

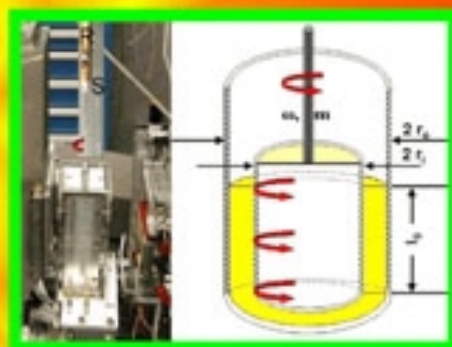
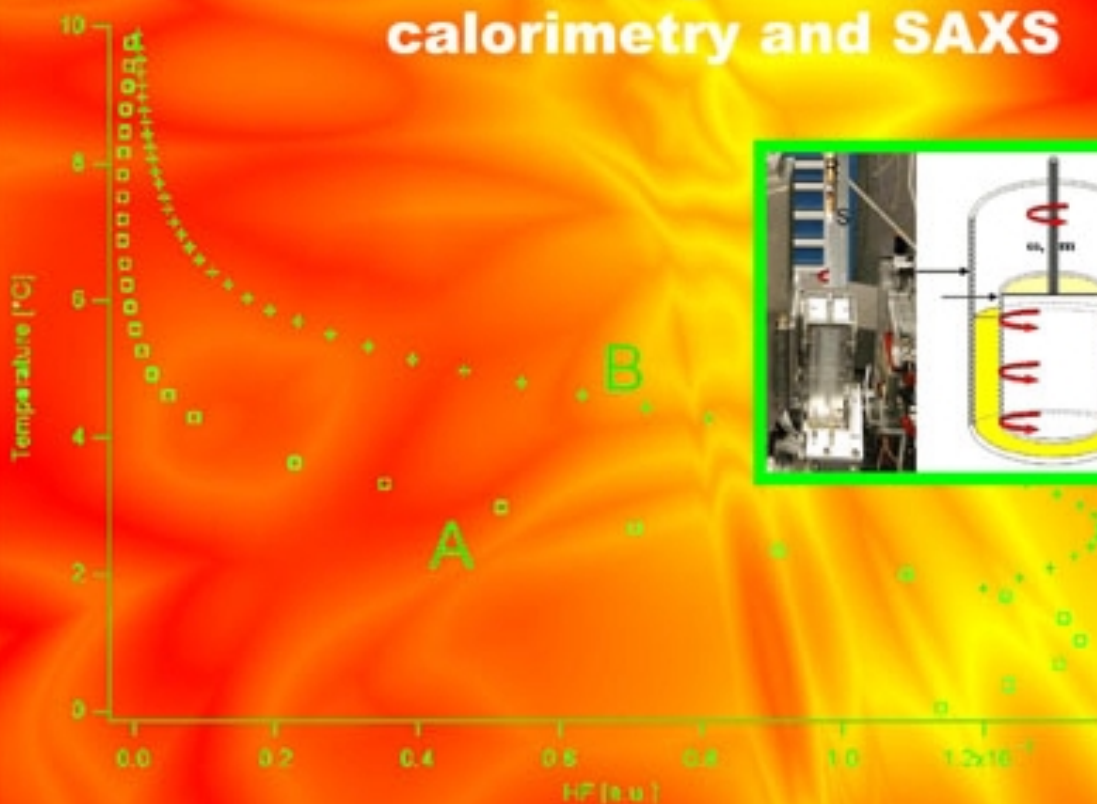
2003



**ANNUAL REPORT
2003**

FOOD & DRUGS:

**Combining shear,
calorimetry and SAXS**



AUSTRIAN SAXS BEAMLINER AT *elettra*



Cover-Pictures: Taken from the user contribution Kalnin et al. *Development of a new vertical couette cell for simultaneous swaxs/dsc/shear experiments as a function of temperature* (page 65)

Austrian Small Angle X-ray Scattering (SAXS) Beamline at ELETTRA

Annual Report 2003

Compiled by the SAXS-Group:

- for IBR: B. Sartori, M. Rappolt & H. Amenitsch
- for ELETTRA: S. Bernstorff

Table of Contents

› Preface	<i>1</i>
› The SAXS-Group	<i>3</i>
› The SAXS-Beamline in General	<i>4</i>
› Application for Beamtime at ELETTRA	<i>8</i>
› List of Institutes Participating in Experiments	<i>10</i>
› List of Performed Experiments	<i>17</i>
› User Statistics	<i>22</i>
› Experimental Possibilities at the SAXS-beamline	<i>26</i>
1. Accessible SAXS and WAXS ranges	<i>26</i>
2. Calibration of the s-axis and flat field correction	<i>27</i>
3. Site laboratories	<i>29</i>
4. Available sample manipulation stages	<i>30</i>
› User Contributions	<i>37</i>
1. Materials Science	<i>38</i>
2. Life Sciences	<i>53</i>
3. Chemistry	<i>82</i>
4. Instrumentation	<i>112</i>
› Publications	<i>116</i>
› Author Index	<i>133</i>

Preface

One year ago I raised here the issue of human resources management, particularly referring to the careers of beamline scientists. I am very glad to see that important progress has already been achieved in the short time since: Through the new I3-Networking Activity: Transnational Exchanges of Scientists (<http://www.elettra.trieste.it/I3/>) established last summer, a fellowship scheme has been created which focuses on the brain-flow between the infrastructure facilities in Europe and their client institutions. The money is there, now it must be used.

Another issue, somewhat related to the first one but still poorly resolved, is the industrial use of synchrotron radiation. SAXS especially, with its wide horizon of applications – “wherever nanostructure counts, SAXS is a key analytical technique” – has an enormous potential to solve questions of interest to industry. Food & drug industry is clearly an extremely promising candidate. The recent developments in techniques, also the one highlighted on the cover of this Annual Report, should prove very attractive in this direction. We now have to transport this message through the right channels. These might be different from those commonly used by academia, the publication in journals, with high impact within but almost no impact beyond the scientific community.

The World Year of Physics 2005 seems an appropriate opportunity to propagate “SAXS for the People”.

I thank again all the users and the management of Elettra for this excellent and smooth collaboration.



A handwritten signature in black ink, appearing to read 'Laggner'.

Peter Laggner
Director
Institute of Biophysics and X-Ray Structure Research
Austrian Academy of Sciences

It is a pleasure to welcome again the appearance of the annual report of the Austrian Beamline at Elettra. Scientists in Materials Science, Life Sciences, Chemistry and related disciplines are taking advantage of this excellent opportunity. The success of their experiments is related to two factors, namely the performance of the electron storage ring and the quality and user-friendliness of the beamline equipment. The program of upgrades of the storage ring made great progress in the last year. The effect of the 3rd harmonic cavity and of the multi-bunch feedback systems on the lifetime and on the stability of the beam is very impressive, and was noticed by the most demanding users. The program of machine upgrades continues, the new injection system under construction being the largest and most important project. As far as the beamline and the related preparation laboratories are concerned, this report details the continuously improving capabilities that are offered to the users.

There is little doubt that partnerships such as this Italian-Austrian venture have been through the years a key element for the success of the Elettra Laboratory. For this reason, the Board of Directors of the Sincrotrone Trieste company, which operates the laboratory, is considering new ways and new instruments to take advantage of the advice of successful partners, such as the Austrian Academy, in the decision-making process for important issues determining the long term strategy of the facility.

I would like to thank the management and the staff of the SAXS beamline for their enthusiasm and dedication to the success of the beamline.



A handwritten signature in black ink, which appears to read "M. Altarelli".

Massimo Altarelli
Director
Elettra Synchrotron Light Laboratory

The SAXS-Group

- HEAD OF PROJECT: Peter Laggner¹⁾
e-mail: Peter.Laggner@oeaw.ac.at
- SENIOR SCIENTISTS: Heinz Amenitsch ^{1), 3)}
e-mail: Heinz.Amenitsch@elettra.trieste.it
Sigrid Bernstorff ²⁾
e-mail: Sigrid.Bernstorff@elettra.trieste.it
- SCIENTIST: Michael Rappolt ^{1), 3)}
e-mail: Michael.Rappolt@elettra.trieste.it
- PHD-STUDENT: Fabian Schmid ^{1), 3)} (since January 2004)
e-mail: Fabian.Schmid@elettra.trieste.it
- VISITING SCHOLAR: Semra Ide (since September 2003)
e-mail: Semra.Ide@elettra.trieste.it
- CHEMICAL ASSISTANT: Barbara Sartori ^{1), 3)} (since April 2003)
e-mail: Barbara.Sartori@elettra.trieste.it
- TECHNICIAN: Christian Morello²⁾
e-mail: Christian.Morello@elettra.trieste.it

1) Institute for Biophysics and X-ray Structure Research, Austrian Academy of Sciences,
Schmiedlstraße 6, 8042 Graz, Austria.

Tel 0043-316-4120 302

Fax 0043-316-4120 390

2) Sincrotrone Trieste, Strada Statale 14, km 163.5, 34012 Basovizza (TS), Italy.

Tel 0039-040-375 81

Fax 0039-040-938 0902

3) Institute for Biophysics and X-ray Structure Research, Austrian Academy of Sciences
c/o Sincrotrone Trieste

The SAXS-Beamline in General

Small Angle X-ray Scattering has become a well known standard method to study the structure of various objects in the spatial range from 1 to 1000 nm, and therefore instruments capable to perform such experiments are installed at most of the synchrotron research centers. The high-flux SAXS beamline at ELETTRA is mainly intended for time-resolved studies on fast structural transitions in the sub-millisecond time region in solutions and partly ordered systems with a SAXS-resolution of 1 to 140 nm in real-space.

The photon source is the 57-pole wiggler whose beam is shared and used simultaneously with a Macromolecular Crystallography beamline. The wiggler delivers a very intense radiation between 4 and 25 keV of which the SAXS-Beamline accepts 3 discrete energies, namely 5.4, 8 and 16 keV. The beamline optics consists of a flat double crystal monochromator and a double focusing toroidal mirror.

A versatile SAXS experimental station has been set-up, and an additional wide-angle X-ray scattering (WAXS) detector monitors simultaneously diffraction patterns in the range from 0.1 to 0.9 nm. The sample station is mounted move-able onto an optical table for optimising the sample detector distance with respect to SAXS resolution and sample size.

Besides the foreseen sample surrounding the users have the possibility to install their own specialised sample equipment. In the design phase, besides technical boundary conditions, user friendliness and reliability have been considered as important criteria.

The optimisation of the beamline with respect to high-flux and consequently high flux density, allows to perform the following experiments:

- Low Contrast Solution Scattering
- Grazing Incidence Surface Diffraction
- Micro-Spot Scanning
- X-ray Fluorescence Analysis
- Time-Resolved Studies $\geq 11 \mu\text{s}$
- Simultaneously Performed Small- and Wide-Angle Measurements (SWAXS) on:
 - Gels
 - Liquid Crystals
 - (Bio) Polymers
 - Amorphous Materials
 - Muscles

Furthermore, using 5.4 and 16 keV energies, the beamline is widely applicable also to very thin, e.g. single muscle fibers, and optically thick (high Z) specimen, as often used in e.g., material science and solid state physics.

THE INSERTION DEVICE

The wiggler for the SAXS beamline consists of three 1.5 m long segments, each having 19 poles. The device can work with a minimum gap of 20 mm, which corresponds to $K=20$ at 2 GeV. The main parameters of the wiggler are:

- Critical Energy 4.1 keV
- Radiation Power 8.6 kW
- Flux 3.5×10^{14} ph/s/mrad/0.1%BW (at 400 mA)

The wiggler radiation cone has a horizontal width of 9 mrad. From this the SAXS-beamline accepts vertically 0.3 mrad, and horizontally +/-0.5 mrad at a 1.25 mrad off-axis position. The resulting source size for 8 keV photons is $3.9 \times 0.26 \text{ mm}^2$ (horiz. x vert.).

THE OPTICS

The optics common with the diffraction beamline consists of:

- C-Filter and Beryllium window assembly to reduce the power load on the first optical elements by a factor of 2 and to separate the beamline vacuum from the storage ring.
- Beam defining slit chamber which allows to define the SAXS beam on three sides before the monochromator in order to reduce the straylight in the downstream beamline sections.

The SAXS beamline optics consists of:

- A double-crystal monochromator consisting of four individual chambers, in which three interchangeable asymmetric Si(111) crystal pairs are used to select one of three fixed energies. Each of the crystal pairs is optimised for the corresponding energy to accomplish a grazing angle of 2° . The energy resolution $\Delta E/E$ of the monochromator is in the range of $0.7 - 2.5 \cdot 10^{-3}$.
- A baffle chamber after the monochromator is used as an adjustable straylight fenditure.
- A segmented toroidal mirror focuses the light in horizontal and vertical direction with a 1/2.5 magnification onto the SAXS-detector.
- An aperture slit reduces the straylight after the monochromator and the toroidal mirror.
- A guard slit defines the illuminated region around the focal spot. The spot size on the detector is 1.6 mm horizontally and 0.6 mm vertically. The calculated flux at the sample is in the order of 10^{13} ph/s at 400 mA. For a maximum sample size of $5.4 \times 1.8 \text{ mm}^2$ correspondingly a flux density of 10^{12} ph/s/ mm^2 has been calculated.

SAMPLE STAGE

The multipurpose sample stage allows to perform fast time-resolved relaxation studies based on temperature- or pressure-jumps as well as stopped flow experiments. Shear jump relaxation experiments are planned. Specifically, T-jumps can be induced by an infra-red light pulse (2 ms) from an Erbium-Glass laser, raising the temperature about 20°C in an aqueous sample volume of 10 μl . A hydrostatic pressure cell with a maximal accessible angular range of 30° for simultaneous SAXS and WAXS measurements is available. P-jumps are realised by switching fast valves between a low and a high pressure reservoir, increasing or decreasing the hydrostatic pressure in the range from 1 bar to 2.5 kbar within a few ms. A Differential Scanning Calorimeter (DSC) allows for DSC-scans simultaneously to SWAXS measurements. Also a 1.5 T magnet is available. In an overview, the following sample manipulations are possible (further details, see page 25-34):

- Temperature Manipulations: Ramps, Jumps and Gradient Scans
- Pressure Manipulation: Scan and Jumps
- Stopped Flow Experiments
- SWAXS Measurements Applying Mechanical Stress
- SWAXS Measurements Applying Magnetic Fields
- Calorimetric measurements

Scientific applications	<p>Low Contrast Solution Scattering, Grazing Incidence Surface Diffraction, Micro-Spot Scanning, X-ray Fluorescence Analysis, Time-Resolved Studies $\geq 11 \mu\text{s}$ and Simultaneously Performed Small- and Wide-Angle Measurements (SWAXS) on:</p> <p>Gels Liquid Crystals (Bio) Polymers Amorphous Materials Muscles</p>																								
Source characteristics	<p><u>Wiggler (NdFeB Hybrid):</u></p> <table border="0"> <tr> <td>Period</td> <td>140 mm</td> </tr> <tr> <td>No. full poles</td> <td>57</td> </tr> <tr> <td>Gap</td> <td>20 mm</td> </tr> <tr> <td>B_{max}</td> <td>1.607 T</td> </tr> <tr> <td>Critical Energy ϵ_c</td> <td>4.27 keV</td> </tr> <tr> <td>Power (9 mrad)</td> <td>8.6 kW</td> </tr> <tr> <td>Effective source size FWHM</td> <td>$3.9 \times 0.26 \text{ mm}^2(\text{HxV})$</td> </tr> </table>	Period	140 mm	No. full poles	57	Gap	20 mm	B_{max}	1.607 T	Critical Energy ϵ_c	4.27 keV	Power (9 mrad)	8.6 kW	Effective source size FWHM	$3.9 \times 0.26 \text{ mm}^2(\text{HxV})$										
Period	140 mm																								
No. full poles	57																								
Gap	20 mm																								
B_{max}	1.607 T																								
Critical Energy ϵ_c	4.27 keV																								
Power (9 mrad)	8.6 kW																								
Effective source size FWHM	$3.9 \times 0.26 \text{ mm}^2(\text{HxV})$																								
Optics	<table border="0"> <tr> <td><u>Optical elements:</u></td> <td>Double crystal monochromator: Si (111) asym. cut, water cooled.</td> <td>Mirror: two-segment, toroidal, Pt coated.</td> </tr> <tr> <td><u>Distance from source:</u></td> <td>18.4 m</td> <td>26.5 m</td> </tr> <tr> <td>Acceptance</td> <td colspan="2">1 mrad/0.3 mrad (HxV)</td> </tr> <tr> <td>Energy (3 selectable)</td> <td colspan="2">5.4, 8, 16 keV (0.077, 0.154, 0.23 nm)</td> </tr> <tr> <td>Energy resolution $\Delta E/E$</td> <td colspan="2">$0.7\text{-}2.5 \times 10^{-3}$</td> </tr> <tr> <td>Focal spot size FWHM</td> <td colspan="2">$1.2 \times 0.6 \text{ mm}^2 (\text{HxV})$</td> </tr> <tr> <td>Spot at Sample FWHM</td> <td colspan="2">$5.4 \times 1.8 \text{ mm}^2(\text{HxV})$</td> </tr> <tr> <td>Flux at sample</td> <td colspan="2">$5 \times 10^{12} \text{ ph s}^{-1}(2 \text{ GeV}, 200 \text{ mA}, 8 \text{ keV})$</td> </tr> </table>	<u>Optical elements:</u>	Double crystal monochromator: Si (111) asym. cut, water cooled.	Mirror: two-segment, toroidal, Pt coated.	<u>Distance from source:</u>	18.4 m	26.5 m	Acceptance	1 mrad/0.3 mrad (HxV)		Energy (3 selectable)	5.4, 8, 16 keV (0.077, 0.154, 0.23 nm)		Energy resolution $\Delta E/E$	$0.7\text{-}2.5 \times 10^{-3}$		Focal spot size FWHM	$1.2 \times 0.6 \text{ mm}^2 (\text{HxV})$		Spot at Sample FWHM	$5.4 \times 1.8 \text{ mm}^2(\text{HxV})$		Flux at sample	$5 \times 10^{12} \text{ ph s}^{-1}(2 \text{ GeV}, 200 \text{ mA}, 8 \text{ keV})$	
<u>Optical elements:</u>	Double crystal monochromator: Si (111) asym. cut, water cooled.	Mirror: two-segment, toroidal, Pt coated.																							
<u>Distance from source:</u>	18.4 m	26.5 m																							
Acceptance	1 mrad/0.3 mrad (HxV)																								
Energy (3 selectable)	5.4, 8, 16 keV (0.077, 0.154, 0.23 nm)																								
Energy resolution $\Delta E/E$	$0.7\text{-}2.5 \times 10^{-3}$																								
Focal spot size FWHM	$1.2 \times 0.6 \text{ mm}^2 (\text{HxV})$																								
Spot at Sample FWHM	$5.4 \times 1.8 \text{ mm}^2(\text{HxV})$																								
Flux at sample	$5 \times 10^{12} \text{ ph s}^{-1}(2 \text{ GeV}, 200 \text{ mA}, 8 \text{ keV})$																								
Experimental apparatus	<p><u>Resolution in real space:</u> 1-140 nm (small-angle), 0.1- 0.9 nm (wide-angle)</p> <p><u>Sample stage:</u> temperature manipulations: ramps, jumps and gradient scans, pressure manipulation: scan and jumps, stop flow experiments, SWAXS measurements applying mechanical stress, SWAXS measurements applying magnetic fields. In-line calorimetric measurements simultaneously with SWAXS.</p> <p><u>Detectors:</u> 1D gas-filled detectors for simultaneous small- and wide-angle (Gabriel type), 2D CCD-detector for small-angle.</p>																								
Experiment control	<p><u>Beamline control:</u> Program-units written in LabView for Windows</p> <p><u>1 D detector control:</u> PC-card and software from Hecus & Braun, Graz.</p> <p><u>2 D detector control:</u> Software from Photonic Science, Oxford.</p>																								

CURRENT STATUS

The beamline has been built by the Institute for Biophysics and X-ray structure Research (IBR), Austrian Academy of Science in collaboration with staff members from Sincrotrone Trieste, and is in user operation since September 1996. The set-up of the beamline started at the beginning of January 1995 with the installation of the support structure. Until the end of 1995, the 8 keV single energy system had been realised. The upgrade to the full three energy system was finished in spring 1998. Time resolved experiments require fast X-ray detectors and data acquisition hard- and software. Depending on the desired resolution in time and in reciprocal space, on isotropic or anisotropic scattering of the sample, one-dimensional position sensitive (delay-line type) or two-dimensional CCD detectors are employed.

In August 2002 our new chemistry and X-ray laboratory went into operation. The chemistry unit serves mainly for sample preparation and analysis for both, in house research and external user groups, whereas the X-ray laboratory allows on-site testing of samples before moving on to the SR beamline (see page 29).

In conclusion, due to wide versatility of the beamline and the highly flexible sample stage, there are nearly no limits for the realisation of an experiment, and you are welcome by our team to propose any interesting and highlighting investigation for the benefit of material and life sciences.

Application for Beamtime at ELETTRA

1. Beamtime Policy at SAXS beamline

According to the agreement from March 2001 regarding the co-operation between the Austrian Academy of Sciences and Sincrotrone Trieste, at the Austrian SAXS-beamline the available beamtime of about 5000 hours/year is distributed as follows:

- 35% for Austrian Users, type: "CRG" (Collaborating Research Group)
- 35% for Users of Sincrotrone Trieste (General Users (GU))
- 30% is reserved for beamline maintenance and in-house research

In both user beamtime contingents also any industrial, proprietary and confidential research can be performed according to the "General User Policy" of Sincrotrone Trieste.

To apply for CRG and GU user beamtime proposals must be submitted according to the rules of Sincrotrone Trieste. The international review committee at ELETTRA will rank the proposals according to their scientific merit assessment. Based on this decision beamtime will be allocated according to the specific quotes for the beamtimes (CRG/GU) either for the following semester ("normal application") or for the next two years ("long term application"). However, at the moment no more than a maximum of 10% of the beamtime will be assigned to "long term" projects.

2. How to apply for beamtime

There are two deadlines each year for proposals, namely August 31st and February 28th. Accepted proposals will receive beamtime either in the then following first or second half year period, respectively. The Application Form must be completed on-line according to the following instructions. In addition, one printed form is also required and must be sent to:

ELETTRA USERS OFFICE
Strada Statale 14 - km 163.5
34012 Basovizza (Trieste), ITALY
Tel: +39 040 3758628 - fax: + 39 040 3758565
e-mail: useroffice@elettra.trieste.it

INSTRUCTIONS GIVEN BY THE USERS OFFICE
(see also: www.elettra.trieste.it/experiments/users_handbook/index.html)

1. Read carefully the following Guidelines.
2. Connect to the Virtual Users' Office: <http://users.elettra.trieste.it> using your favorite browser with JavaScript enabled.
3. Select the Virtual Users Office link.

4. When prompted, insert your ID and password. If you are a new user fill in the registration form with your data and choose your institution with the search button; in case your institution does not appear in the list, please contact useroffice@elettra.trieste.it giving all the details about it. When registered, you will receive an acknowledgment with your ID and password. You can change your password, if you wish. In case you forget your password, please don't register again but contact useroffice@elettra.trieste.it. At any moment you can select the help button and view more detailed instructions. By inserting your ID and password you will be able to continue.
5. Select the proposals button in the User functions group.
6. Select add and fill in on-line the proposal form. Please, type your proposal in English. Repeat this procedure for each proposal you intend to submit.
7. In case of continuation proposal: a) attach the experimental report of previous measurements; b) give your previous proposal number.
8. When finished, submit the proposal electronically, selecting the save button.
9. Print the proposal form together with each related safety form.
10. Sign the safety form(s).
11. Mail one complete printed copy to the Users Office.

NOTE

From July 2002 on there exists a new possibility for users from developing countries to apply for financial support for their travel expenses. For all other users everything remains as before. For further information, please have a look into the web-pages

http://www.elettra.trieste.it/experiments/users_handbook/index.html)

or contact the USERS OFFICE.

List of Institutes Participating in Experiments

Austria

Austrian Academy of Science, Institute for Biophysics and X-ray Structure Research, Graz

AMENITSCH Heinz
DEUTSCH Günter
FERNANDEZ-VIDAL Monica
JOCHAM Philipp
KOSCHUCH Richard
KRIECHBAUM Manfred
LAGGNER Peter
LOHNER Karl
PABST Georg
POZO-NAVAS Beatriz
RAPPOLT Michael
SARTORI Barbara
SEVCSIK Eva
VOLPE Luigia

Technical University, Institut of Applied Synthetic Chemistry, Division of Macromolecular Chemistry, Vienna

KUNZ Michael
BINDER Wolfgang H.
MACHL Doris
KLUGER Christian
PETRARU Laura

Technical University, Institute of Materials Chemistry, Vienna

HAUBENBERGER Ulrike
HÜSING Nicola
KICKELBICK Guido
KOGLER Franz Rene
RAAB Christina
TORMA Viktoria
GIESENHENG Thomas
BRANDHUBER Doris

University of Technology, Institute of Structural Analysis, Computational Biomechanics, Graz

HOLZAPFEL G.A.
SCHULZE-BAUER Christian A.J.
SOMMER Gerhard
SCHMID Fabian

University of Vienna, Institute of Materials Physics

KERBER Michael
PETERLIK Herwig
SCHAFLER Erhard
ZEHETBAUER Michael

University of Vienna, Institute of Materials Physics, and ARC
Seibersdorf Research GmbH

ZEIPPER Leonhard

Croatia

"Ruder Boskovic" Institute, Zagreb

BULJAN Maya
DESNICA-FRANKOVIC Ida-Dunja
DESNICA Uros
DUBCEK Pavo
KOVACEVIC Ivana
MAROHNIC Zeljko
MEDUNIC Zvonko
PIVAC Branko
RADIC Nikola

University of Zagreb, Institute for Physics, Zagreb

SABOLEK Stjepan
SALAMON Kresimir
IVKOV J.

Faculty of Sciences, Zagreb

TONEJC A.

Czech Republic

Academy of Sciences of the Czech Republic, Institute of Macro- molecular
Chemistry, Prague

BALDRIAN Josef
SIKORA Antonín

Joint Laboratory of Solid State Chemistry of Institute of
Macromolecular Chemistry of Academy of Sciences and University of
Pardubice, Pardubice

BENES Ludvik
MELÁNOVÁ Klara
ZIMA Vitezslav

University of Pardubice, Department of Physics, Pardubice

STEINHART Milos

University of Pardubice, Faculty of Chemical Technology, Pardubice
KASPAROVÁ J.

Finland

Åbo Akademi University, Dept. of Physical Chemistry, Materials Research
Group, Turku

LINDÉN Mika
TEIXEIRA Cilaine Veronica

France

Equipe Physico-Chimie des Systèmes Polyphasés, UMR CNRS 8612,
Chatenay-Malabry

KALNIN Daniel
KELLER Gerhard
OLLIVON Michel

Université Pierre et Marie Curie, Chimie de la Matière Condensée,
Paris

BABONNEAU Florence
BACCILE Niki
BOISSIÈRE Cédric
COUPÉ Aurélie
GROSSO David
SANCHEZ Clément

Germany

Max-Planck-Institute for Coal Research, Department of Hetero-
geneous Catalysis, Mülheim / Ruhr

SCHMIDT Wolfgang

Max-Planck-Institute for Colloids and Interfaces, Golm / Potsdam

CÖLFEN Helmut

Max-Planck-Institute for Polymer Research, Mainz

GRÖHN Franziska

Research Center Rossendorf, Dresden

MUELLER Gudrun
VAN OUYTSEL Kristel

Universität Augsburg, Institut für Physik

GROSSHANS I.
KARL Helmut
STRITZKER B.

Universität Bremen, Institut für Festkörperphysik

ALEXE Gabriela
CLAUSEN Torben
FALTA Jens
GANGODADYHAY Subhashis
HOMMEL Detlev
KRUSE C.
SCHMIDT Thomas
UETA A.

Universität–GH Siegen, Fachbereich Physik, Siegen

BESCH Hans-Juergen
MARTOIU Sorin
NURDAN K.
ORTHEN Andre'
WAGNER Hendrik
WALENTA Albert Heinrich
WERTHENBACH U.

Hungary

Eötvös University, Department of General Physics, Budapest

NYILAS Krystian
RIBARIK Gabor
SIMON Kornel
UNGÁR Tamas

India

Indian Institute of Science, Solid State and Structural Chemistry Unit, Bangalore

SAPRA Sameer
SARMA Dipankar Das
VISWANATHA Ranjani

Italy

CNR, Istituto Processi Chimico-Fisici, Messina

LOMBARDO Domenico
TRIOLO Alessandro

I.N.F.M. - Laboratorio TASC, Trieste

COJOC Danut-Adrian
DI FABRIZIO Enzo
FERRARI Enrico

Istituto Motori C.N.R., Aerosol and Nanostructures Lab, Napoli

DI STASIO Stefano
VERRENGIA G.

Sincrotrone Trieste, Trieste

BERNSTORFF Sigrid

MENK Ralf

MORELLO Christian

Università di Firenze, Dip. Scienze Fisiologiche, Firenze

BAGNI Maria Angela

CECCHI Giovanni

COLOMBINI Barbara

Università di Padova, Dep. of Mechanical Engineering, Padova

FALCARO Paolo

Università di Palermo, dipartimento di Chimica Fisica, Palermo

TRIOLO Roberto

Università di Perugia, Dipartimento di Fisica, Perugia

CINELLI Stefania

ONORI G.

ORTORE Maria Grazia

Università del Piemonte Orientale “A.Avogadro”, Dip. Scienze e
Tecnologie Avanzate (DISTA), Alessandria

CROCE Gianluca

MILANESIO Marco

VITERBO Davide

Università Politecnica delle Marche, Dipartimento di Scienze Applicate ai Sistemi
Complessi, sez. Scienze Fisiche, Ancona

DI GREGORIO Giordano M.

FEDERICONI Francesco

FERRARIS Paolo

MARIANI Paolo

MATTIONI Michele

PACCAMICCIO Lydia

SPAGNOLI Rachele Pie

SPINOZZI Francesco

Università Politecnica delle Marche, Dipartimento di Fisica e Ingegneria dei
Materiali e del Territorio, Ancona

FRANCESCANGELI Oriano

STANIC Vesna

Università Politecnica delle Marche, Dipartimento di Scienze dei Materiali e della Terra, Ancona

CASTAGNA Riccardo
CLEMENTONI Daniela
CONTI Carla
PISANI Michela

Università di Roma-II-Tor Vergata

ESPORTO Vincenzo

Università di Sassari, Dipartimento di Architettura e Pianificazione, Laboratorio di Scienza dei Materiali e Nanotecnologie, Alghero

INNOCENZI Plinio

University of Trieste

VOLTOLINA Francesco

Poland

University of Mining and Metallurgy, Crakow

MIKULOWSKI Borys

Russia

Institute of Chemical Kinetics and Combustion, Siberian Branch of the Russian Academy of Sciences, Novosibirsk

ONISCHUK A.

Slovenia

University of Ljubljana, Department of Physics, Faculty of Mathematics and Physics, Ljubljana

BLINC R.

Spain

Instituto de Investigaciones Químicas y Ambientales de Barcelona – Consejo Superior de Investigaciones Científicas (IIQAB-CSIC), Dep. Tecnología de Tensioactivos, Barcelona

CAELLES Jaime
CÓCERA Mercèdes
CARRERA Immaculada
LOPEZ Olga
DE LA MAZA A.
PEREIRA LACHATAIGNERAIIS Joedmi
PONS Ramon

Sweden

University of Lund, Institute for Physical Chemistry 1

ALFREDSSON Viveka
FLODSTRÖM Katarine

University of Uppsala, Department of Physical Chemistry 1

ALMGREN M.

Switzerland

Nestle Research Center, Lausanne

SCHAFER Olivier

United Kingdom

UCB Surface Specialties, Wigton, Cumbria

JESCHKE M.

University Laboratory of Physiology, Oxford

ASHLEY Christopher C
GRIFFITHS Peter J.

USA

Illinois Institute of Technology, Department of Chemical Engineering, Chicago

ERDEMIR Deniz
EVANS James M.B.
MYERSON A. S.

Illinois Institute of Technology, Department of Biological, Chemical
and Physical Sciences, Chicago

SEGRE Carlo U.

MR-CAT, Advanced Photon Source, Argonne National Laboratory, Argonne,
Illinois

CHATTOPADHYAY Soma

University of California, Department of Chemistry and Biochemistry, Los Angeles

RILEY A.
TOLBERT S.

List of Performed Experiments

2003 (first half year)

Proposal	Proposer	Institution	Country	Title	Research Area
2001115	BESCH Hans-Juergen	Universität GHS Siegen, Dept. of Physics	Germany	Detector development for time- resolved SAXS (long term proposal)	Instrumen- tation
2001229	LAGGNER Peter	Inst. of Biophysics and X-Ray Structure Research (IBR), Austrian Academy of Sciences (AAS), Graz	Austria	(long term proposal): as prop 2002385	Life Sciences
2002319	DI STASIO Stefano	C.N.R. - Istituto Motori, Napoli	Italy	<in-situ> TR-SWAXS experiments of zinc nanoparticles undergoing an oxidation process	Chemistry
2002385	LAGGNER Peter	IBR, AAS, Graz	Austria	1. Phospholipid main phase transition in oriented bilayers: sterol impact 2. Structural and thermo-dynamical properties of POPC at low sterol conc. studied by p- scanning SAXS 3. p-induced subunit dissociation structure and fluctuations in the anomalous swelling regime of PC 4. X-Ray diffraction of mixed chain PE and PG 5. The non-equilibrium formation of the cubic diamond phase in monolein/water systems	Life Sciences
2002389	ZEHETBAUER Michael	Univ. Wien, Institut für Materialphysik	Austria	Time and Space Resolved Scanning Synchrotron X-ray Profile Analyses during Plastic Deformation of BCC and HCP Metals	Materials Science
2002394	TRIOLO Alessandro	Istituto per i Processi Chimico- Fisici – CNR, Messina	Italy	Phase diagram of polyolefin-resin mixtures	Chemistry
2002427	DUBCEK Pavo	Rudjer Boskovic Institute, Zagreb	Croatia	Study of the surface treatment influence on soft magnetic properties of nanocrystalline Fe- Cu-Nb-Si-B alloys	Materials Sciences
2002450	BABONNEAU Florence	Université Paris 6, Chimie de la Matiere Condensee, Paris	France	In-situ SAXS study of the formation of surfactant templated silicas with 3D-periodic structures.	Chemistry
2002479	HÜSING Nicola	Technische Universität Wien - Institut für Materialchemie, Vienna	Austria	Time resolved SAXS investigation of sol-gel materials prepared from (MeO) ₃ Si-R- M(OMe) ₃ or (MeO) ₃ Si-R- M(OMe) ₂ -R-Si(OMe) ₃	Chemistry
2002491	HÜSING Nicola	Technische Universität Wien - Institut für Materialchemie, Vienna	Austria	In-situ SAXS Investigation of the Formation of Mesostructured Silica Monoliths	Chemistry

2002555	VAN OUYTSEL Kristel	Research Center Rossendorf, Dresden	Germany	SAXS and WAXS to characterize the damage around the crack tip in Al-alloys.	Materials Sciences
2002585	LOMBARDO Domenico	CNR, Istituto per I Processi Chimico- Fisici, Messina	Italy	Structural Investigation in Aqueous Solution of Complex Polyelectrolytes Systems	Chemistry
2002593	MARIANI Paolo	Università di Ancona - Ist. di Scienze Fisiche	Italy	Structural and energetic effects of hydrostatic pressure on lyotropic phases from biologically relevant molecules	Life Sciences
2002594	MARIANI Paolo	Università di Ancona - Ist. di Scienze Fisiche	Italy	Pressure-assisted cold denaturation of metmyoglobin by SAXS	Life Sciences
2002601	INNOCENZI Plinio	Università di Padova - Dip. Ingegneria Meccanica (Settore Materiali)	Italy	Small angle X-ray scattering of self-assembled mesoporous thin films doped with fullerene derivatives and push-pull chromophores	Chemistry
2002612	OLLIVON Michel	CNRS UMR 8612, University Paris- Sud, 5	France	Triglyceride crystallisation in emulsions : Study of the crystalline structures and phase transitions by coupling of Differential Scanning Calorimetry and High Resolution Small Angle X-ray Scattering.	Life Sciences
In-house	BERNSTORFF Sigrid, RADIC Nikola et al.	Sincrotrone Trieste + Rudjer Boskovic Institute, Zagreb	Italy / Croatia	Microstructure and phase distribution in sputter-deposited tungsten films	Materials Sciences
In-house	BERNSTORFF Sigrid, PIVAC Branko et al.	Sincrotrone Trieste + Rudjer Boskovic Institute, Zagreb	Italy / Croatia	GISAXS study of oxygen precipitation in silicon	Materials Sciences
In-house	STEINHART Milos	Czech Academy of Sciences - Inst. of Macromolecular Chemistry, Prague	Czech Republic	Study of Phase Properties of Intercalates by SWAXS	Chemistry
In-house	AMENITSCH Heinz, COELFEN Helmut et al.	IBR, AAS Graz + Max Planck Institute of Colloids and Interfaces, Golm, Potsdam + Max- Planck-Institute for Polymer Research, Mainz	Austria / Germany	Ultrafast free jet study of crystallization reactions by synchrotron small angle X-ray scattering (SAXS)	Chemistry
In-house	AMENITSCH Heinz, VITERBO Davide CROCE Gianluca et al.	IBR, AAS Graz + DISTA, Università del Piemonte Orientale, Alessandria	Austria / Italy	Thermal SAXS study of siliceous spicules Thetya Aurantium	Life Sciences
Pilot	SARMA Dipankar Das	Indian Institute of Science, Solid State and Structural Chemistry Unit, Bangalore	India	Study of the growth of semiconducting ZnS nanoparticles	Chemistry

2003 (second half year)

Proposal	Proposer	Institution	Country	Title	Research Area
2003021	GROSSO David	Université Paris 6, Chimie de la Matiere Condensee	France	Self-assembly mechanisms during aerosol generation of mesostructured macro-spheres.	Chemistry
2003035	GRIFFITHS Peter John	University Laboratory of Physiology, Oxford	United Kingdom	Investigation of Substates in the Power Stroke Event of the Myosin Molecular Motor.	Life Sciences
2003036	EVANS James CHATTO- PADHYAY Soma	Illinois Institute of Technology - Center of Crystallization and Particle Technology, Chicago	USA	Fundamental study of the nucleation process from a supersaturated solution	Chemistry
2003059	LOPEZ Serrano Olga	Consejo Superior de Investigaciones Cientificas - Instituto de Investigaciones Quimicas y Ambientales de Barcelona	Spain	Role of the electrostatic charge on the kinetic of the first steps of liposome solubilization: adsorption of surfactant and desorption of mixed micelles	Life Sciences
2003063	PONS Ramon	Dep. Tecnologia de Tensioactius, IIQAB-CSIC, Barcelona	Spain	Dynamics of emulsification by temperature jump	Chemistry
2003064	FRANCES- CANGELI Oriano	Univ.di Ancona, Dip. di Scienze e dei Materiali della Terra, sez. Fisica, Ancona	Italy	Structural study of self- assembled Liposome-DNA-Metal Complexes	Life Sciences
2003068	LINDEN Mika	ÅBO Academi University, Dept. of Physical Chemistry, Materials Research Group, Turku	Finland	First in-situ synchrotron SAXS/XRD study of the formation of triblock copolymer templated mesostructured silica in solution	Chemistry
2003090	BINDER Wolfgang	Technische Universität Wien - Institut of Applied Synthetic Chemistry, Division of Applied Synthetic Chemistry, Vienna, Austria	Austria	Nanostructural Investigations on Phase Separated Supramolecular Polymers	Chemistry

2003093	LAGGNER Peter	IBR, AAS, Graz	Austria	1. Phospholipid main phase transition in oriented bilayers: sterol impact 2. Structural and thermo-dynamical properties of POPC at low sterol conc. studied by p- scanning SAXS 3. p-induced subunit dissociation structure and fluctuations in the anomalous swelling regime of PC 4. X-Ray diffraction of mixed chain PE and PG 5. The non-equilibrium formation of the cubic diamond phase in monolein/water systems	Life Sciences
2003095	MARIANI Paolo	Università di Ancona - Ist. di Scienze Fisiche	Italy	Phase behaviour, molecular conformation and compressibility of lipid systems	Life Sciences
2003110	MARIANI Paolo	Università di Ancona - Ist. di Scienze Fisiche	Italy	Pressure induced subunit dissociation of dimeric beta-Lactoglobulin	Life Sciences
2003145	BALDRIAN Josef	Czech Academy of Sciences - Inst. of Macromolecular Chemistry, Prague	Czech Republic	Cocrystallization Dynamics in Lamellar Systems of Polymer Blends in Vicinity of Melting Temperature	Physics
2003200	TORMA Viktoria	Technische Universität Wien - Institut für Materialchemie, Vienna	Austria	Formation of inorganic gels prepared from tailored precursors	Chemistry
2003211	TORMA Viktoria	Technische Universität Wien - Institut für Materialchemie, Vienna	Austria	Formation of inorganic-organic hybrid materials using oxometallate particles	Chemistry
2003272	AMENITSCH Heinz	IBR, AAS, Graz	Austria	Layer and Age Specific Tensile Testing of Human Cardiac Arteries	Life Sciences
2003294	ZEHETBAUER Michael	Univ. Wien Institut für Materialphysik	Austria	Investigation of Microstructure by Means of Synchrotron Multi-Reflection X-Ray Profile Analysis (MXPA) in Ultrafine-Grained Metals Produced by High Pressure Torsion (HPT)	Materials Sciences
In-house	AMENITSCH Heinz INNOCENZI Plinio	IBR, AAS Graz + Lab. di Scienza dei Materiali e Nanotecnologie, Università di Sassari, Alghero	Austria / Italy	Orthorombic mesostructured silica film with high thermal stability	Chemistry
In-house	BERNSTORFF Sigrid, DESNICA Uros	Sincrotrone Trieste + Rudjer Boskovic Institute, Zagreb	Italy / Croatia	Compound semiconductor Quantum Dots formed by ion implantation of constituent atoms	Materials Sciences
In-house	BERNSTORFF Sigrid, DESNICA- FRANKOVIC Ida-Dunja	Sincrotrone Trieste + Rudjer Boskovic Institute, Zagreb	Italy / Croatia	Ion beam synthesized CdSe Quantum Dots	Materials Sciences

In-house	BERNSTORFF Sigrid FALTA Jens	Sincrotrone Trieste + Universität Bremen -Institut für Festkörperphysik	Italy / Germany	Ordering of CdSe quantum dots	Materials Sciences
In-house	BERNSTORFF Sigrid PIVAC Branko	Sincrotrone Trieste + Rudjer Boskovic Institute, Zagreb	Italy / Croatia	GISAXS study of noble gas ions implanted silicon	Materials Sciences
In-house	BERNSTORFF Sigrid RADIC Nikola	Sincrotrone Trieste + Rudjer Boskovic Institute, Zagreb	Italy / Croatia	Microstructure and phase distribution in sputter-deposited tungsten films	Materials Sciences
In-house	STEINHART Milos	Sincrotrone Trieste + Rudjer Boskovic Institute, Zagreb	Czech Republic	Study of Phase Properties of Intercalates by SWAXS	Chemistry
Pilot	COJOC Dan et al.	TASC-INFN National Laboratory, Trieste	Italy	Combined microSAXS- microscopy studies on colloidal dispersions	Life Sciences

User Statistics

1. Number of submitted proposals and assigned shifts from 1995 until December 2004

The Austrian SAXS-beamline at ELETTRA opened to users in September 1996. Since then many experiments have been performed related to the fields of life science, materials science, physics, biophysics, chemistry, medical science, technology and instrumentation.

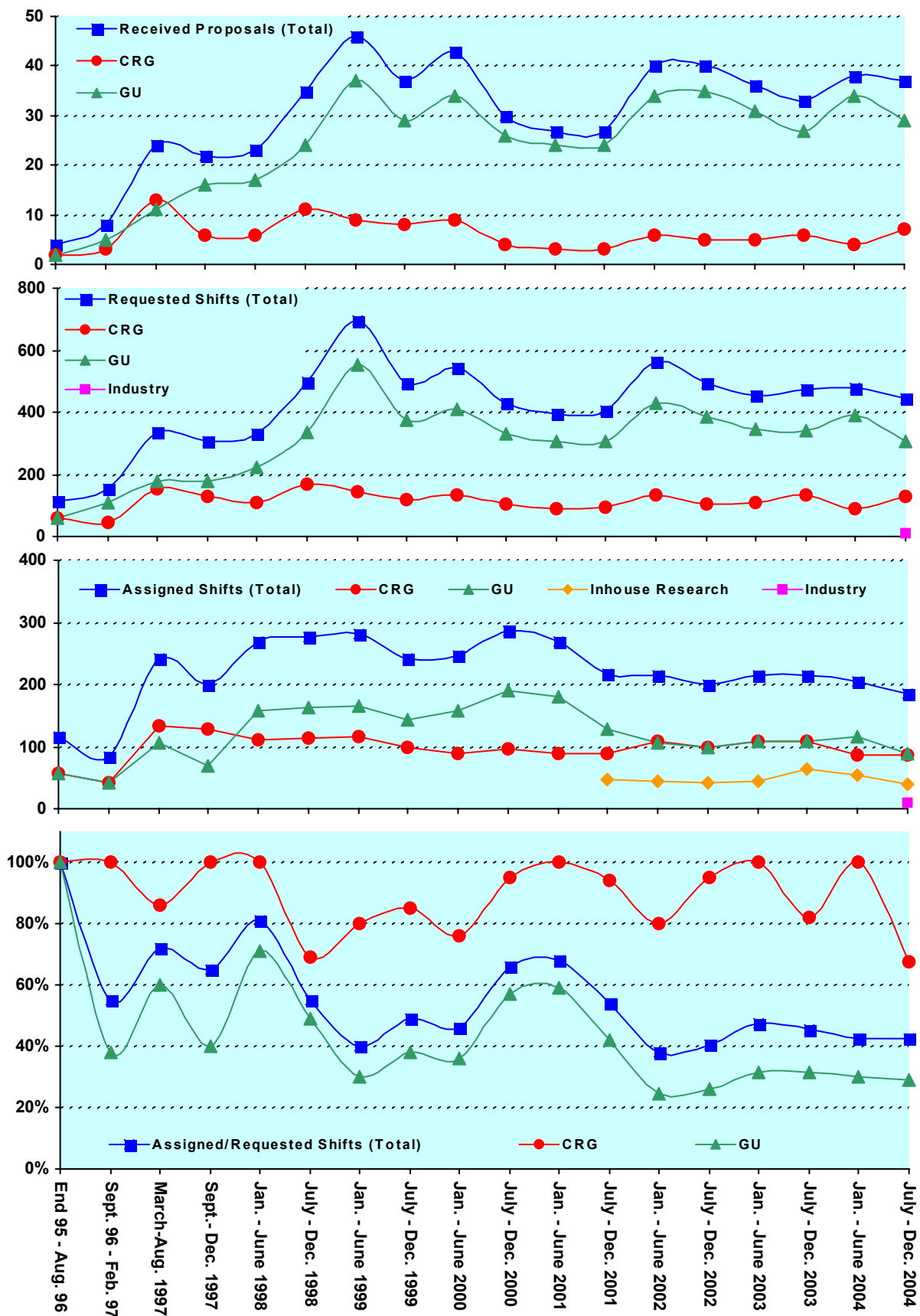
From September 96 on users gained access to the SAXS-beamline on the basis of the proposals received for the periods shown in Fig. 1. The assignment of beamtime at this beamline is done separately for the group of "General Users" (GU) and the "Collaborating Research Group" (CRG), i.e., the Austrian users. Beamtime was assigned to the proposals of each group in the order of the rating received by the Scientific Committee, and up to the maximum number of shifts available to each group according to the contract between "The Austrian Academy of Sciences" and the "Sincrotrone Trieste". Until December 1997 up to 30 % of the beamtime was given to CRG, up to 55 % to GU, and 15% was reserved for maintenance purposes. From January 98 to June 2001 the quota for beamtime was up to 35 % for CRG, up to 50 % for GU, and again 15% reserved for maintenance purposes. From July 2001 on the two contingents for user proposals from CRG and GU receive up to 35% of the beamtime each. The remaining 30 % of beamtime are used for inhouse research projects as well as for maintenance purposes.

Fig. 1 gives an overview of the numbers of received proposals, the numbers of requested and assigned shifts, as well as the percentage between assigned and requested shifts. Included in Fig.1 are also the same data for the period End 1995 - August 1996, during which some beamtime had been given already to users in order to perform first pilot- and test-experiments together with the beamline staff. These first experiments during the commissioning phase were not yet based on proposals, since the goal was mostly to evaluate and improve the performance of the beamline and the equipment of its experimental station. As can be seen in Fig.1, the request for beamtime at the SAXS-beamline increased continuously and strongly until the first half year of 1999 (also during the period Sept.-Dec. 1997, if one takes into account that this period was only 4 instead 6 month long, and that for this reason less proposals were submitted). Then, probably due to the high rejection rates, the number of submitted proposals decreased somewhat during 2001, which resulted in a better ratio of accepted / rejected proposals. This oscillating behaviour of beamtime request can also be seen for the period 2002 - 2004, where after higher numbers of submitted proposals slightly reduced request periods follow.

In 2003, in total 69 proposals (11 from CRG, and 58 from GU) were submitted. From these 18 proposals (5 from CRG and 13 from GU) were submitted by "new" usergroups, i.e. groups which so far had never beamtime at the SAXS beamline. From these 9 proposals (5 CRG and 4 GU) were officially accepted, while 1 GU proposal received some shifts for a first „pilot“ experiment.

Figure 1 (Next page). The statistical information about the beamtime periods since end of 1995 are given for the groups "CRG", and "GU" separately, as well as for both together ("Total"). Shown are, for all beamtime periods (from top to bottom):

- Number of received proposals, ● Number of requested shifts,
- Number of assigned shifts, and ● Relation between assigned and requested shifts



2. Provenience of users

During 2003, 159 users from 53 institutes in 17 countries have performed experiments at the SAXS beamline. In Fig. 2 are shown both the provenience of these users, and of their respective institutes. Each user or institute was counted only once, even though many users performed experiments in both beamtime periods of 2003.

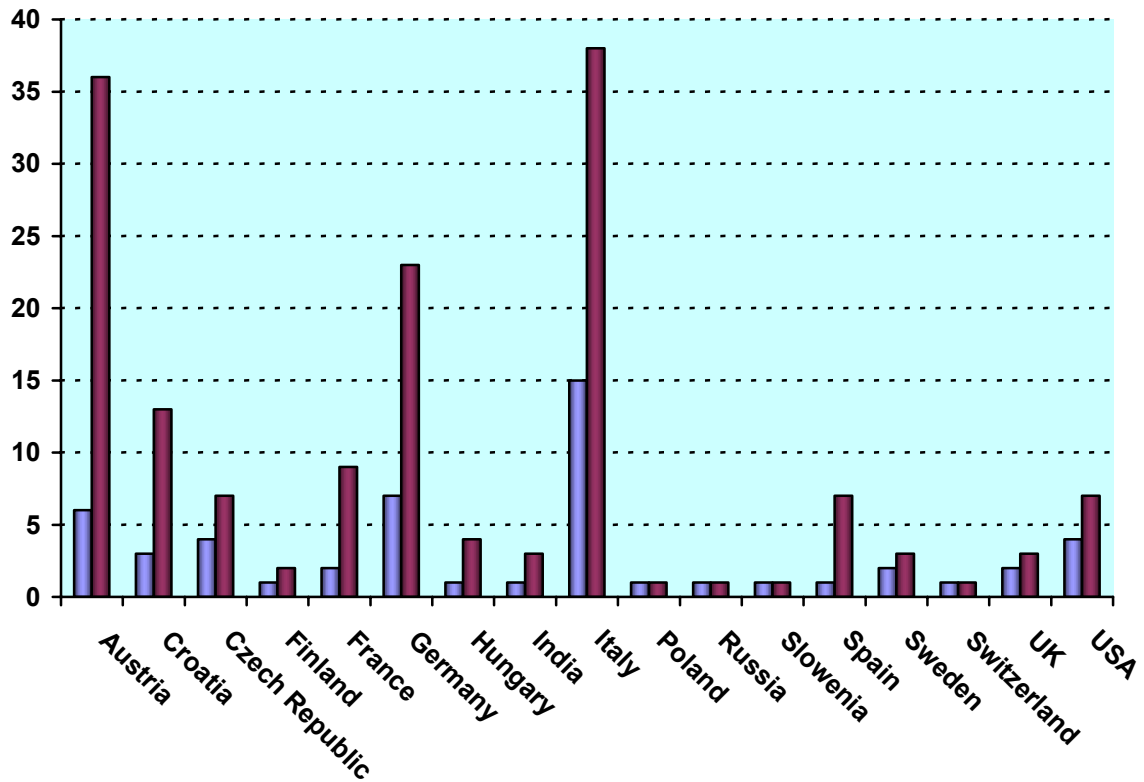


Figure 2. Provenience of users (dark grey) and of their corresponding institutes (light grey).

3. Documentation of experimental results

As could be expected, with the start of user-operation at the SAXS-beamline the number of contributions to conferences started to increase strongly. With a delay of one year - the average time needed for paper publications - also the number of publications increased accordingly, as can be seen in Fig. 3.

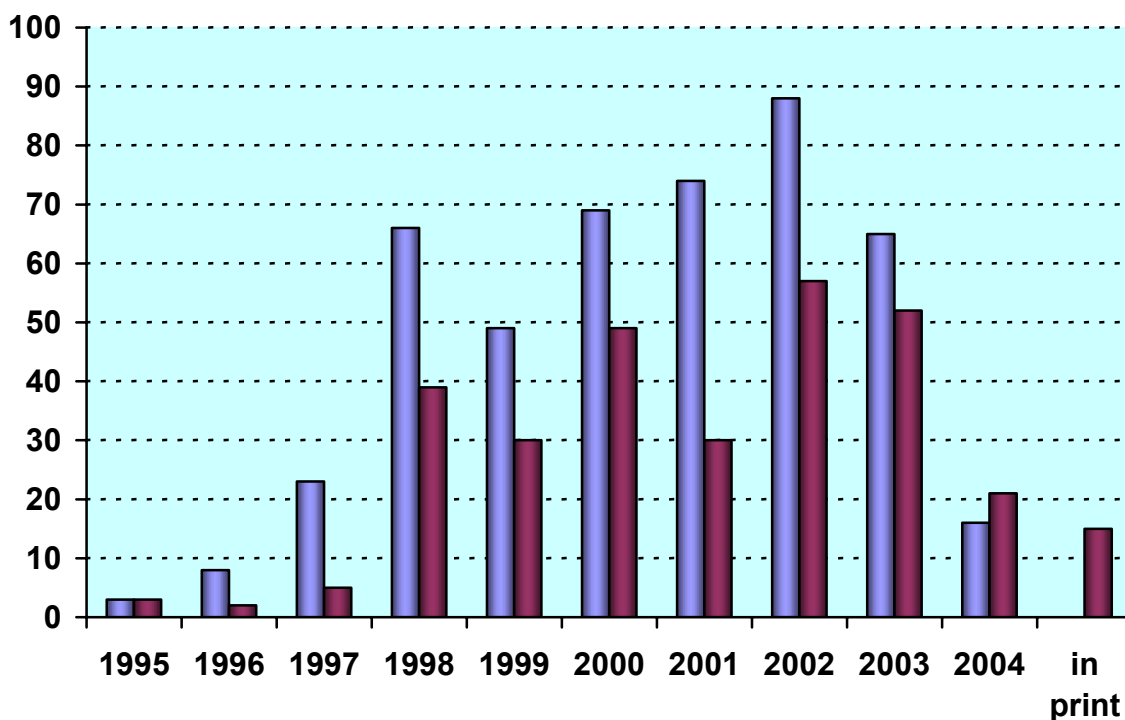


Figure 3. Number of conference contributions (light grey) and of refereed paper publications (dark grey) for the years 1995-2003. Also contributions, which have been published until July 2004 as well as those in print at that time are included.

In addition, from 1995 until July 2004, the following documentations based on instrumentation of the SAXS-beamline, or on data taken with it, have been produced.

Unrefereed publications:

Technical Reports on Instrumentation:	5
Contributions to Elettra Newsletters:	15
Contributions to Elettra Highlights:	17
Habil Thesis:	2
PhD Thesis:	36
Master Thesis :	21

Experimental Possibilities at the SAXS-beamline

1. Accessible SAXS and WAXS ranges

Simultaneous SAXS- and WAXS-measurements can be performed using a linear sensitive gas detector (Gabriel type, windows size 8 x 100 mm, active length 86.1 mm with a resolution of 0.135 mm/channel) for the WAXS-range, and either a second linear Gabriel type detector (windows size 10 x 150 mm, active length 134 mm with a resolution of 0.159 mm/channel), or the 2D CCD-system for the SAXS-range. A specially designed vacuum chamber (SWAXS-nose, see Annual Report of 1996/97, p. 32) allows to use both scattering areas below (for SAXS) and above (for WAXS) the direct beam, respectively.

Depending on the photon energy maximum SAXS resolutions of 2000 Å (5.4 keV), 1400 Å (8 keV) or 630 Å (16 keV) are available. The available possible WAXS-ranges are summarised in Table 1. The overall length of the SWAXS-nose in the horizontal direction, measured from the sample position, is 512 mm and the fixed sample to WAXS-detector distance is 324 mm. At the shortest SAXS camera-length an overlap in the d-spacings covered by the SAXS- and WAXS-detectors, respectively, is possible: then, the common regime lies around 9 Å.

Table 1. Possible d-spacing ranges in the WAXS-regime at the SAXS-beamline at ELETTRA. Since the WAXS-detector can be mounted at four different fixed positions on the SWAXS-nose (range 1-4), with the three possible energy choices (5.4, 8 and 16 keV) this results in 12 different d-spacing regimes. In italic the most common choice (8 keV, range 1) is highlighted. This range is suited for experiments, e.g., on lipid-systems and (bio)polymers.

Range	2 θ [deg]	d-spacing (Å)		
		8 keV	5.4 keV	16 keV
1	9.4	<i>9.40</i>	14.03	4.27
	27.6	<i>3.23</i>	4.82	1.47
2	27.4	3.25	4.86	1.48
	45.6	1.99	2.97	0.90
3	45.4	2.00	2.98	0.91
	63.6	1.46	2.18	0.66
4	63.4	1.47	2.19	0.67
	81.6	1.18	1.76	0.54

2. Calibration of the s-axis and flat field correction

At the SAXS beamline various standards are used for the angular (s-scale) calibration of the different detectors:

rat tail tendon for the SAXS detector - high resolution (rtt*.dat)

Silver behenate for the SAXS detector – medium and low resolution (agbeh*.dat)

Para-bromo benzoic acid for the WAXS detector – WAXS range 1 and 2 (pbromo*.dat)

Combination of Cu, Al foils and Si powder for the WAXS detector – WAXS range 2 and higher

In Fig. 1 a typical diffraction pattern of rat tail tendon is shown, depicting the diffraction orders (from the first to the 14th order) measured with a "high" resolution set-up (2.3 m) and the delay-line gas detector. The d-spacing is assumed to be 650 Å, but this value can vary depending on humidity up to 3%. Thus, the rat tail tendon is often used only to determine the position of the direct beam (zero order), while the absolute calibration is performed using the diffraction pattern of Silver behenate powder. Fig. 2 depicts a diffraction pattern of Silver behenate measured with "medium" resolution set-up (1.0 m) from the first to the 4th order (repeat spacing 58.4 Å) [1].

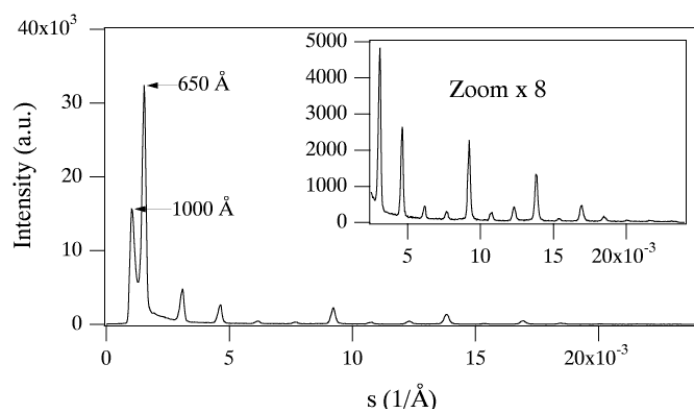


Figure 1. SAXS diffraction pattern of the collagen structure of rat tail tendon fibre at a distance of 2.3 m.

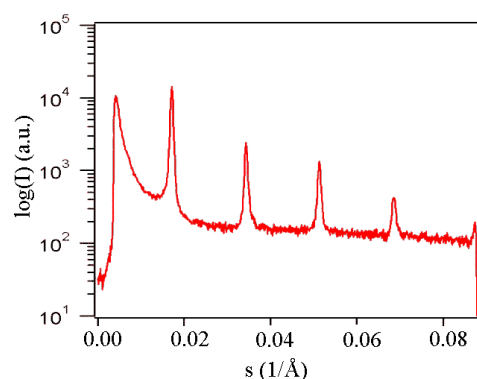


Figure 2. SAXS diffraction pattern of Ag behenate powder at a distance of 1.0 m

In Fig. 3 a typical WAXS pattern of p-bromo benzoic acid is shown. The diffraction peaks are indexed according to the values given in Table 2, taken from [2].

Table 2. d-spacings and relative intensities of p-bromo benzoic acid according to [2].

d-spacing/Å	rel. intensity	d-spacing/Å	rel. intensity
14.72	18000	4.25	490
7.36	1200	3.96	2380
6.02	330	3.84	10300
5.67	980	3.74	26530
5.21	6550	3.68	1740
4.72	26000	3.47	760

p-bromo benzoic acid: calculated intensities

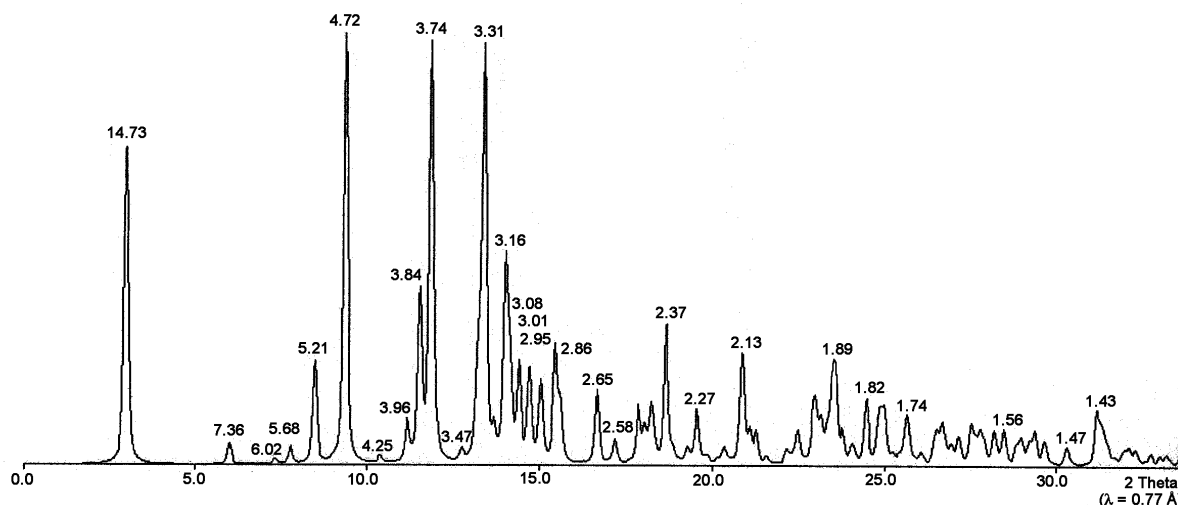


Figure 3. Calculated diffraction pattern of p-bromo benzoic acid. d-spacings are given in Å.

The s-scale for both, the SAXS and the WAXS range, can be obtained by linear regression, i.e., the linear relation between the known s-values of the calibrant versus the measured peak positions has to be found.

A further correction is regarding the flat field response (efficiency) of the detectors. For this correction, the fluorescence light of various foils are used to illuminate the detectors rather homogeneously:

At 8 keV: iron foil (100 μm thick), fluorescence energy: 6.4 keV K_{α} , 7.1 keV K_{β} (effic*.dat)

At 16 keV: copper foil (> 100 μm thick), fluorescence energy: 8.028 keV $K_{\alpha 2}$, 8.048 keV $K_{\alpha 1}$, 8.905 keV K_{β} (effic*.dat)

The measured scattering patterns are corrected for the detector efficiency simply by dividing them by the fluorescence pattern. Note: The average of the detector efficiency data should be set to unity and a small threshold should be applied to avoid any division by zero.

[1] T.N. Blanton et. al., Powder Diffraction 10, (1995), 91

[2] K. Ohura, S. Kashino, M. Haisa, J. Bull. Chem. Soc. Jpn. 45, (1972), 2651

3. Site laboratories

In August 2002 our new chemistry and X-ray laboratory went into operation. The 70 m² big laboratory is divided in two parts, in which the bigger share of 43 m² is occupied by the chemistry lab. This unit serves mainly for sample preparation and analysis for both, in house research and external SAXS user groups. In the X-ray laboratory the set-up of a SWAX camera for simultaneous small and wide angle scattering has been completed (Hecus-M. Braun, Graz, Austria: www.hecus.at), which allows on-site testing of samples before moving on to the SR beamline. The chemistry lab is meanwhile equipped with:

- micro centrifuge (max. 13200 rpm; model 5415D from Eppendorf , Hamburg, Germany)
- chemical fume hood (model GS8000 from Optolab, Concondordia, Italy)
- vacuum drying oven (min. pressure 1 mbar; max. T: 200 °C; Binder WTB, Tuttlingen, Germany)
- balance (min.-max.: 0.001 - 220 g; model 770 from Kern & Sohn, Balingen, Germany)
- magnetic stirrer with heating plate and a vortexer for microtubes (model MR 3001 and REAX; both from Heidolph, Schwabach, Germany)
- two water baths (the model Unistat CC is freely programmable in range from -30 to 100 °C from Huber, Offenburg, Germany; the model M3 from Lauda can only heat; Lauda-Könighofen, Germany)

Further, two working benches (one with a water sink), two fridges and a separate freezer (- 20 °C), standard glassware, syringes and needles of different sizes, μ -pipettes (10 - 50 - 200 - 1000), as well as some standard solutions (e.g., chloroform, ethanol, methanol) and de-ionized water are available.



Figure 4. Typical lab activity: Barbara Sartori loads the centrifuge (September 2003).

4. Available sample manipulations stages

1. General

Usually the sample is mounted onto the sample alignment stage which allows the user to place the sample into the beam with a precision of 5 μm (resolution: 1 μm). In Fig. 4 the ranges for vertical and horizontal alignment as well as the maximum dimensions of the sample holders are given. The maximum weight on the sample stage is limited to 10 kg. In case the envelope dimensions of a sophisticated sample station provided by the users are slightly larger than those given in Fig. 4, the user can ask the beamline responsible for a check up of his space requirements. If it does not fit at all to these specifications, user equipment can also be mounted directly onto the optical table, which allows much larger spatial dimensions.

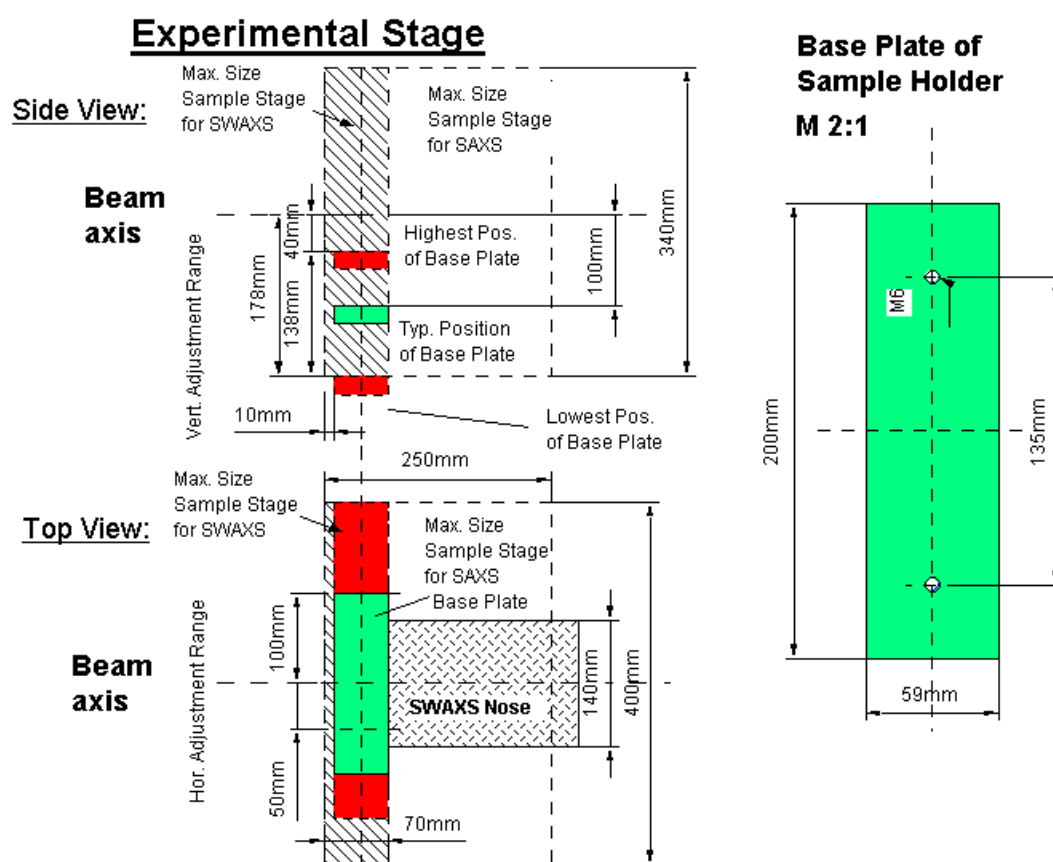


Figure 5. Maximum dimensions and alignment range of the sample holder to be mounted via a base-plate onto the standard alignment stage (left), and dimensions of the base-plate (right).

2. Sample holders

As standard equipment for liquid samples Paar capillaries (diameter: 1 and 2 mm) are used thermostated with the KHR (electrical heating) or KPR (Peltier heating/cooling) sample holders (Anton Paar, Graz, Austria). For use in these sample holders flow through capillaries and Gel holders are standard equipment. Temperature scans can be performed with KHR and/or KPR in the range from 0 to 150 $^{\circ}\text{C}$, typically the precision and the stability of this systems is < 0.1 $^{\circ}\text{C}$. Additionally thermostats for temperature control or cooling proposes can

be used at the beamline (0-95 °C, at present). Helium and Nitrogen gas bottles are available at the beamline, for other gases please contact the beamline responsible.

Multiple-sample holders can be mounted onto the standard sample manipulator. At present holders are available for measuring in automatic mode up to 30 solid samples at ambient temperature or up to 4 liquid or gel samples in the temperature range 0 – 95 °C.

3. Online exhaust system

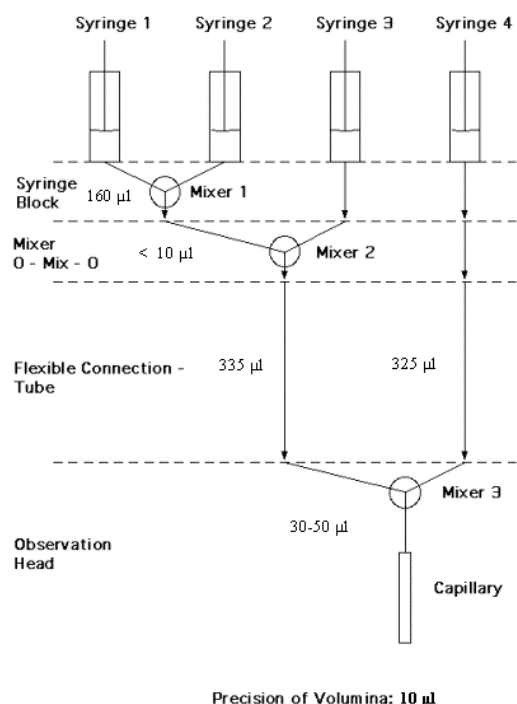
At the experimental station is available a custom-built fume cover and chemical exhaust system for toxic gases. Thus it is possible to e.g. study in-situ chemical reactions, during which toxic gases might develop.

4. Magnet System

For studying magnetic effects in samples, capillaries or sample holders with suitable dimensions can be mounted inside an electromagnet. Up to now a sample holder for standard Paar capillaries (Anton Paar, Graz, Austria) is available for ambient temperature only. The alignment of the magnetic field is horizontal or vertical (transversal to the photon beam). For short times the maximum magnetic field can be up to 1.5 T, and 1.0 T for continuous operation, respectively, assuming a pole gap of 10 mm for both.

5. Stopped Flow Apparatus

A commercial stopped flow apparatus (manufactured by Bio-Logic, Paris, France), especially designed for Synchrotron Radiation SAXS investigations of conformation changes of proteins, nucleic acids and macromolecules, is available. The instrument consists of a 4 syringe cell with 3 mixer modules manufactured by Bio-Logic. Each syringe is driven independently from the others by an individual stepping-motor, which allows a high versatility of the mixing sequence (flow-rate, flow duration, sequential mixing). For example, injection sequences using one or up to 4 syringes, unequal filling of syringes, variable mixing ratio, reaction intermediate ageing in three- or four-syringe mode etc.. The solution flow can be entirely software-controlled via stepping motors, and can stop in a fraction of a millisecond.



The software allows the set-up of the shot volumes of each of the 4 syringes in a certain time interval. Up to 20 mixing protocols can be programmed. Additionally macros for the repeated execution of individual frames can be defined. Furthermore, the input and output trigger accessible for user operation can be programmed. In the usual operation modus the start of rapid mixing sequence is triggered from our X-ray data-acquisition system (input trigger).

After the liquids have been rapidly mixed, they are filled within few ms into a 1 mm quartz capillary - situated in the X-ray beam- , which is thermostated with a water bath. Depending on the diffraction power of the sample time resolutions of up to 10 ms can be obtained.

Figure 6. Sketch of the stop flow system.

The main parameter of the system are:

- Thermostated quartz capillary (1 mm)
- Temperature stability 0.1 °C
- Total sample used per mixing cycle (shot volume): 100 µl
- Maximum 2θ angle of 45°
- Total Volume 8 ml
- Dead volume 550 µl
- Speed: 0.045 – 6 ml/s
- Duration of flow 1 ms to 9999 ms/Phase
- Dead time: 1 ms
- Reservoir volume: 10 ml each

Further information can be found in the homepage: <http://www.bio-logic.fr/>

6. Grazing Incidence Small Angle X-ray Scattering

Grazing incidence studies on solid samples, thin film samples or Langmuir-Blodgett-films can be performed using a specially designed sample holder, which can be rotated around 2 axes transversal to the beam. Furthermore the sample can be aligned by translating it in both directions transversal to the beam. The precisions are 0.001 deg for the rotations and 5 µm for the translations. Usually the system is set to reflect the beam in the vertical direction. According to the required protocol and the actual assembly of the rotation stages ω , θ , 2θ and ϕ scans can be performed.

7. Temperature Gradient Cell

A temperature gradient cell for X-ray scattering investigations on the thermal behaviour of soft matter manybody-systems, such as in gels, dispersions and solutions, has been developed. Depending on the adjustment of the temperature gradient in the sample, on the focus size of the X-ray beam and on the translational scanning precision an averaged thermal resolution of a few thousands of a degree can be achieved.

8. IR-Laser T-Jump System for Time-Resolved X-ray Scattering on Aqueous Solutions and Dispersions

The Erbium-Glass Laser available at the SAXS-beamline (Dr. Rapp Optoelektronik, Hamburg, Germany) delivers a maximum of 4 J per 2ms pulse with a wavelength of $1.54 \mu\text{m}$ onto the sample. The laser-beam is guided by one prism onto the sample, which is filled in a glass capillary (1 or 2 mm in diameter) and Peltier or electronically thermostated in a metal sample holder (A. Paar, Graz, Austria). With a laser spotsize of maximal 7 mm in diameter a sample-volume of maximal $5.5 \mu\text{l}$ or $22 \mu\text{l}$, respectively, is exposed to the laser-radiation. In a water-solutions/dispersions with an absorption coefficient of $A = 6.5 \text{ cm}^{-1}$ T-jumps up to $20 \text{ }^\circ\text{C}$ are possible.

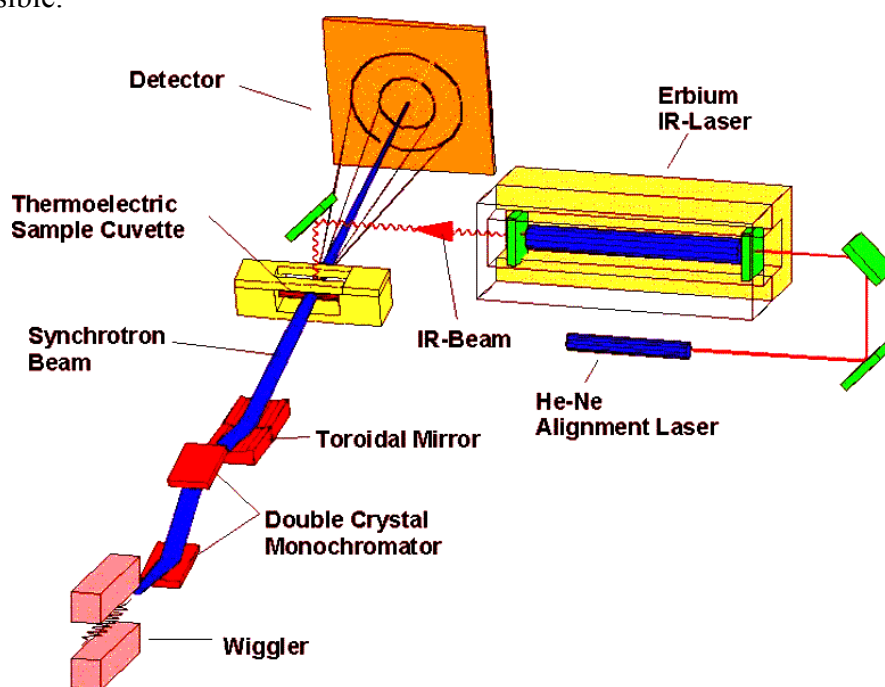


Figure 7. Sketch of the T-jump set-up.

9. High Pressure Cell System

SWAXS measurements of samples under pressure can be performed from 1 to 2500 bar, from 0 to $80 \text{ }^\circ\text{C}$ in the scattering angle region up to 30 degrees, both in the static or time-resolved mode, e.g. p-jump or p-scan, with a time-resolution down to the ms range. Precise pressure scans of any speed within a broad range (e.g. ca. 1.0 bar/s - 50 bar/s in the case of water as pressurising medium, and a typical sample volume) can be performed. Alternatively, dynamic processes can be studied in pressure-jump relaxation experiments with jump amplitudes up to 2.5 kbar/10ms in both directions (pressurising and depressurising jumps).

In most applications diamond windows of 0.75 mm thickness (each) are used. The transmission of one pair (entrance and exit window) is 0.1 at 8 keV, i.e. lower than 0.3, the value for the originally used 1.5 mm thick Be-windows. However the loss in intensity is more than compensated for by the considerably lower background scattering of diamond thus leading to higher q-resolution in the experiments.

The sample thickness can be 0.6-4.0 mm, with a volume of approximately 0.5-3 mm³ completely irradiated by pin-hole collimated (< 1.0 mm diameter) X-rays.

The pressure cell system is flexible and can be built according to the needs of the particular experiment. Normally, a liquid (water, ethanol or octanol) is used as pressurising medium. But in principle, also gaseous media can be employed as well. N₂ has been successfully tested, and measurements in supercritical CO₂ became frequent.

Beside bulk measurements on samples in transmission set-up, also grazing incidence experiments using silicon wafer with highly aligned samples on its surface inserted in the high-pressure cell have been carried out successfully.

10. Oxford Cryostream Cooler

The Cryostream cooler creates a cold environment only a few millimeters from the nozzle position. The temperature and the flow of the nitrogen gas stream is controlled and regulated by a Programmable Temperatur Controller based on an 'in stream' heater and a thermo-sensor before it passes out over the sample.

The system has been especially developed for X-ray crystallography to perform diffraction experiments on e.g. shock frozen bio-crystals. However, the programmable temperature controller allows further implication for SAXS-experiments, e.g., rapid temperature drops in solvents. The design of the Cryostream Cooler facilitates:

- nitrogen stream temperatures from -190 to 100 °C,
- a stability of 0.1 °C,
- a system that can be refilled without creating any disturbance of the temperature at the sample,
- temperature ramps can easily be carried out remotely controlled with
- scan rates up 6 °C/min
- individual temperature protocols can be cycled
- T-jumps in both directions can be performed by rapid transfer of the sample in a pre-cooled or -heated capillary using an fast syringe driver reaching a minimum temperature of -80 °C. Here, typical scan rates are about 15 °C/sec with a total process time in the order of 10 sec.

11. In-line Differential Scanning Calorimeter (DSC)

The in-line micro-calorimeter built by the group of Michel Ollivon (CNRS, Paris, France) allows to take simultaneously time-resolved synchrotron X-ray Diffraction as a function of the Temperature (XRDT) and high sensitivity DSC from the same sample.

The microcalorimetry and XRDT scans can be performed at any heating rate comprised between 0.1 and 10 °C/min with a 0.01 °C temperature resolution in the range -30/+130 °C. However, maximum cooling rates are T dependent and 10°C/min rates cannot be sustained below 30°C since cooling efficiency is a temperature dependent process. Microcalorimetry

scans can be recorded independently, and also simultaneously, of X-ray patterns. The microcalorimeter head can also be used as a temperature controlled sample-holder for X-ray measurements while not recording a microcalorimetry signal. Isothermal microcalorimetry is also possible when a time dependent thermal event such as meta-stable state relaxation or self-evolving reaction, is expected. The sample capillaries have a diameter of 1.5 mm and are filled over a length of 10 mm.

12. The 2D CCD-camera system

The CCD has a 115 mm diameter input phosphor screen made of a gadolinium oxysulphide polycrystalline layer. The screen is coupled by means of a fiber optic to the image intensifier. The image intensifier is coupled again with an additional taper to the CCD itself. The achieved spatial resolution of a pixel is 79 μm for the whole set-up.

The number of pixels is 1024 x 1024 and they can be pinned down to 2 x 2 and 4 x 4. The dynamic range of the CCD is 12 bit. The dark current of the CCD is in the order of 100 ADU (off-set) and the readout noise (read out speed: 10 MHz) is in the order of 6 ADU. (The CCD is cooled by multistage Peltier element for reducing the dark noise.) The intensifier gain is adjustable between 200 and 20000 photons full dynamic range. Typical readout times and exposure times are 150 ms and 100 ms, respectively. The readout times can be reduced down to 100 ms by using the pinning mode of the CCD. Between the frames additional wait times can be programmed e.g. for reducing the radiation damage in the sample or to extend the time for measuring long time processes.

For the external control a TTL trigger signal is provided (active low, when the CCD is accumulating an image), which is used to control the electromagnetic fast shutter of the beamline on one hand. On the other hand this signal can be used also to trigger processes as requested by the user.

The CCD is controlled by Image Pro+, which also includes non too sophisticated data treatment capabilities. The program is featuring a comprehensive set of functions, including:

- flat fielding/background corrections
- enhanced filters and FFT
- calibration utilities (spatial and intensity)
- segmentation and thresholding
- arithmetic logic operations
- various measurements, like surface, intensity, counts, profiles
- advanced macro management

The data are stored in 12 bit – TIFF format. At the present state up to 300 full images (1024 x 1024) can be recorded by the system, but a strict conservation of the timing sequence is maintained only for the first 15 - 17 frames until the RAM memory is full. Afterwards the images are stored in the virtual memory on the hard disk. At present a software development for the CCD readout system is under way to improve the stability of the readout cycles.

For the complete treatment of the 2D data Fit2D available from the ESRF is used, which is able to perform both interactive and "batch" data processing (homepage: http://www.esrf.fr/computing/expg/subgroups/data_analysis/FIT2D/index.html, programmed by Dr. Andy Hammersley), which supports a complete spatial correction, flat field correction and background correction. Furthermore more elevated data-treatment can be performed within this software package, like circular integration, segment integration and similar.

13. Tension cell

Together with the external user group Schulze-Bauer/Holzapfel the research team constructed a general-purpose tension cell. This particular cell was designed for *in-situ* tensile testing with the particular feature that the sample could be completely immersed in a solvent (e.g. physiological solution), which is of particular interest for the blood vessel or collagen fiber testing. The sample container can be attached to a thermal bath to control the temperature in the range from 5 to 95 °C. A screw with an appropriate opening for the passage of the X-ray beam can adjust the optical thickness of the sample container continuously and optimize the set-up for different sample geometries.

The fully remote controlled system allows to control not only the fiber extension from 0 to 50 mm, but also it records simultaneously the force signal in the range from 0 to 25 N and as an option the optically determined Video extensometer signal to measure the transversal contraction of the sample.

User Contributions

1. Materials Science

GISAXS STUDIES OF CORRELATED STACKS OF CdSe/ZnS_{Se} QUANTUM DOTS

G. Alexe¹, T. Clausen¹, Th. Schmidt¹, S. Bernstorff², C. Kruse¹, A. Ueta¹, D. Hommel¹,
and J. Falta¹

1.) Institut für Festkörperphysik Universität Bremen, P.O.Box 330440, 28334 Bremen, Germany

2.) Sincrotrone Trieste, ARÉA Research Park, I-34012 Basovizza / Trieste, Italy

CdSe quantum dots embedded in Zn(S)Se have attracted a large interest for applications in light emitting devices because a smaller laser threshold is expected [1,2] and degradation effects due to defect formation are expected to be diminished. Besides the chemical composition and strain state of the CdSe quantum dot layers [3,4], ordering and correlation effects in stacked layers play an important role in the homogeneity of the quantum dot size distribution, which is desirable for many device applications.

An ordering of the CdSe quantum dots due to stacking was demonstrated for structures consisting of at least five sheets of quantum dots separated by ZnS_{Se} spacer layers with thicknesses up to 4.5 nm [5]. The ordering is described as a self-organized process with strain being the driving force. However, stacking faults could also be considered as determining the quantum dots spatial correlation. This is supported by the definite $\langle 110 \rangle$ azimuthal anisotropy observed for the lateral ordering that coincides with the anisotropic orientation of staking faults in the CdSe/ZnS_{Se} material system. Moreover, the accumulated strain in stacked quantum dot layers rapidly leads to the formation of stacking faults [4,6]. The ordering is observed to be increasing with the number of sheets in stacks, as it is expected also for the density of stacking faults. Therefore, the influence of the two possible determining factors on ordering must be discriminated.

A series of CdSe quantum dot stacks in ZnS_{Se} grown by molecular beam epitaxy on GaAs(001) substrates was investigated. Samples, each consisting of five layers of nominally 1.8 monolayers CdSe separated by 4.5 nm thick ZnS_{Se} spacers for strain compensation were deposited on a 50 nm thick ZnSe buffer layer and overgrown by a 10 nm ZnSe cap layer. Different substrate temperatures of 230°C, 280°C and 310°C were used for the growth of the five-fold CdSe/ZnS_{Se} layer sequence. The low temperature sample presents a higher density of stacking faults as principally observed by high resolution x-ray diffraction [3]. Low temperature photoluminescence shows a shift of the signal towards lower energy indicating an increase in the Cd contents with decreasing growth temperature. The strong decrease of the photoluminescence intensity for the 230°C sample is consistent with the higher density of stacking faults. The influence of the stacking faults on the spatial correlation of quantum dots in the stacks can therefore be studied.

Grazing incidence small angle x-ray scattering (GISAXS) experiments were performed at the SAXS beamline at various incidence angles in order to obtain direct information on ordering at a mesoscopic scale. Vertical and lateral ordering of quantum dots in stacked layers is observed by the presence of satellite spots in the perpendicular and parallel directions in the reciprocal space. The experimental results are summarized in Fig. 1.

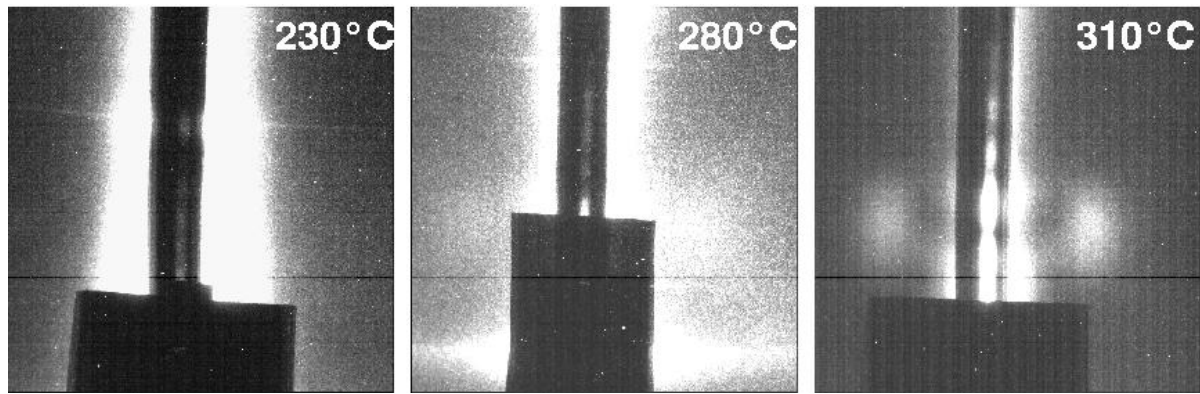


Figure 1. Grazing incidence small angle x-ray scattering images for five-fold CdSe quantum dot stacks grown at different substrate temperatures (indicated on every image) showing lateral satellites for the samples grown at 280°C and 310°C but not for 230°C.

For the sample grown at the standard substrate temperature of 280°C lateral satellites were observed depending on the crystallographic direction, showing a mean lateral quantum dot distance of about 14 nm comparable with previous results [5]. The sample prepared at 320°C presents well defined satellites in the [1-10] direction. For this sample a slightly smaller correlation length of the dot-dot distance is observed in comparison to the sample prepared at 280°C. This is consistent with the decreased deposited amount due to the higher growth temperature, leading to thinner spacer layers. However, the low temperature sample (230°C) shows no lateral satellites, even though the density of stacking faults for this sample is higher. These results, combined with other structural data, confirm that the ordering process is strain driven and not determined by stacking faults.

References:

- [1] Y. Arakawa and H. Sakaki; Multidimensional quantum well laser and temperature dependence of its threshold current; *Appl. Phys. Lett.* **40**, 939-941 (1982)
- [2] M. Klude, T. Passow, R. Kröger, and D. Hommel; Electrically pumped lasing from CdSe quantum dots; *Electron. Lett.* **37**, 1119-1120 (2001)
- [3] T. Passow, H. Heinke, J. Falta, K. Leonardi, and D. Hommel; Nondestructive detection of stacking faults for optimization of CdSe/ZnSe quantum-dot structures; *Appl. Phys. Lett.* **77**, 3544-3546 (2000)
- [4] T. Passow, K. Leonardi, and D. Hommel; Optical and structural properties of CdSe/Zn(S)Se quantum dot stacks; *phys. stat. sol. (b)* **224**, 143-146 (2001)
- [5] Th. Schmidt, T. Clausen, J. Falta, S. Bernstorff, G. Alexe, T. Passow, and D. Hommel; Investigation of CdSe/ZnSSe quantum dot ordering by grazing incidence small angle X-ray scattering; *phys. stat. sol. (b)* **241**, 523-526 (2004)
- [6] R. Engelhardt, U.W. Pohl, D. Bimberg, D. Litvinov, A. Rosenauer, and D. Gerthsen; Room-temperature lasing of strain-compensated CdSe/ZnSSe quantum island laser structures; *J. Appl. Phys.* **86**, 5578-5583 (1999)

DIRECT ION BEAM SYNTHESIS OF II-VI NANOCRYSTALS

U.V. Desnica¹, I.D. Desnica-Frankovic¹, M. Buljan¹, P. Dubcek¹, S. Bernstorff²

1.) R. Boskovic Institute, Bijenicka 54, 10000 Zagreb, Croatia
 2.) Sincrotrone Trieste, SS 14 km163.5, 34012 Basovizza (TS), Italy

There is an intense research activity going on to develop technology for the efficient and controllable synthesis of nanocrystals or quantum dots (QDs) [1-3]. The main interest in wide band-gap semiconductors QDs comes out from the strong size-dependent quantum confinement, which enables tunability of the bandgap and powerful visible photoluminescence, offering a number of potential applications in semiconductor and other industries [1].

We are demonstrating here the possibility of direct synthesis of CdS, ZnTe, CdTe and PbTe quantum dots by ion implantation of large and equal doses ($0.4 \cdot 10^{17}/\text{cm}^2$) of constituent atoms into SiO₂ substrate. Grazing incidence small angle X-ray scattering (GISAXS) reveals the successful synthesis of QDs already after ion implantations (left of Fig. 1, odd numbers of samples), performed either at RT (samples 1-4) or at LN₂ temperature (samples 5-10). The ring-like GISAXS signal indicates the establishment of a well-defined, isotropically distributed 3D ensemble of spherical aggregates (diameter 4-6 nm) embedded in the substrate). Annealing at 800° -1000° C temperature (Fig. 1, even numbers of samples) increased the nanoparticle size typically for 20-30%.

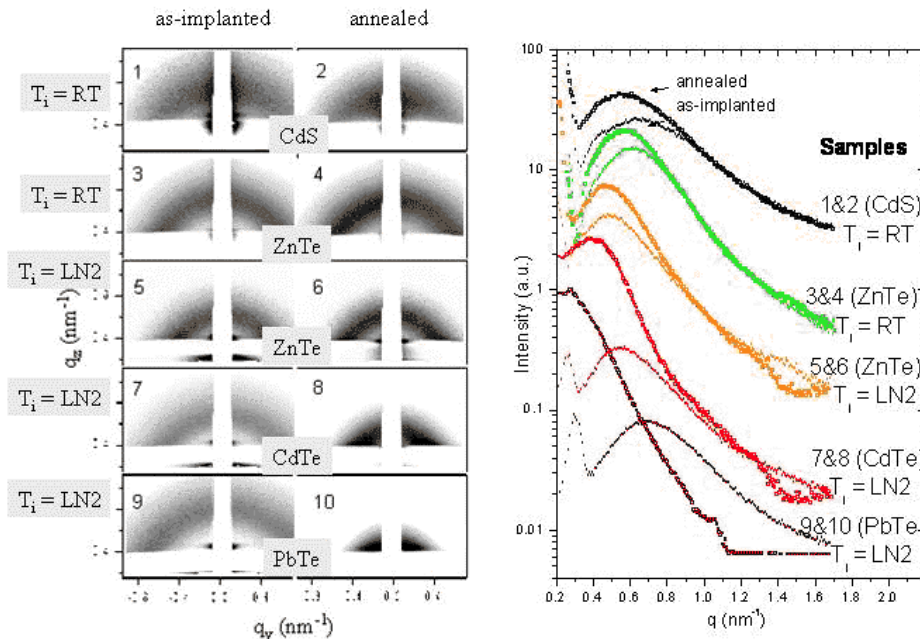


Figure 1. GISAXS Results. Left: Two-dimensional GISAXS patterns of double-species ion implanted SiO₂. Samples implanted with Cd+S are indicated as CdS, etc. Implant temperature, T_i, being either room temperature (RT) or liquid nitrogen (LN₂) is also indicated. Numbers 1,2.. 10 refer to the No. of samples. Right: 1D intensity profiles from the 2D spectra shown in Fig. 1. left, taken along the detector polar angle of 70°.

The same samples were also studied by Raman spectroscopy (RS) and transmittance measurements (T). Both optical methods confirm the synthesis of crystalline QDs after annealing, showing specific LO peaks in RS spectra and characteristic optical gaps in T measurements (Fig. 2). However, these crystalline phase-related signals were missing altogether in RS and T spectra of as-implanted samples.

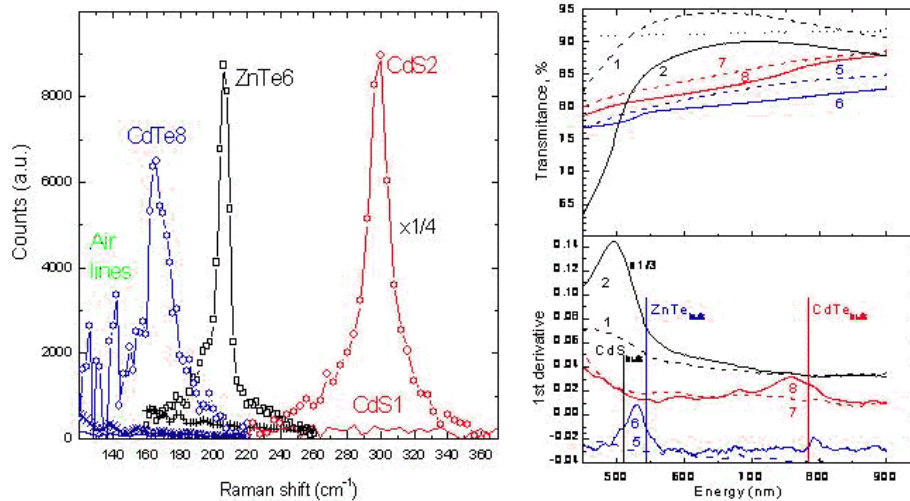


Figure 2. Optical Characterization. Left: Raman spectra of several samples from Fig. 1; CdS1 and CdS2 referring to as-implanted and annealed CdS samples, respectively, etc. The 2.41 eV line was used for excitation. Right: Transmission spectra (upper panel), and their 1st derivative (lower panel), of the same samples: as-implanted samples (dashed lines) and implanted/annealed samples (full lines): 1 = CdS1, 2 = CdS2, 5 = ZnTe5, 6 = ZnTe6, 7 = CdTe7, 8 = CdTe8, see Fig. 1. The transmittance of SiO₂ is also shown (dots in the upper panel). The bulk values of gap energy E_g for CdS, CdTe and ZnTe are indicated in the lower panel.

The apparent contradiction between GISAXS results (which suggest that implanted ions aggregate already during implantation) and optical methods (which both find that nanocrystals are formed only after annealing) leads to the conclusion that in as-implanted samples implanted atoms aggregate into non-crystalline nanoparticles (amorphous or strongly disordered). Post-implantation annealing, then, leads to the crystallization of the amorphous/disordered nanoparticles. The consequences of these experimental findings are important both from the fundamental and practical point of view:

Results suggest that the present paradigm that NCs are formed by thermal diffusion of implanted species and small NCs might not be valid for high-dose implants. In the new paradigm the process of obtaining nanocrystals would reduce primarily to the crystallization of amorphous aggregates that have been formed already during high-dose implants.

Practical consequences could be also worthwhile: the re-crystallization of amorphous phase into crystalline requires, generally, considerably lower annealing temperatures, so high-T annealings could be avoided in obtaining NCs. That is very desirable as thermally driven thermodynamical processes at high T tend to broaden the size distribution of NCs, since the size increase of larger QDs is energetically more favorable (larger decrease of free energy) than the size increase of smaller QDs. Hence, the combination of high-ion dose and low-T post-implantation annealing could give a better chance to obtain a narrower size distribution at a desired average QD size.

References:

- [1] Meldrum, R.F. Haglund, Jr., L.A. Boatner, C.W. White, *Advanced Materials* 13 (2001) 1431.
- [2] J.D. Budai, C.W. White, S.P. Wiothrow, M.F. Chisholm, J. Zhu, R.A. Zuhr, *Nature* 390 (1997) 384.
- [3] U. V. Desnica, P. Dubcek, I.D. Desnica-Frankovic, M. Buljan, S. Bernstorff, S.W. White, *J. Appl. Cryst.*, 36, 443-446 (2003)

CdSe NANOCRYSTALS SYNTHESIZED IN THERMALLY GROWN SiO₂

I.D. Desnica-Frankovic¹, P. Dubcek¹, U.V. Desnica¹, S. Bernstorff², H. Karl³, I. Großhans³, B. Stritzker³

1.) R. Boskovic Institute, P.O.Box 180, 10000 Zagreb Croatia

2.) Sincrotrone Trieste, SS 14, km 163.5, 34012 Basovizza, Italy

3.) Universität Augsburg, Universitätsstr. 1, D-86135 Augsburg, Germany.

Physical properties of material comprising buried nanoparticles depend on the characteristics of the ensemble of QDs. Those features could be optimized for a particular application by controlling the concentration and the size of precipitated QDs. However, a number of implantation and post-implantation treatment parameters influence the properties of QDs. Here, we are presenting our studies on nucleation and growth of CdSe QDs formed by implanting energetic ions into the thermal SiO₂ under different implant and annealing conditions.

Samples were produced by implanting ¹¹²Cd and ⁸⁰Se ions into 0.5 μm thick thermally grown SiO₂ on (100)-Si at LN₂ temperature. The energy was 190 keV for Cd and 134 keV for Se, to obtain the overlapping implantation profile and a projected range of approx. 80 nm, according to the results of TRIM simulations. The dose of Se was always 4.79x10¹⁶ cm⁻², whereas the dose of Cd was varied so as to achieve a series of under- (from -32%) or over- (up to +114%) stoichiometric deviation to Se. Rapid-thermal annealing was done at 800°, 900°, or 1000°C, under Ar+H₂ or pure Ar atmosphere.

GISAXS patterns were recorded with a 2D detector, 1024x1024 pixels. Spectra were corrected for background intensity and detector response, and then for refraction and absorption effects

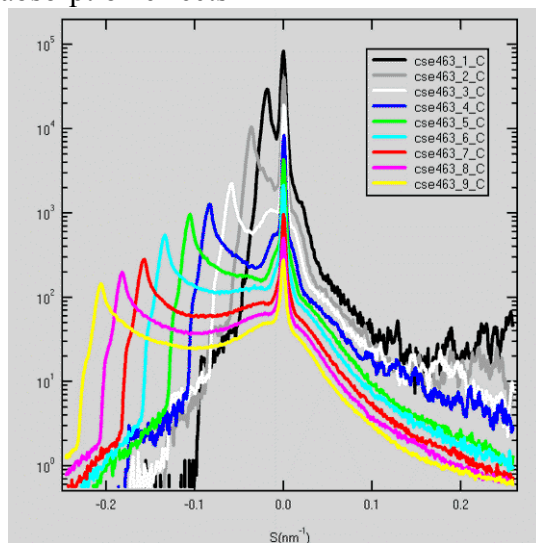


Figure 1. 1D GISAXS spectra vs. offset from specular angle for a stoichiometrically balanced sample annealed at 800°C in Ar+H₂. The incidence angle was increased from the critical angle $\alpha_i = \alpha_c$, (trace _1) in incremental steps of 0.02°.

In the spectra contributions from bimodal distribution of particles are resolved: in the subsurface region (i.e. trace _3) a pronounced interference maximum close to the specular peak results from the closely spaced population of large particles with narrow size distribution. The shoulder just starting to emerge at larger S comes from second group of considerably smaller particles of broader size distribution. As α_i is further increased, the contribution of small particles becomes more important and dominates deeper in the layer (trace _9) When Guinier-plot analysis was applied to the respective spectra average Guinier radius of 5–7 nm was obtained for smaller particles, the radius increasing with the increase in annealing temperature. The distribution of bigger particles was centered between 50 and 60

nm diameters, again somewhat, but not substantially, increasing with Ta. These findings are confirmed by cross-sectional TEM as shown in Figure 2.

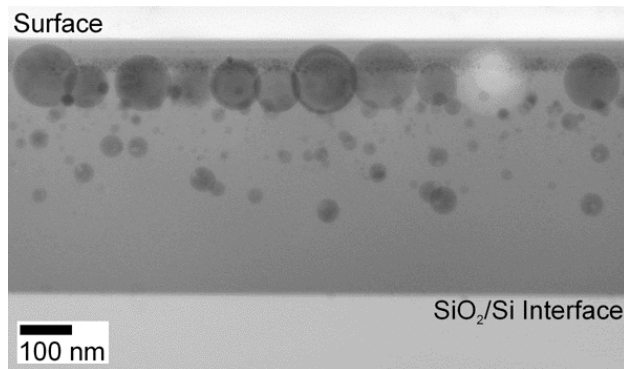


Figure 2. Cross-sectional TEM image: Size distribution for CdSe nanocrystals in SiO₂ after annealing at 1000 °C, 30s, Ar. A closely spaced layer of bigger particles is located near the surface. Deeper in, smaller particles are randomly dispersed, with broader size distribution.

When substantial stoichiometry deviation was present as for the sample depicted in Fig. 3, a much broader size distribution is present through the layer, smaller and larger particles being spatially intermixed.

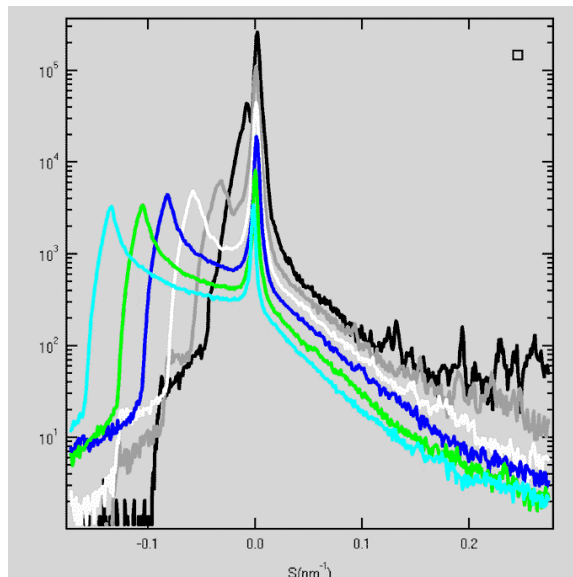


Figure 3. 1D GISAXS spectra for a sample implanted with a 95% surplus of Cd compared to Se.

In conclusions, we have investigated a number of ion beam synthesized nanoparticles obtained by implanting Cd and Se ions into thermal SiO₂. Although synthesis of nanoparticles was confirmed in all studied cases, their spatial and size and shape distributions differed substantially, depending on the chosen implant- or post-implant-treatment parameters and in particular on the stoichiometric deviations of Cd versus Se concentration. Some selected cases are presented in the results.

SAXS STUDY OF OXYGEN PRECIPITATION IN SILICON

B. Pivac¹, P. Dubcek¹, I. Kovacevic¹ and S. Bernstorff²

1.) R. Boskovic Institute, Bijenicka 54, Zagreb, Croatia

2.) Sincrotrone Trieste, SS 14, km163.5, 34012 Basovizza (TS), Italy

Czochralski-grown dislocation-free silicon crystals contain typically $5-18 \times 10^{17}$ interstitial oxygen atoms per cm^3 . During crystal growth, oxygen is dissolved from the silica crucible containing the molten silicon and is incorporated in the bulk of material. When the heating cycles are performed on such material necessary for device fabrication the oxygen atoms diffuse and agglomerate to form amorphous SiO_2 precipitates. Such precipitates may have disastrous effects if they are formed in the active regions of a device. In regions away from the active components, however, precipitates have advantageous effects, since they punch out dislocations which act as gettering centers for the unwanted metallic impurities. In addition, the dissolved oxygen inhibits the dislocation slip that may be produced by differential expansion or contraction during the thermal treatments of the processing stage. In spite of the technological significance of oxygen precipitation in silicon there are still unresolved scientific problems concerning the oxygen diffusivity, the size and number density of the precipitates and problems associated with formation of electrical active defects (thermal donors) during heat treatments at around 450 C [1].

To describe completely the precipitation process of oxygen in silicon the size, number density, shape and crystallographic orientation of the precipitates must be determined, as well as the concentration of oxygen in the matrix. In the past diverse methods have been used to obtain some of these parameters. One of methods successfully applied for that purpose was small-angle neutron scattering (SANS) [2]. One of the advantages of SANS technique is that large samples could be measured, however, this is at the same time a disadvantage since thin samples, resembling wafers, could not be measured. At the same time small-angle X-ray scattering (SAXS) - a complementary technique to SANS - was considered ineffective due to high absorption of X-rays in silicon. However, it is our intention to show that by employing high brilliance synchrotron sources, SAXS can be effectively used for study of oxygen precipitation in silicon. We have recently shown that with the SAXS technique by using 8 keV radiation small objects formed by oxygen clustering in single crystal silicon can be detected. The aim of this study was to perform a detailed study of oxygen nucleation and precipitation process in silicon wafers subjected to different thermal treatments.

In this respect we selected single crystal Si wafers with close oxygen content and all samples were taken from the same ingot and were closely spaced in the ingot prior to slicing.

The interstitial oxygen content was determined prior and after thermal treatments by infrared spectroscopy both at room temperature and at liquid helium temperature. All samples were subjected to homogenization thermal treatment to reduce the possible effects of thermal prehistory. Subsequently samples were subjected to different sequences designed to create specific nucleation and/or precipitation stages of oxygen clustering. Such obtained samples were chemically thinned to approx 100 μm and SAXS measurements were performed in transmission geometry.

The 2D-SAXS pattern in Figure 1 shows that the SAXS technique can provide information about the different shapes of oxygen precipitates formed in the bulk. Further studies are necessary to verify this information.

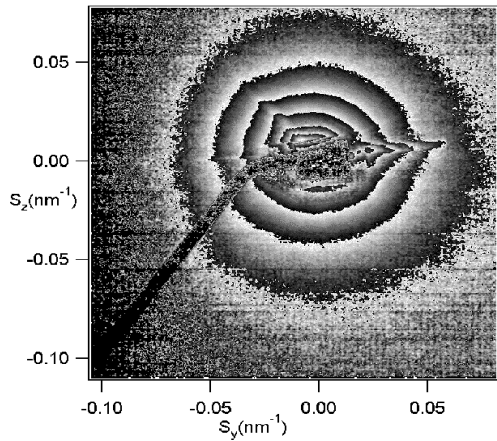


Figure 1. 2-D SAXS pattern of oxygen precipitates formed in the silicon bulk.

In Fig. 2 are shown the results – based on our SAXS-measurements – of calculated distributions of oxygen agglomerated in particles, formed upon specific thermal treatment designed to grow precipitates. The increasing sample number denotes the increasing duration of precipitation process. The results are in good qualitative agreement with the expected oxygen

behavior. However, a closer analysis reveals that the nucleation as well as precipitation process is far more complex and the two cannot be simply separated. Namely, since we were not able to detect particles larger than about 150 nm due to limitations of our setup, we could not monitor all the way the fully-grown precipitates. This is the reason why the samples with higher number do not follow smooth shift of size distribution to larger values. Nevertheless, we found that the nucleation process coexists along with the precipitation process. The competition between the two processes leads to the observed complex behavior, as shown in Fig. 2. On the other hand, shown in Fig. 3., when only the nucleation process was monitored, the size distribution of the formed nuclei follows the smooth increase with the process duration. The detailed analysis of the results is underway.

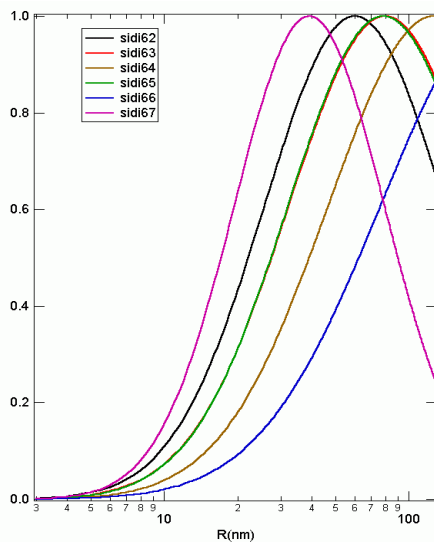


Figure 2. Distribution of radii of aggregated oxygen formed upon thermal annealing designed to grow precipitates.

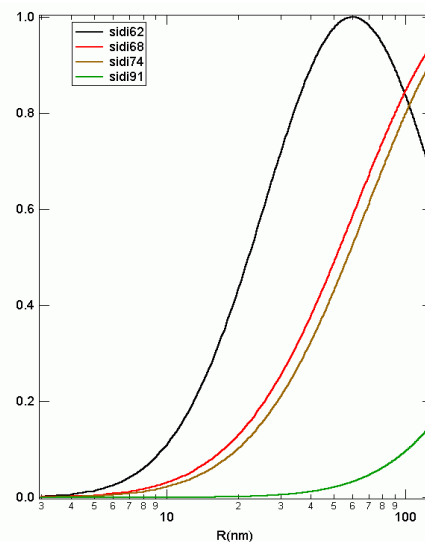


Figure 3. Distribution of radii of oxygen nuclei formed upon nucleation process.

References:

- [1] A. Borghesi, B. Pivac, A. Sassella and A. Stella; J. Appl. Phys. 77, 4167-4244 (1995).
- [2] S. Messoloras, J.R. Schneider, R.J. Stewart and W. Zulehner, Nature 336, 364-365 (1988).
- [3] B. Pivac, P. Dubcek, S. Bernstorff, A. Borghesi, A. Sassella, and M. Porrini, Nucl. Instrum. Methods in Phys. Res. B 200, 105-109 (2003).

SPUTTER-DEPOSITED AMORPHOUS-LIKE TUNGSTEN

N. Radić¹, A. Tonejc², J. Ivkov³, P. Dubček¹, S. Bernstorff⁴, Z. Medunić¹

1.) Rudjer Bošković Institute, Bijenička 54, Hr-10000 Zagreb, Croatia,

2.) Faculty of Sciences, Bijenička 34, HR-10000 Zagreb, Croatia,

3.) Institute of Physics, Bijenička 46, HR-10000 Zagreb, Croatia,

4.) Sincrotrone Trieste, SS 14 km 163,5, I-34012 Basovizza (TS), Italy

The sputter-deposited films tend to have high residual stress, which changes from strongly compressive to tensile with increasing working gas pressure. Simultaneously, the phase composition of tungsten films changes from predominantly α -W form to β -W modification. The formation and stabilization of β -W in case of sputter-deposited tungsten films is attributed to the incorporation of oxygen in the film.

Thin tungsten films were prepared in a sputtering system with two cylindrical magnetrons, and equipped with a diffusion pump and auxiliary titanium sublimation pump. Base pressure in the system was about 10^{-4} Pa. Working gas (argon, 5N) pressure was varied in the range of 0.7 – 3.5 Pa, and the partial pressure of spectroscopically pure oxygen was varied in a 0-8 % range with a total pressure kept constant at 1.4 Pa. A d.c. magnetron discharge operated in a continuous gas flow. Pure tungsten was used as cylindrical targets, and the average current density at the cathodes was 3.3 mA/cm^2 . Substrates were discs of about 1 cm diameter made of sapphire, fused silica and monocrystalline silicon, and mounted onto rotating holder in order to achieve lateral homogeneity of the films. Deposition rate was about 0.2 nm/s, and the final film thicknesses were in the 150-200 nm range.

The oxygen content of the films was determined by nuclear reaction $^{16}\text{O}(\text{D,p})^{17}\text{O}$, with 0.85 MeV deuterons. A Mylar foil was placed in front of the silicon detector in order to suppress the detection of deuteron particles. For quantitative determination a reference standard of anodically oxidized tantalum was used [1].

Grazing incidence measurements were taken at different, fixed grazing angles on the sample, using a 2-D CCD detector (1024x1024 pixels) at a fixed position. The scattering was also measured with the beam entering the film perpendicularly to the surface (SAXS).

The SAXS intensities, measured on amorphous-like tungsten, are shown in Fig.1, where the substrate contribution has been subtracted. No anisotropy in the scattering has been observed, and therefore the integral intensity is shown. Using the Guinier fit, we obtained $R_G=1.42 \text{ nm}$ for the radius of gyration. The significant depletion of intensities at very small angles is a result of particle-particle correlation. The SAXS data from α -W and β -W are displayed for comparison. While the β -W displays similar scattering, with the radius of gyration slightly smaller ($R_G=1.26 \text{ nm}$), much lower scattering intensity and considerably smaller particle sizes ($R_G=0.83 \text{ nm}$) are found for α -W.

GISAXS contour patterns (logarithmic) for amorphous-like tungsten are shown in Fig.2. Apart from the broadened Yoneda peak at $q_z=0.6 \text{ nm}^{-1}$, the scattering is of flattened particle type for the critical grazing angle value, i.e. minimum penetration depth, Fig.2a. A more complex pattern for $\alpha_G = \alpha_{\text{CRIT}} + 0.6^\circ$ (Fig.2b) suggests a considerable variation of the particle sizes deeper within the film.

From the above results, the amorphous-like tungsten films might be conceived as composed of nanosized grains of pure tungsten (with only a small amount of interstitial oxygen) separated by oxygen-stuffed voids and grain boundaries.

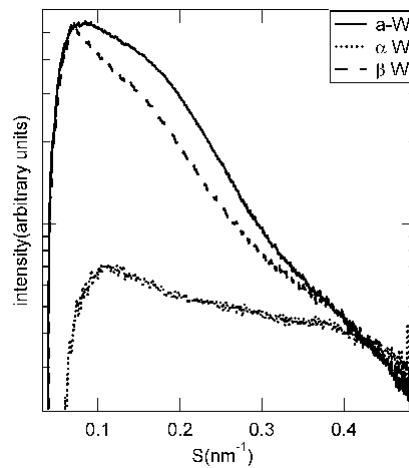


Figure 1. The SAXS intensities for amorphous-like tungsten, α -W, and β -W phase deposited onto monocrystalline silicon vs. scattering angle $S=2\theta/\lambda$. The intensities were obtained from a 2-D pattern by azimuthal integration.

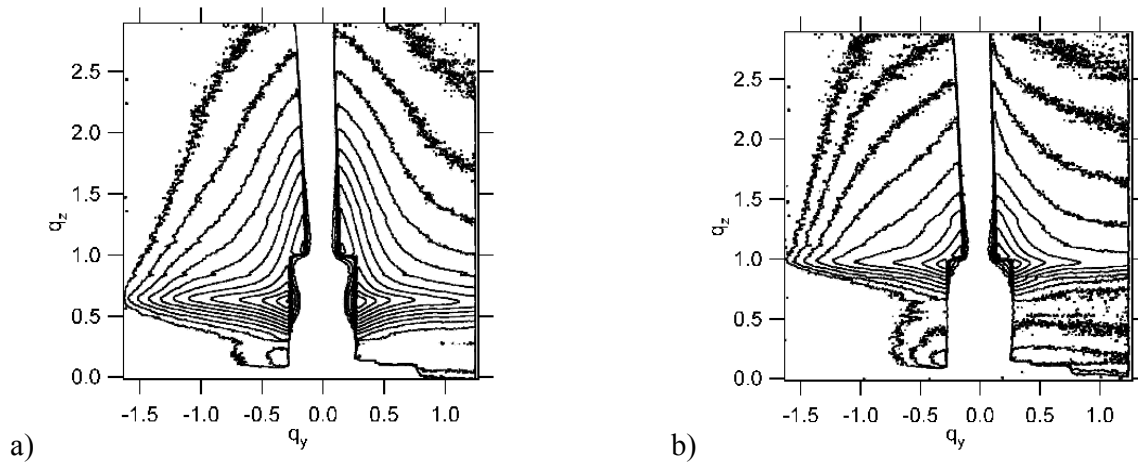


Figure 2. A 2-D GISAXS contours (logarithm of intensity) of amorphous-like tungsten for the grazing angle equal to critical angle, and 0.6° above the critical angle, a) and b), respectively.

References:

[1] N. Radic, A. Tonejc, J. Ivkov, P. Dubcek, S. Bernstorff and Z. Medunic, Surface and Coatings Technology. 180-181, pp. 66-70 (2004)

MICROSTRUCTURE OF POST-DEFORMED NANOCRYSTALLINE TI AS INVESTIGATED BY SYNCHROTRON MULTIPLE X-RAY LINE PROFILE ANALYSIS

E. Schafler^{1,3}, K. Nyilas², S. Bernstorff⁴, L. Zeipper^{1,5}, T. Ungàr², M. Zehetbauer¹

1.) Institute of Materials Physics, University of Vienna, A-1090 Wien, Austria

2.) Department of General Physics, Eötvös University Budapest, H-1518 Budapest, Hungary;

3.) Institute for Materials Science, Austrian Academy of Sciences, A-8700 Leoben, Austria

4.) Sincrotrone Trieste, AREA Research Park, I-34012 Basovizza / Trieste, Italy

5.) ARC Seibersdorf research GmbH, A-2444 Seibersdorf, Austria

The production of ultrafine-grained or even nanocrystalline bulk metals (Fig. 1) by modes of severe plastic deformation (SPD) such as Equal Channel Angular Pressing (ECAP) (Fig. 2) and High Pressure Torsion (HPT) now has become a prominent way to improve the mechanical properties of metals, especially strength and fatigue life time, with the same or even higher ductility than conventional metals [1]. In case of Ti, these outstanding properties combined with the low weight and the excellent bio-compatibility suggest the use of nanoSPD Ti as material for medical implants and hip prostheses not at least because biologically dangerous alloying elements like Vanadium can be omitted.

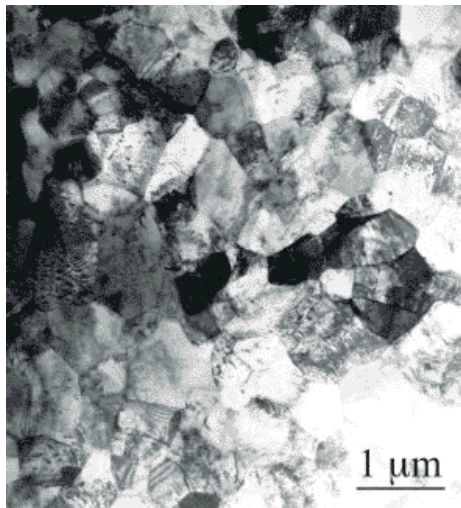


Figure 1. TEM micrograph showing the nanocrystalline structure of CP-Ti resulting from ECAP deformation (8 passes, route B_C, 450°C) and annealed at 450°C (from [1]).

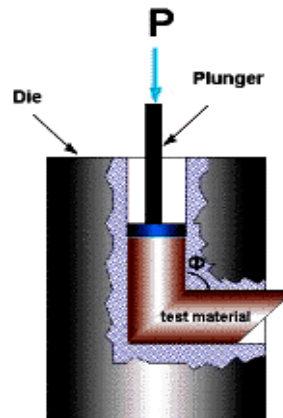


Figure 2. Tool for Equal Channel Angular Pressing (ECAP) producing ultrafine grained and nanocrystalline metals by severe plastic deformation [1].

In order to explain the particular mechanical properties of such materials in the as-produced nanocrystalline state as well as after additional (“post”) deformation and to perform model simulations [2], certain structural parameters like the density of lattice line defects and/or the typical structural size (-distribution) have to be necessarily known. There is the method of MXPA (Multi reflection X-ray Bragg Peak Analysis [3, 4]) which gives a direct experimental access to these parameters. The combined use of high intensity Synchrotron radiation not only ensures a sufficient number of reflections but permits also investigations with high resolution in time and space which will be tried in our next experiments at ELETTRA.

In the present work, samples from CP α -Ti which has been ECAP deformed at 450°C for 8 passes in route B_C was subjected to compression up to 80% of true strain.

Employing 4 position sensitive linear detectors (PSD) at the SAXS beamline of ELETTRA, diffraction patterns with up to 11 reflections were recorded and analysed by Multiple Whole Profile Fitting (MWP) [5]. The eleven possible dislocation slip systems of hexagonal Ti were considered in terms of the three groups of possible Burgers vectors [6] being $\langle -2110 \rangle$, $\langle -2113 \rangle$ and $\langle 0001 \rangle$. In the current investigation it turned out that the first two of these three groups are dominating for all different extents of the “post” deformation. For the initial as-ECAP deformed sample state, the area weighted mean coherently scattering domain size was found to be about 40nm. With increasing post-deformation by compression, the size distribution was found to slightly increase (Fig.3) while the mean domain size did not change. However, the still high dislocation density of the as-ECAP state was observed to significantly increase with further deformation (Fig.4 and [7]) so that an increase of dislocation density in the domain boundaries seems to be responsible for the post-deformation strengthening behaviour.

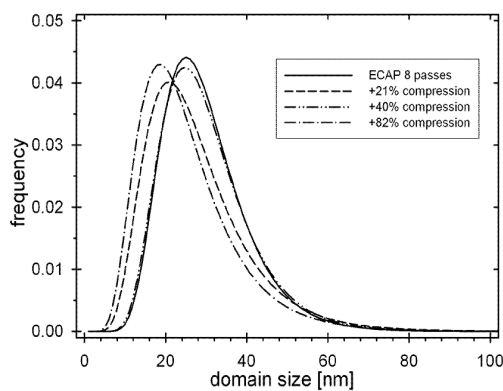


Figure 3. Distribution of coherently scattering domain size for ECAP nanocrystalline CP-Ti and for different extents of post-deformation by compression (as indicated). The evaluation of the area weighted mean domain size is found to be constant and to amount to about 40nm.

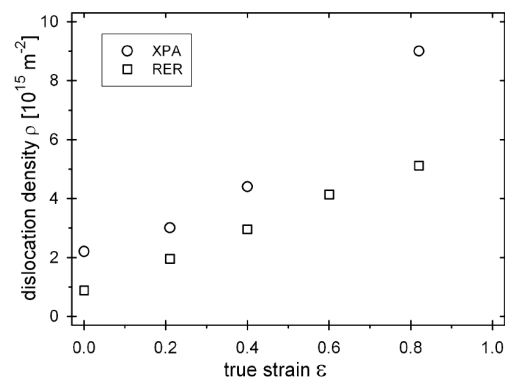


Figure 4. Dislocation density as a function of post-deformation compression strain ϵ . Data from X-Ray Profile Analysis have been roughly confirmed by electrical residual resistivity measurements [7].

References:

- [1] Proc. 2nd Int.Conf. on Nanomaterials by Severe Plastic Deformation: Fundamentals –Processing – Applications, Wien, Austria (Dec. 9-13, 2003), eds. M.J.Zehetbauer & R.Z.Valiev, J.Wiley VCH Weinheim, Germany (2004)
- [2] M.Zehetbauer, H.P.Stüwe, A.Vorhauer, E.Schafner, J. Kohout, Adv.Eng.Mater. 5 (2003) 330
- [3] T. Ungár, J. Gubicza, G. Ribárik, A. Borbély, J. Appl. Cryst. 34 (2001) 298.
- [4] E. Schafner, M. Zehetbauer, T. Ungar, Mater.Sci.Eng. A, 319-321 (2001) 220
- [5] I.C. Dragomir, T. Ungár, J. Appl. Cryst. 35 (2002) 556.
- [6] R. Kuzel jr., P. Klimanek, J. Appl. Cryst. 22 (1989) 299.
- [7] A.Korznikov, L.Zeipper, E.Schafner, V.Gröger, M.Zehetbauer, unpublished results

DEVELOPMENT OF A SAXS-METHOD TO CHARACTERIZE THE DAMAGE ZONE AROUND A CRACK TIP IN METALS

K. Van Ouytsel and G. Müller

Forschungszentrum Rossendorf e.V., Institut für Sicherheitsforschung, Postfach 51 01 19, 01314 Dresden, Germany

The aim was to characterize the damage zone around a crack tip in technical aluminium alloys using Small Angle X-ray Scattering (SAXS).

The method involved the following steps: optimal location of the crack tip, a very small beam size to accurately map the strong damage gradients existing at the tip of a crack, an optimal beamstop to allow the investigation of small angles close to the beamstop, recording 2d-SAXS images (ccd-camera) combined with WAXS-data (Wide Angle X-ray Scattering).

Finding the optimal parameters, beam size, detector distance, beamstop size and position, scan duration are all interrelated and needed to scan a region around the crack tip sufficiently large to make an assessment about the size and shape of the damage zone, [1].

Experiments to ascertain these parameters were conducted at the Austrian SAXS beamline, at ELETTRA in Trieste from the 18th-24th of February 2003.

Trial and error tests allowed us to establish an optimal method to locate the crack (crack tip) with high accuracy using a photodiode. Beam size reduction was optimized for the scattering intensity of the specimen with the maximum beam intensity. This proved to be time consuming because originally it was hoped to arrive at a beam size of $\approx 40 \mu\text{m} \times 40 \mu\text{m}$. With such a small beam, however, the intensity was insufficient. With a beam size of $\approx 60 \mu\text{m} \times 200 \mu\text{m}$ we were able to locate the crack and scan a sufficient number of locations around the crack tip. The larger beam size implied a larger disturbance from grain boundary scattering, but this could not be avoided, [2].

Four specimens of the commercial 2024-T351 aluminium alloy were investigated. Three of these specimens had a grain size of about $20 \mu\text{m}$. One of them was undeformed, another deformed in tension (M(T), middle tension) and the third deformed by three-point bending (SENB).

The fourth specimen, a CT-specimen (compact tension), had a grain size of about $70 \mu\text{m}$ by $150 \mu\text{m}$, which is large enough to expect grain boundary scattering, which was indeed observed. This allowed us to prove that indeed this pattern in the scattering is visible when the spot is at a grain boundary made visible with metallographical techniques. Though there remained a difficulty in specimen thickness; the specimens are on average thicker than a few grains and therefore not only the grain boundaries from the surface contribute to the scattering. Yet, to assess correspondence between the anisotropy observed for a number of scan points, e.g. Fig. 1, and the grain boundaries from the metallographic photographs, the two surfaces of the specimens were accurately prepared and photographed to reveal the grain boundaries. There seems to be a correlation between the position of scan point, grain boundaries and the observed anisotropic scattering pattern, but this is not sufficiently reliable yet, and more data are required. The CT-specimen also revealed, very surprisingly, a strongly varying shape of the scattering images, it is not yet clear how to interpret all these different shapes, but it promises to be very interesting especially since the other specimens did not reveal a change in the scattering shape.

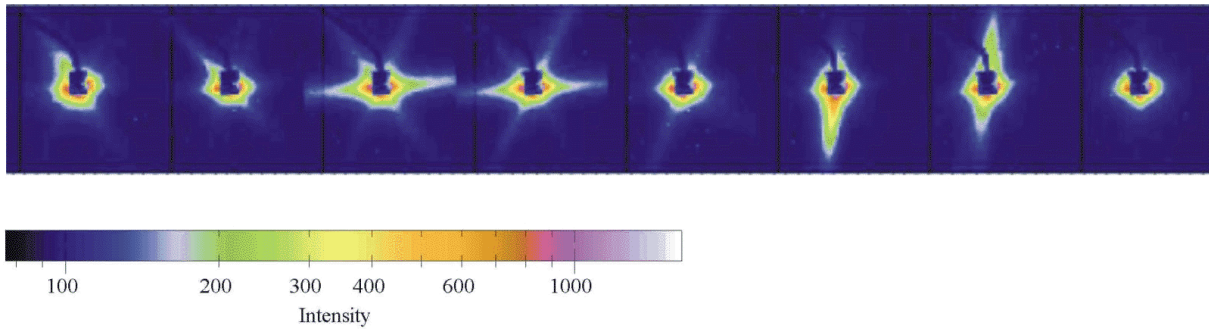


Figure 1. Anisotropic grain boundary scattering of Al 2024, CT-specimen

No clear analysis could, however, be made to ascertain the scattering centres responsible for the SAXS-patterns, this is also attributed to the complexity of the material. The grain boundary scattering superpose the anisotropic scattering of the deformation induced defect structures and further investigations are necessary to determine the nature of the scattering entities, like sheared coherent precipitates and strain-induced variations of the dislocation arrangement, that may contribute to the scattering contrast.

References:

- [1] K. Van Ouysel, J. Böhmert and G. Müller; A Small Angle X-ray Scattering Method to investigate the crack tip in metals; FZR-388 (2003)
- [2] M. Große, J. Böhmert and C. Riekel, Investigations of the structural changes ahead of a crack tip in ductile aluminium, using scanning microbeam, small angle X-ray scattering, Journal of Materials Science Letters 17 (1998) 1631-1634

2. Life Science

MYOFILAMENT OVERLAP AFFECTS X-RAY SIGNALS FROM SKELETAL MUSCLE FIBRES.

H. Amenitsch¹, C.C. Ashley², M.A. Bagni³, S. Bernstorff⁴, G. Cecchi³, B. Colombini³ and P.J. Griffiths²

- 1.) Institute of Biophysics and X-ray Structure Research, Austrian Academy of Sciences, Schmiedlstr. 6, A-8042 Graz, Austria
- 2.) University Laboratory of Physiology, Parks Road, Oxford, OX1 3PT, U.K.
- 3.) Dipartimento di Scienze, Università degli Studi di Firenze, Viale G.B. Morgagni 63, Firenze, I-50134, Italy
- 4.) Sincrotrone Trieste, Area Science Park, Basovizza/TS, I-34012, Italy

Myosin motors are transducers of the chemical free energy of ATP hydrolysis into mechanical work, which is performed by myosin translation along filaments of G-actin. Linear molecular motors (i.e. dynein, kinesin and myosin) are involved in cell division, directional transport of intracellular organelles, exo-, endo- and pinocytosis, sound transduction into electrical signals in the ear, and the contraction of all forms of muscle tissue. 17 classes of myosin motor have been identified, but myosin II (responsible for all muscle contractility) has the unique advantage that it aggregates into highly ordered filaments. In skeletal muscle, these 'thick' filaments overlap 'thin' (actin) filaments in a hexagonal array, giving a quasi-crystalline structure and enabling simultaneous collection of X-ray diffraction and mechanical data from a working population of myosin motors. The subfragment 1 (S1) moiety of myosin is sufficient to produce motor activity, and is composed of a 'motor domain' bearing the actin and ATP binding sites, and a 9 nm long 'lever arm', which is proposed to tilt during the motor power stroke [1], producing ca. 4-10 nm translational movement or 2-4 pN of force.

The meridional X-ray reflection (M3) originates from the 3-fold helical projection of S1 'crowns' along the thick filament backbone. Its intensity (IM3) detects changes in S1 structure during the power stroke, and its behaviour during the synchronized power stroke, which accompanies a step change in actin-myosin overlap, is consistent with a change in lever arm tilt. In this respect, X-ray diffraction studies were in conflict with data from complementary structural investigations. These earlier studies, using optical or spin label probes of molecular orientation, failed to detect changes in S1. It is now apparent that this was because such probes were bound at locations on the motor domain, which is now thought not to tilt. More recently, using probes bound to the lever domain, evidence of tilting was detected, but the relatively small changes in probe orientation could be accounted for by the expected degree of tilting only if the fraction of working S1s were very small (ca 12%), in agreement with findings from motility studies. This calls into question the interpretation of X-ray studies: if 88% of the S1 population are not participating in force generation and are behaving as relaxed S1 moieties, why does their contribution to IM3 not swamp that of the much smaller population of working S1, making the relative amplitude of power stroke-related IM3 signals so small as to be undetectable? During activation there is relatively little change in IM3, yet IM3 undergoes very large intensity changes during muscle length changes, suggesting that the bulk of the IM3 signal arising from actin-bound S1. Furthermore, shortening at high velocity, which is known to produce large scale S1 detachment, causes virtual disappearance of IM3, instead of restoration of the resting intensity level. We investigated the contribution of non-cycling S1s to the X-ray signal by variation in the fraction of working S1 using reduction in the overlap between thick and thin filaments, since S1 binding to actin can only occur in regions of overlap.

We studied the two dimensional X-ray pattern of small bundles of tibialis anterior fibres from *Rana temporaria* in the relaxed state and during isometric tetanic contractions. Patterns were

collected on a 2D CCD detector during a 300ms X-ray exposure, and were corrected for background scattering and spatial aberrations in the detector response. Reflection intensities were measured by projection onto the meridian or the equatorial, then by fitting with gaussian intensity distributions superimposed on a polynomial background. We examined patterns over a sarcomere length range from 2.2 μm (full filament overlap) to 3.6 μm .

Increase in sarcomere length resulted in broadening of M3 along the equator. This effect was present in both relaxed and tetanised muscle. This effect was roughly twice as large in the activated state, except at very long sarcomere lengths, where the tetanised M3 broadening was frequently smaller than the corresponding relaxed state. This broadening is probably due to the loss of axial alignment of the myofilaments under load. The variation in IM3 with sarcomere length is affected by this disordering, since the 2D detector shows only a 'slice' of the 3D lattice point in reciprocal space. Since disordering is radially uniform, M3 can be assumed to broaden to the same extent in all directions perpendicular to the fibre axis, so multiplication of integrated IM3 by the change in width of the 2D reflection compensates for the change in volume of the 3D lattice point in reciprocal space. In addition, IM3 was corrected for the reduction in number of diffracting elements in the X-ray beam due to stretching, taking both a linear and a square law dependence of IM3 on bundle length. Corrected IM3 was increased 3 fold by activation at full filament overlap, but fell linearly towards the relaxed level as the bundles were stretched (fig. 1). It was not possible to distinguish between square and linear dependencies on fibre length, which both produced very similar dependencies to fig. 1. These findings support the results of Linari et al. [1], who proposed that activated IM3 arises almost entirely from actin-bound S1 in the overlap region. The intersection of activated and relaxed plots close to zero overlap in fig. 1 suggests that the intensity contribution from S1 outside the filament overlap zone is unaffected by activation, and that the absence of a free S1 IM3 contribution at full overlap is the result of axial disordering effects, and not a direct effect of activation on free S1 structure.

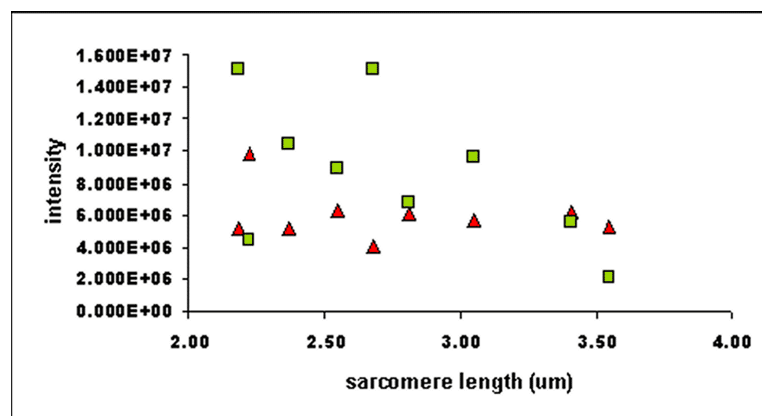


Figure 1. Variation in relaxed (triangles) and activated (squares) I_{M3} with sarcomere length from a single fibre bundle corrected for linear dependence of intensity on fibre length exposed to x-rays. Sarcomere length of 2.2 μm represents full overlap of actin and myosin filaments; 3.6 μm zero overlap.

References:

- [1] M. Linari, G. Piazzesi, I. Dobbie, N. Koubassova, M. Reconditi, T. Narayanan, O. Diat, M. Irving and V. Lombardi. Interference fine structure and sarcomere length dependence of the axial x-ray pattern from active single muscle fibres. *PNAS*, **97**, 7226-7231 (2000).

PHOSPHOLIPID MAIN PHASE TRANSITION IN ORIENTED BILAYERS: STEROL IMPACT

H. Amenitsch, M. Rappolt, B. Sartori, and P. Laggner

Austrian Academy of Sciences, Institute of Biophysics and X-ray Structure Research, Schmiedlstraße 6, A-8042 Graz, Austria

In the plasma membrane of mammalian cells cholesterol takes part in the regulation of membrane fluidity and influences the activity of many membrane-bound proteins. It has been demonstrated that changes in cholesterol content induce modification in cellular function, which e.g. depend on the recognition of an external signal [1]. To investigate whether the different plant sterols such as sito- and stigmasterol play similar roles in plant cells, we carried out simultaneous differential scanning calorimetry (DSC) and small angle X-ray scattering on the main phase transition of different dipalmitoylphosphatidylcholine/sterol/water systems. First results show, that the thermodynamical behavior among the different lipid/sterol/water systems is quite similar (see Figure 1), but the sterol impact on the bilayer stacking does show some significant variations.

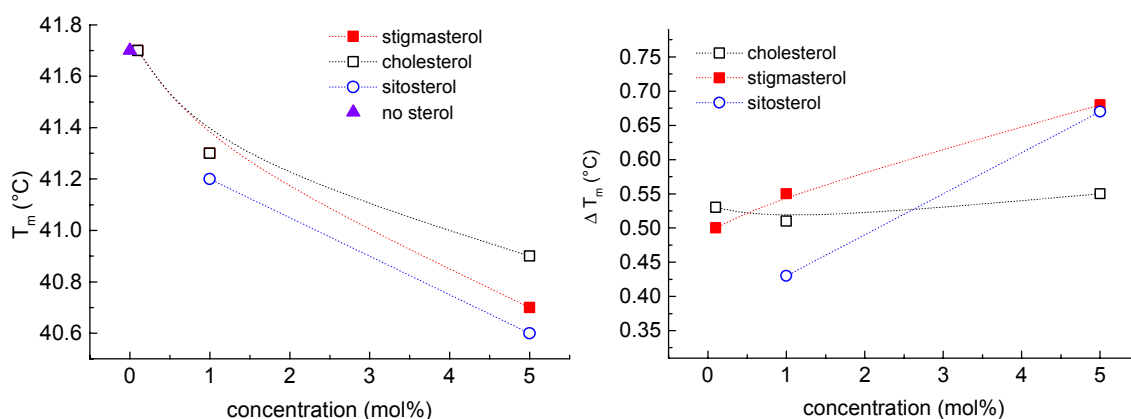


Figure 1. Comparison of the main transition temperatures T_m (left) and transition width ΔT_m (right) as a function of sterol concentration. All samples were heated with a scan rate of 1 °C/min.

References:

- [1] M. Rappolt, M., M. Vidal, M. Kriechbaum, M. Steinhart, H. Amenitsch, S. Bernstorff and P. Laggner. Structural, dynamic and mechanical properties of POPC at low cholesterol concentration studied in pressure/temperature space. *Eur. Biophys. J.* **31**, 575-585 (2003).

EVAPORATION INDUCED SELF-ASSEMBLY OF PHOSPHOLIPIDS STUDIED WITH SURFACE DIFFRACTION

H. Amenitsch¹, M. Rappolt¹, B. Sartori¹, G. Pabst¹, D. Grosso² and P. Laggnier¹

1.) Institute of Biophysics and X-ray Structure Research, Austrian Academy of Sciences, Schmiedlstr. 6, A-8042 Graz, Austria

2.) LCMC, Université Pierre et Marie Curie, 4 place Jussieu 75252 Paris Cedex 5, France

Phospholipids are the major constituent of biomembranes and form complex morphologies depending on the hydration level. In particular surface deposited structures are widely used as model systems for structural investigations, e.g. to study the evolution of cell parameters or phase behavior, or in applications, e.g. such as biosensors or biomimetic coatings. The evaporation induced self-assembly process (EISA) [1] and particular dipcoating [2] is a powerful method to create high quality coatings for mesoporous thin films. We have applied this method for phospholipids in order to study their self-assembly process *in situ* on one hand and to optimize the conditions of film deposition in terms of film quality on the other hand.

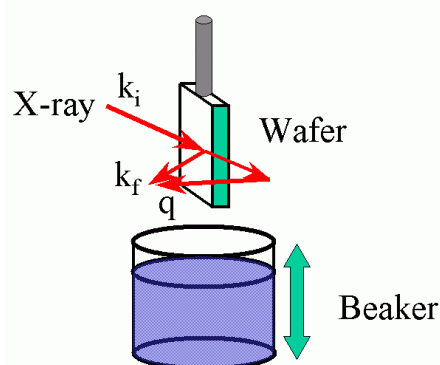


Figure 1. Schematic sketch of the set-up of the dipcoater and the chosen diffraction geometry.

Fig. 1 shows the schematic sketch of the dipcoating device. To start the process the beaker is moved upwards to immerse the wafer in the phospholipid solution. The removal of the beaker deposits a thin liquid film on the wafer surface and the subsequent assembly process on the surface is driven by the evaporation of the solvent and the up-take of humidity, which is controlled within a surrounding dipcoater chamber. Simultaneously with the removal of the beaker the data acquisition is started. As one representative result, Fig 2a shows the final diffraction pattern after such a self-assembly process, which was recorded at constant grazing angle. For this experiment, soya-phosphatidylcholine/isopropanol (40mg/ml) was used as coating solution. The final phase is a hexagonal phase in which the columns are ordered parallel to the surface as easily recognized by the two out-of-plane reflections (OPR) indicated in the figure. The time evolution of the self assembly process of the same solution is given in Fig 2b. In this graph the integrated intensities of the in-diffraction plane are represented versus time. In the beginning and in contrary to the final hexagonal phase an intermediate lamellar phase is formed with a d-spacing of 7 nm between approximately 20 to 40 s which is almost by 50% larger than the d-spacings of final phase with 4.8 nm. The final hexagonal phase forms after 60 s from a lamellar phase having the same d-spacing.

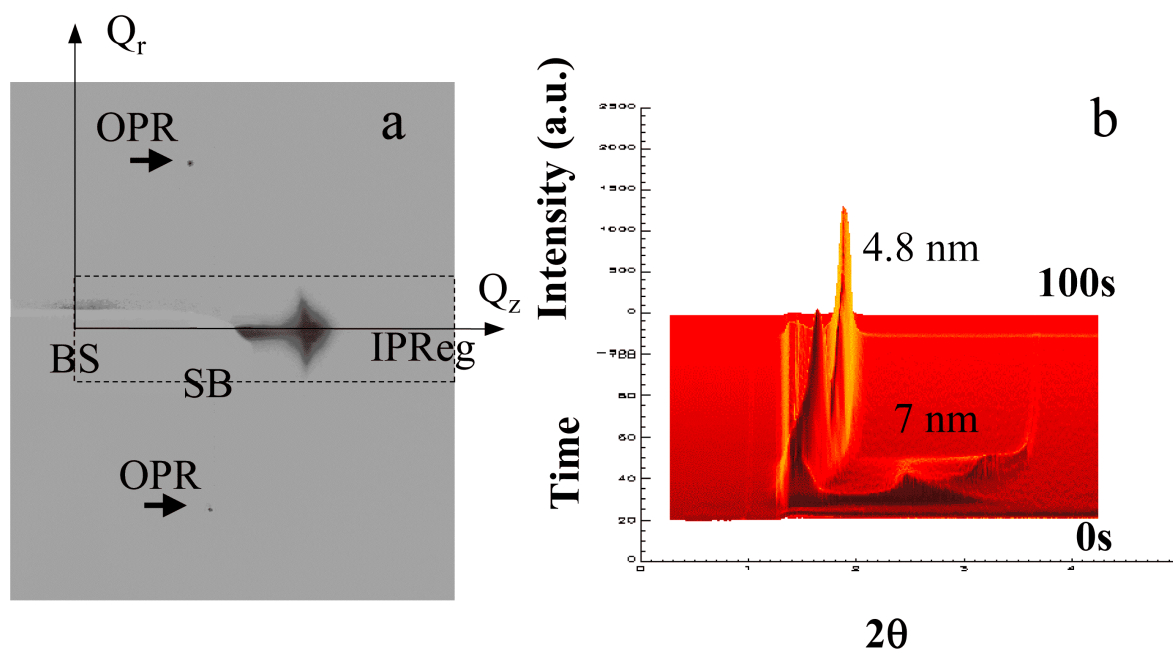


Figure 2. (a) Final diffraction pattern of Soya-PC revealing a hexagonal phase with a d-spacing of 4.8 nm. BS stands for the beam stop, SB for the specular reflected beam, OPR for the out-of-diffraction-plane reflections and IPReg for the in-plane diffraction region over which the single pictures have been integrated in (b). (b) Time evolution of the integrated diffraction image during the evaporation process.

Concluding, this method applied for phospholipids has enormous advantages to the conventionally used methods and allows the production of thin films under controlled and reproducible conditions. Grazing incidence small angle X-ray diffraction is the method of the choice to check the order, quality of the films and enables even to study in-situ the self-assembly process of the lipids after the dipcoating.

References :

- [1] Y. F. Lu et al., *Nature* 398, 223-226 (1999).
- [2] F. Cagnol et al., *Journal of Materials Chemistry* 13, 61-66 (2003).

THERMAL SAXS STUDY OF SILICEOUS SPICULES *THETYA AURANTIUM*

Gianluca Croce¹, Davide Viterbo¹, Marco Milanesio¹, Michael Rappolt² and Heinz Amenitsch²

1.) DISTA, Università del Piemonte Orientale, Piazza G. Ambrosoli 5, I-15100 Alessandria, Italy

2.) IBR, Austrian Academy of Science, A-4082 Graz, Austria

Sponges are primitive marine animals consisting of organized cells supported by a skeleton of fibres known as spicules. Spicules are usually composed of calcium carbonate or of silica and their secretion is due to specialised cells called sclerocytes. The two most important functions of the spicules are to provide support for the soft part of the sponges and to play a defence role. Their inorganic envelope generally contains an organic axial filament, made of a protein called *Silicatein* [1], which plays an important role in the biomineralization process. An important and unsolved question is the mechanism leading to the formation of spicules, which may show very different and complex shapes.

For our study we used siliceous spicules extracted from *Thetya aurantium* sponges, belonging to demosponge family and collected in the coastal lagoon of Porto Cesareo (Apulian Coast). These spicules have an elongated shape with one sharp and one rounded tip and a length of few mm [2]. The presence of central cavities inside the inorganic envelop is revealed by electron microscopy on ground samples. These cavities are the sites where the *Silicatein* proteins, responsible for the spicule growth, are hosted. The SAXS measurements were carried out in order to obtain some structural information on the organic filaments inside the spicules and to achieve a more detailed picture of their organisation. The shape and length of these spicules permitted us to collect diffraction patterns from a still sample composed by a bundle of almost parallel spicules. The *Thetya aurantium* spicules were also subjected to a thermal treatment, in the range from RT to 250°C, in order to shed some light on the structural rearrangements accompanying the thermal degradation of the organic material, already described by Croce et al [3].

The diffraction pattern collected at RT (fig1a) reveals three sharp independent spots. The more intense spot is in the equatorial position, while the other two are in non-equatorial positions. The first spot has a spacing value of about 0.200 nm, typical of spicules belonging to the demosponge family [3]. The thermal treatment induces an increase both in intensity and in sharpness of these three spots, as well as a small shift of the maxima towards lower angles. Besides at higher temperatures new spots emerge and in the final diffraction pattern at 250°C (fig1b) eleven independent spots are observed.

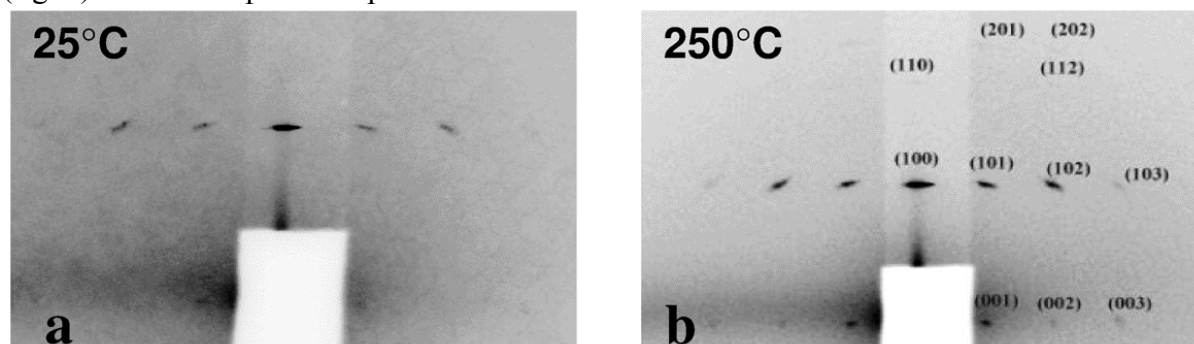


Figure 1. Diffraction pattern of a bundle of *T. aurantium* spicules collected at RT(a) and at 250°C(b).

These peaks can be indexed in an hexagonal lattice and from their position and distribution it is possible to derive some structural features. Indeed they indicate that the protein units are

packed in an hexagonal way and act as templates for the formation of a regular pattern within a silica matrix. The higher order observed at 250°C is probably due to the unfolding and/or decomposition of the protein units inside the spicules and to the reorganisation of the siliceous ordered pattern.

From the eleven peaks acquired at 250°C we also carried out the calculation of electron density maps, using a multiresolution direct method approach [4] to solve the phase problem. With such a small number of reflections only low resolution maps can be obtained but some more realistic ones can be selected. As an example the map in fig.2 clearly shows a hexagonal packing of low density (dark) regions, due to the protein template, on the (001) face, while along the spicule [001] elongation axis the low density regions are arranged as a lamellar phase.

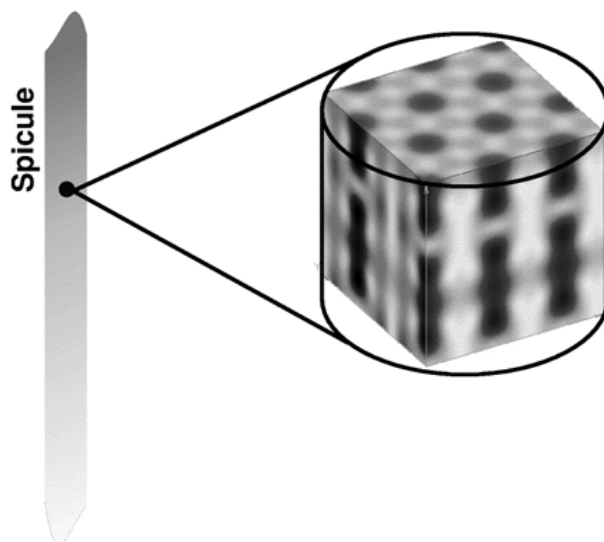


Figure 2. An example of the calculation of electron density map

References:

- [1] Cha, J. N. et al. Silicatein filaments and subunits from a marine sponge direct the polymerization of silica and silicones in vitro. *Proc. Natl. Acad. Sci. USA* (1999.) 96:361–365.
- [2] De Vos et al editors. *Atlas of Sponge Morphology* (1991) Smithsonian Institute, Washington, DC.
- [3] G. Croce et al. Structural Characterization of Siliceous Spicules from Marine Sponges. *Bioph. J.* (2004) 86: 526–534
- [4] M. M. Woolfson. Structure Determination by the Method of Permutation Syntheses. *Acta Crystallogr* (1954) 7:65-67

STRUCTURE, STABILITY AND ENERGETIC OF FOLIC ACID LIQUID CRYSTALLINE PHASES

F. Federiconi¹, M. Mattioni¹, H. Amenitsch², S. Bernstorff³ and P. Mariani¹

- 1.) Dipartimento di Scienze Applicate ai Sistemi Complessi, sez. Scienze Fisiche, Università Politecnica delle Marche
- 2.) Institute of Biophysics and X-Ray Structure Research, Austrian Academy of Sciences, Graz, Austria
- 3.) Sincrotrone Trieste, Area Science Park, Trieste, Italy

Self-assembly and self-organization have been reported for both organic and inorganic molecules. The property of biological molecules to self-associate in water is of particular interest.

The folic acid, as well as guanosine derivatives, self-associate in water [1]. This behavior is related to the similarity between guanine and pterine moieties, which both possess a particular pattern of H-bond donor and acceptor groups leading to self-recognition and self-assembly. In both cases a planar disk-shaped quartet formed by four Hoogsteen hydrogen-bonded molecules was found. These quartets, because of their amphiphilic properties, stack each on the top of the other at the typical distance of 3.4 Å to form chiral columns. This tendency to self-associate has another important consequence: the analysis of the aggregation properties revealed an extended columnar lyotropic polymorphism, characterized by the presence of Hexagonal and Cholesteric phases depending on the concentration, temperature, and salt type [2, 3].

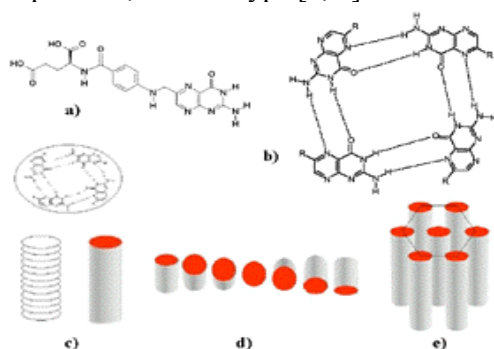


Figure 1. The self-assembly process of the folic acid: a) the molecular structure of folic acid, b) the quartets and c) their stacking, d) cholesteric and e) hexagonal phase.

To obtain further information on the self-association properties of folic acid, we decided to investigate extensively by X-ray diffraction methods the polymorphic behavior of folate sodium and potassium salt, as a function of pressure and ionic strength. The sodium and potassium folate were prepared by neutralization of folic acid (dihydrate, from Sigma) with sodium and potassium hydroxide, respectively. Samples were prepared by mixing the folic acid derivative with freshly bidistilled water, from 25% to 75% and for the potassium folate also with 1 M KCl solution; after an equilibration of at least one day, samples have been investigated by X-ray diffraction at the SAXS Austrian beamline of ELETTRA synchrotron (Trieste, Italy), in combination with the high pressure cell. Measurements were performed (at constant temperature of 25°C) from 0 to 2 Kbar with steps of about 100 bar; the Q-range was from 0.03 to 0.6 Å⁻¹ and an additional wide-angle scattering detector was used to monitor diffraction patterns in the Q-range from 0.7 to 2.5 Å⁻¹.

In each experiment, a number of reflections were observed and their spacings measured following usual procedures [3]. Typical X-ray diffraction patterns are reported in Figure 2. The low angle peaks (from 2 to 5, depending on sample concentration) can be indexed in a 2D hexagonal lattice and the unit cell dimension *a*, (i.e., the lateral interaxial distance between the helices) was then derived as a function of pressure. Note that in the same diffraction region, a diffuse band would indicate the presence of the cholesteric phase. The narrow band observed in the wide angle region is the indication of the columnar nature of the H phase: this reflection is indeed related to the tetramer stacking and from its position the distance between the neighboring tetrads, can be obtained.

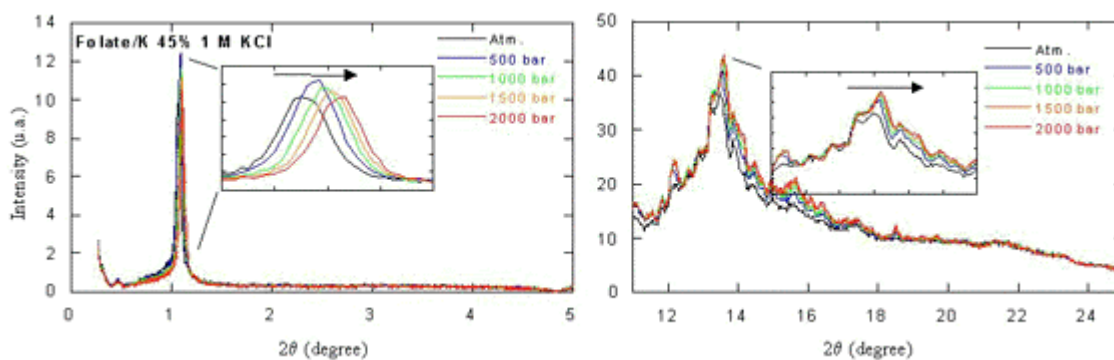


Figure 2. X-ray diffraction profiles obtained from folic acid in water. a) low-angle profile, b) high angle profile.

Two main features emerge from the X-ray data: the absence of phase transitions in the investigated concentration range and the pressure dependence of the positions of the diffraction peaks. Some quantitative results are reported in Figure 3: at all concentrations, both the unit cell dimension a , and the tetramer repeat distance reduces as a function of pressure.

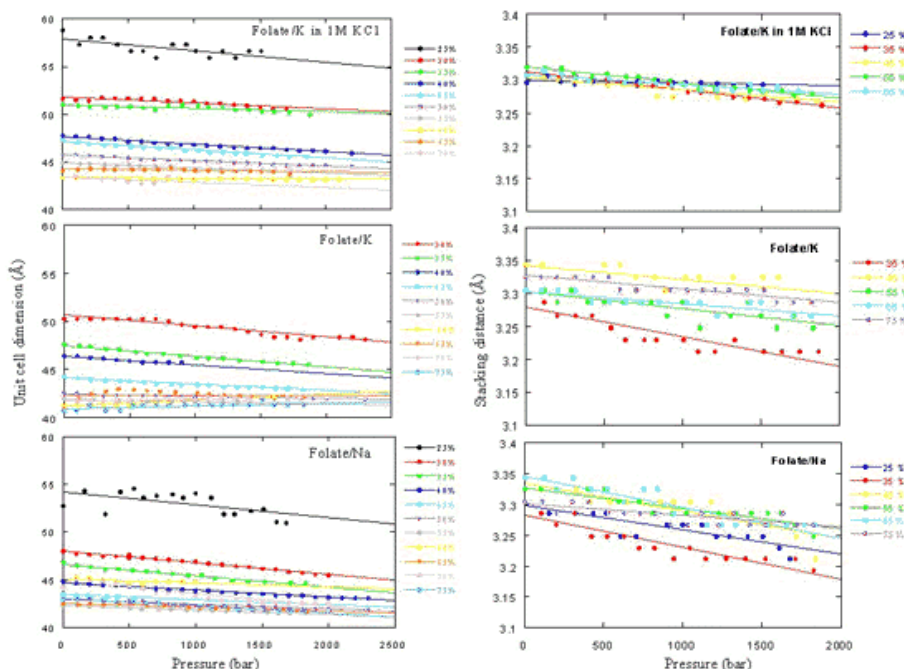


Figure 3. Pressure dependence of the 2D hexagonal unit cell (on the left) and of the stacking distance of the tetramers (on the right). Folic acid concentrations are indicated in the graph. Lines are guides to the eyes.

References:

- [1] Bonazzi, S., De Morais, M. M., Gottarelli, A., Mariani, P., & Spada, G.P., Self-assembly and liquid crystal formation of folic acid salts, *Angew. Chem., Int. Ed. Engl.* **32**, 248-250, 1993.
- [2] Ciuchi, F., Di Nicola, G., Franz, H., Gottarelli, G., Mariani, P., Ponzi Bossi, M. G., & Spada, G. P., Self-recognition and self-assembly of folic acid salts: Columnar liquid Crystalline Polymorphism and the column growth process, *J. Am. Chem. Soc.*, **116**, 1994.
- [3] Gottarelli, G., Spada, G.P., & Mariani, P., The self assembly of guanosine derivatives and folic acid, *Crystallography of Supramoleculouar Compounds*, 307-330, 1996

STRUCTURAL STUDY OF SELF-ASSEMBLED LIPOSOME-DNA-METAL COMPLEXES

O. Francescangeli¹, M. Pisani², V. Stanic.¹, C. Conti², R. Castagna², D. Clementoni², S. Bernstorff³

1.) Dipartimento di Fisica e Ingegneria dei Materiali e del Territorio, Universita' Politecnica delle Marche, Via Brecce Bianche, 60131 Ancona, Italy

2.) Dipartimento di Scienze dei Materiali e della Terra, Universita' Politecnica delle Marche, Via Brecce Bianche, 60131 Ancona, Italy

3.) Sincrotrone Trieste, 34012 Basovizza /Trieste, Italy

The association between liposomes and DNA has been object of several investigations over the last two decades. These materials are able to mimic certain characteristics of natural viruses in their ability to act as efficient chemical carriers of extracellular DNA across outer cell membranes and nuclear membranes (transfection). In order to study new biological materials of potential interest for gene therapy, we have carried out a detailed study of the structure and morphology of the triple complex dioleoylphosphatidilcholine (DOPC)-DNA-Mn²⁺ [1,2]. We performed this preliminary x-ray diffraction study at the SAXS beamline at ELETTRA. The data have shown the self-assembled formation of DOPC-DNA-Mn²⁺ complexes. This complex is formed in a self-assembled manner when solution of lipid, DNA and metal ions are mixed, which represents a striking example of supramolecular chemistry. A typical SAXS x-ray diffraction patterns of the DOPC-DNA-Mn²⁺ is shown in Fig.1. It shows two sets of peaks, the first one corresponds to unit cell $d_1=73.4 \text{ \AA}$ associated to the L^c_α phase of the triple complex; the second one corresponds to unit cell $d_2=60.4 \text{ \AA}$ associated to the L_α phase of the pure DOPC. The complex is characterized by the lamellar symmetry of the L^c_α phase, the structure consists of an ordered multilamellar assembly where the hydrated DNA helices are sandwiched between the lipid bilayers.

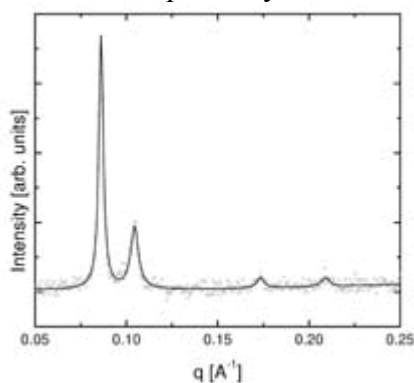


Figure 1. Synchrotron XRD pattern of DOPC-DNA-Mn²⁺ at 3:4:12 molar ratio.

The condensation of the DNA in the complex is promoted by the metal cations that bind the lipid polar heads with the negatively charged phosphate groups of DNA. In the present experiment we have studied new complexes differing in the nature of the neutral lipid and metal cations ($\text{Me}^{2+} = \text{Mg}^{2+}, \text{Mn}^{2+}, \text{Fe}^{2+}$ and Co^{2+}). These experiments have confirmed the previous results and have shown a similar behavior for dilinoeylphosphatidilcholine (DLPC)-DNA-Me²⁺ and dipalmitoylphosphatidilcholine (DPPC)-DNA-Me²⁺. All these complexes exhibit the lamellar symmetry of the liquid crystalline L^c_α . In addition we have studied the effects of the temperature on the structure and phase stability of the DOPC-DNA-Mn²⁺ complex as well as on the equilibrium coexistence of the triple complex in the L^c_α phase with the multilamellar vesicles of the neutral lipid L_α phase of the DOPC. In Fig 2. we report a

series of x-ray diffraction patterns as a function of temperature of the DOPC-DNA-Mn²⁺ complex at molar ratio 3:4:3. Moreover, we have carried out a series of experiments on the DOPC-DNA-Mn²⁺ at different concentrations of DOPC. The results (Fig. 3) show that the volume ratio of the two structures (L^c , L_α) depends on the molar ratio of the components. On increasing the relative concentration of the DOPC a continuous reduction of the relative volume ratio of the complex is observed until a critical value is reached where the formation of the complex is inhibited. These are only preliminary results and a more detailed interpretation of the measurements will require a complete analysis of the overall data, which is still in progress.

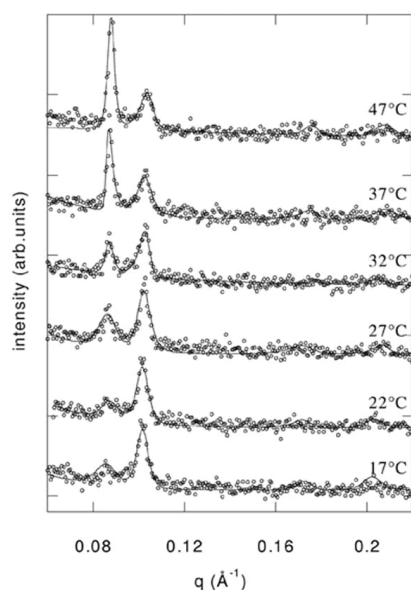


Figure 2. X-ray diffraction patterns of DOPC:DNA:Mn²⁺ at 3:4:3 molar ratio as a function of temperature.

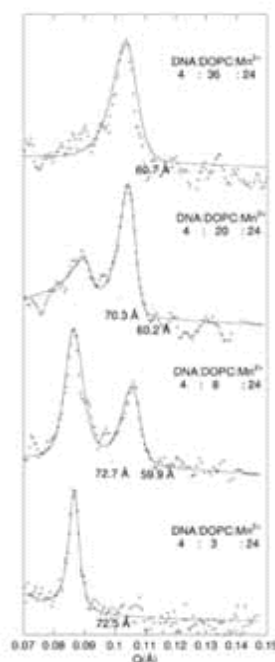


Figure 3. X-ray diffraction patterns of DOPC:DNA:Mn²⁺ as a function of different molar ratio of the DOPC

References:

- [1] O. Francescangeli, V. Stanic, L. Gobbi, P. Bruni, M. Iacussi, G. Tosi, S. Bernstorff; Structures of self-assembled liposome-DNA-metal complexes; *Phys. Rev. E*, **67**, 011904, (2003).
- [2] O. Francescangeli, V. Stanic, D.E. Lucchetta, P. Bruni, M. Iacussi, F. Ciongolani; X-Ray Diffraction Study of Dioleoylphosphatidylcholine-DNA-Mn²⁺ complexes; *Mol. Cryst. Liq. Cryst.*, **398**, 259-267, (2003) .
- [3] O. Francescangeli, M. Pisani, V. Stanic, P. Bruni, T. Weiss; Evidence of an Inverted Hexagonal Phase in Self-Assembled Phospholipi-DNA- Metal Complexes; submitted to *Europhysics Letters*

DEVELOPMENT OF A NEW VERTICAL COUETTE CELL FOR SIMULTANEOUS SWAXS/DSC/SHEAR EXPERIMENTS AS A FUNCTION OF TEMPERATURE

D. Kalnin¹, O. Schafer², G. Keller¹, S. Bernstorff³, H. Amenitsch⁴, M. Ollivon¹

1.) UMR CNRS 8612, Equipe Physico-Chimie des Systèmes Polyphasés, 92296 Chatenay-Malabry, France

2.) Nestlé Research Center NRC, Vers-Chez-les-Blanc, 1000 Lausanne 26, Switzerland;

3.) Sincrotrone Trieste, Strada Statale 14, km 163.5, 34012 Basovizza (TS), Italy.

4.) Institute of Biophysics and X-Ray Structure Research, Austrian Academy of Sciences, Graz, Austria

Combining insoluble substances is a key processing step in many industries. In fact many drugs, flavors and colorants can be mixed in form of “dispersions” comprising all sorts of lipidic particles, emulsions, liposomes, etc.. Emulsions however raise many problems due to the fact that emulsion technology and formulation is rather based on empirical methods. Only a few key parameters such as apparent stability are nearly understood due to of the lack of analyzing methods. Low concentration of the “dispersed” phase mostly impedes its investigation just as the numerous added constituents. Therefore the dispersed phase is generally studied in bulk - which cannot lead to its appropriate characterization, because it forfeits all properties related to dispersion such as influence of interface curvature. For this reason emulsions have to be investigated as such using more and more refined analyzing methods.

Lipid in water emulsions essentially containing triacylglycerols (TAGs) find widespread applications in pharmaceutical and food industries. Food preservation implies storage after manufacturing at low temperatures where at least partly crystallized emulsion droplets occur whereas for approval, pharmaceuticals have to be stable for even longer time periods at higher temperatures close to ambient. In the majority of cases when liquid or liquid crystalline metastable phases are present solubility changes drastically with recrystallization into more stable species. It is of importance to understand the effect of mechanical and thermal stresses on emulsions.

In order to elucidate the influence of mechanical stress on the crystallization behavior of dispersed systems we developed a vertical temperature controlled shear device working in synchrotron X-ray beam and associating calorimetry detection (Fig.1 left). Model emulsions of different lipid concentrations ranging up to 20% lipid content of different origin (cocoa butter, anhydrous milk fat, palm oil fractions) were investigated and their polymorphic behavior was investigated varying the emulsifier concentration and type.

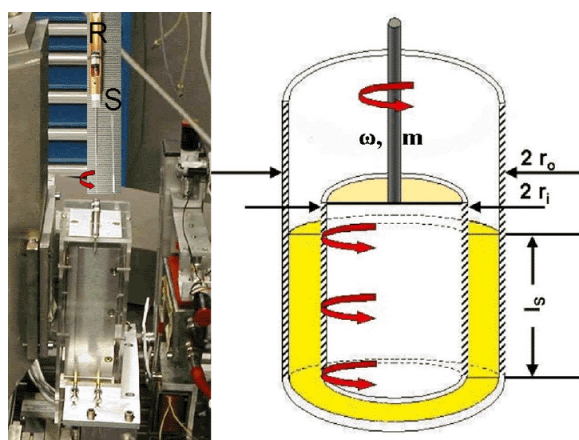


Figure 1. Schematic of the shear module consisting of two concentric Müller quartz-glass capillaries of 1.5 and 1.0 mm hand calibrated diameter and its implementation inside the vertical DSC cell mounted in the X-ray beam of the SAXS beamline.

Glass capillaries – the inner one qualified to rotate at different velocities controlled by an electronic module capable of maintaining the velocity at a constant rate exert lamellar flow on

the sample (Fig.1 right)- assure good heat transfer and present still sufficient mechanic properties in order to avoid capillary breakage when shear is applied. Verticalness assures that the samples not showing to much capillarity stay in the beam and inside the measurement cell for calorimetric measurements.

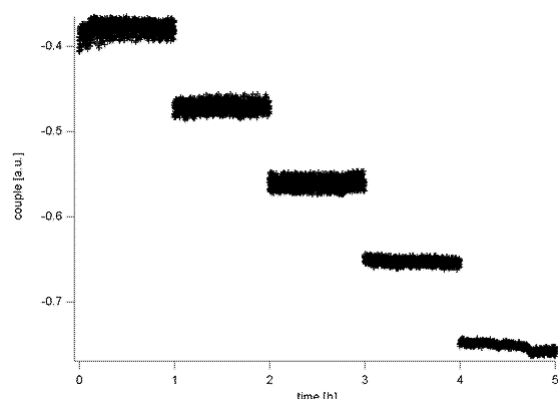


Figure 2. Signal of the current necessary to keep the shear velocity constant measured between rotor and stator capillary inside the temperature controlled sample holder at the given temperature of 20°C. The couple imposed was increased measuring a protein stabilized emulsion for 5 hours.

Shear experiments during a long time period showed (Fig. 2) that shear can be applied without the significant emulsion modification [1], which is very important as lipids in bulk represent totally different crystallization behavior than in emulsion. Different shear velocities show different couple measurable producing a signal with decreasing noise increasing the rotation speed. Medium shear rates are applied to all emulsions studied.

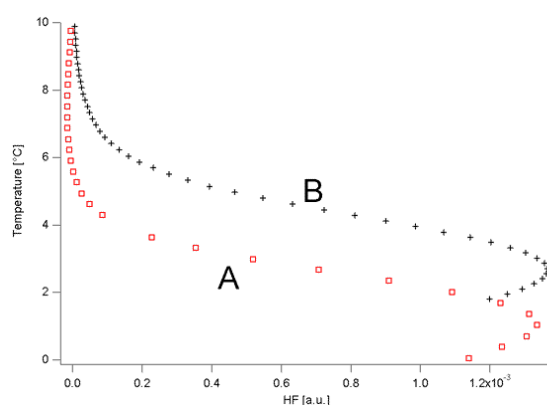


Figure 3. DSC signal recorded on cooling at $r_C = 4\text{k/min}$ Emulsion crystallizing without any mechanical stress (A) and with the application of a constant shear rate (B).

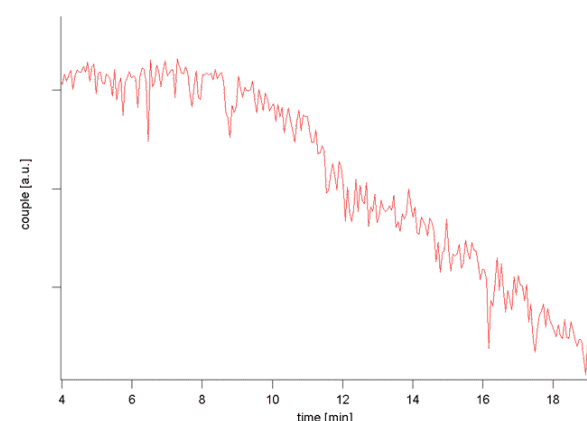


Figure 4. Signal of shear force at a medium imposed rotation speed measured between rotor and stator capillary inside the DSC cell as a function of the temperature during cooling from 60 to 0°C at $r_C = 4\text{ K/min}$.

This setup allows for the simultaneous measurement of shear forces, heat exchanges and SWAXS from a single sample. We found as a general feature of all kinds of emulsified lipids that the application of mechanical stress increases the T_{ON} of the lipid crystallization such as some emulsifiers do[2] (Fig. 3) not affecting the apparent emulsion viscosity (Fig. 4).

In addition this mechanical stress influences the structural properties of emulsified TAGs in such a way that crystallization seems to direct the polymorph toward more stable crystal forms. This is even more surprising since the monotropic polymorphism (valuable for equilibrium conditions) foresees a different behavior. Different data sets comprising fats of different origin, and various emulsifiers in different concentration were investigated of which data evaluation is still under way.

References:

- [1] S. A. Vanpalli, J. N. Coupland; Emulsions under shear- the formation and properties of coalesced lipid structures; *Food Hydrocoll.* 15, 507-512 (2001)
- [2] D. Kalnin, O. Schafer, H. Amenitsch, M. Ollivon; Fat Crystallization in Emulsion: Influence of the emulsifier concentration on triacylglycerol crystal growth and polymorphism; submitted to *Crystal Growth and Design*

STRUCTURAL AND THERMODYNAMICAL PROPERTIES OF POPC AT LOW STEROL CONCENTRATIONS STUDIED BY PRESSURE-SCANNING SAXS

M. Kriechbaum¹, M.F. Vidal¹, M. Steinhart², M. Rappolt¹, H. Amenitsch¹, S. Bernstorff³ and P. Laggner¹

- 1.) Institute of Biophysics and X-Ray Structure Research, Austrian Academy of Sciences, Graz, Austria.
- 2.) Institute of Macromolecular Chemistry, Czech Academy of Sciences, Prague, Czech Republic.
- 3.) Sincrotrone Trieste, Strada Statale 14, km 163.5, Basovizza (Trieste), Italy.

We have completed the studies on the structural and mechanical properties of 1-palmitoyl-2-oleoyl-phosphatidylcholine (POPC) and the sterol cholesterol binary mixtures by slow pressure scanning SAXS measurements [1] and have extended these studies including 2 other plant sterols, sitosterol and stigmasterol, respectively (Fig.1). No significant differences were found with the POPC/sitosterol and POPC/stigmasterol mixtures compared to POPC/cholesterol. Adding either sterol, the transition enthalpy ΔH_m for the gel-fluid transition of POPC decreases from 19kJ/mol (0% sterol) to 7kJ/mol (20% sterol) using the reciprocal Clapeyron relation $dp_m/dT = \Delta H_m / (\Delta V_m T_m)$, where dp_m/dT denotes the change in transition pressure p_m with temperature T, ΔV_m the associated volume change (taken from literature) and T_m the gel-fluid transition temperature (see compilation of the values in Table 1).

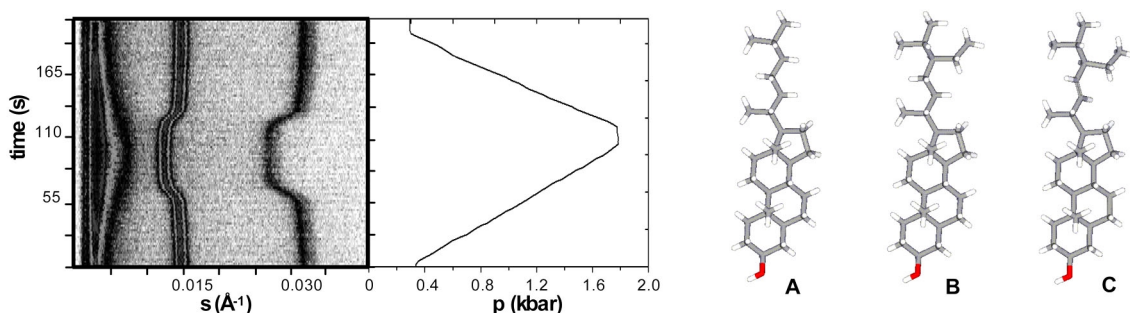


Figure 1. Time-resolved SAXS patterns of the gel-fluid transition of POPC (+ 1 mol% cholesterol) during a pressurizing and subsequent depressurizing scan at 20°C. The picture to the left shows 110 diffraction patterns with an exposure time of 2 s for each frame and next to it the respective pressure (scan rate ~ 15 bar/s). To the right, the molecular structures of cholesterol (A), sitosterol (B) and stigmasterol (C) are shown.

Table 1. Thermodynamic properties for the gel-fluid transition of POPC with increasing cholesterol concentration. Values for dp_m/dT were obtained from pressure scanning SAXS measurements and ΔH_m calculated by the Clapeyron relation (see text).

Cholesterol (mol%)	dp_m/dT (bar/°C)	ΔH_m (KJ/mol)
0	45	18.9
1	37	14.5
5	46	15.8
10	46	13.3
20	37	6.7

References:

- [1] Rappolt, M., Vidal, M.F., Kriechbaum, M., Steinhart, M., Amenitsch, H., Bernstorff, S. & Laggner, P. (2003): Structural, dynamic and mechanical properties of POPC at low cholesterol concentration studied in pressure/temperature space. *Eur. Biophys. J.* **31**, 575-585.

STUDYING THE EFFECT OF THE IONIC STRENGTH ON THE SOLUBILIZATION OF CHARGED LIPOSOMES USING TIME RESOLVED SAXS

O. López¹, M.Cócerca¹, J. Pereira¹, J. Caelles¹, H. Amenitsch², A. de la Maza¹, I. Carrera¹, R. Pons¹

1.) IIQAB-CSIC, Jordi Girona 18-26 08034 Barcelona, Spain.

2.) Institute of Biophysics and X-ray Structure Research, Austrian Academy of Sciences, Schmiedlstr. 6, A-8042 Graz, Austria

The mechanism that induces the solubilization of liposomes by surfactants consists in a monomeric adsorption of surfactant on the bilayers and a desorption of mixed micelles from the liposome surface to the aqueous medium. Extremely fast rates have been associated with these two processes [1]. This fact makes necessary the use of high time resolution techniques as stopped-flow time resolved small angle X-ray scattering (SAXS) using a Synchrotron radiation source. Earlier experiments performed at ELETTRA have reported interesting information about the kinetics of these initial steps of solubilization, as well as about the effect in this process of a small amount of electrostatic charge. Our results showed the coexistence of different structures (bilayers, pure micelles and mixed micelles) in short time intervals during the solubilization. The electrostatic charges could either accelerate or slow down the processes involved [2, 3].

In this work we seek to study the effect of the liposome electrostatic charge and the ionic strength on the solubilization of liposomes. Neutral liposomes as well as liposomes containing 20% in weight of ionic lipids (negative and positive) were formed. This amount of surface charge mimicks the proportion presents in some biological membranes. The anionic surfactant sodium dodecyl sulfate (SDS) was mixed with the liposomes using a stopped-flow cell and the changes produced in the systems were monitored by SAXS. In order to evaluate the effect of the ionic strength, the experiments were carried out in deionized water and in Tris buffer 5mM with 100 mM NaCl.

The x-ray scattering curves showed clearly two bands in all the lipid-surfactant systems. Figure 1 shows the scattering curves of the interaction of neutral liposome with SDS after different times from mixing. The band corresponding with the bilayer was detected at q values about 0.100 \AA^{-1} , which correspond with bilayer thickness of about 63 \AA . Other band was detected approximately at $q=0.151 \text{ \AA}^{-1}$. After fitting to a two shell model [4], this band was attributed to spherical particles of 41 \AA . Both, pure micelles and mixed micelles could contribute to this band.

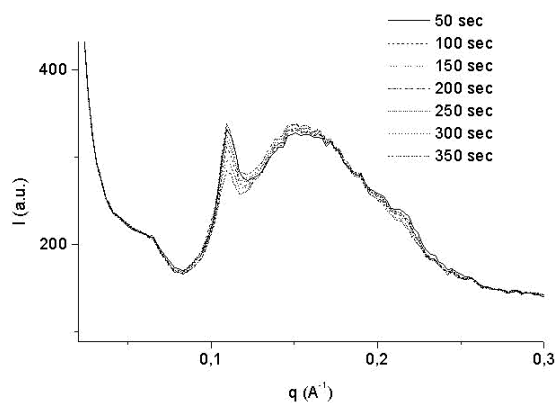


Figure 1. X-ray scattering patterns for the system neutral liposome-SDS after different times from mixing.

The analysis of the intensity variation of each scattering band (corresponding to liposomes and micelles) as a function of time at low and high ionic strength are shown in Figures 2 and 3 respectively.

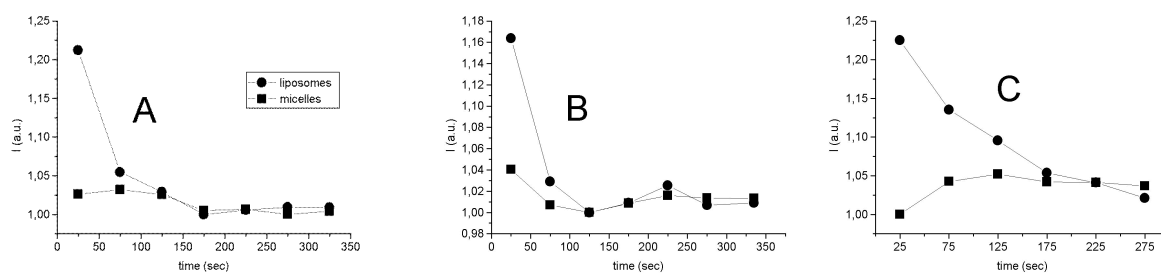


Figure 2. Intensity of the bands associated with the liposome bilayer (●) and micelles (■) as a function of time. Liposomes used were cationic (A), anionic (B) and non-ionic (C) at low ionic strength

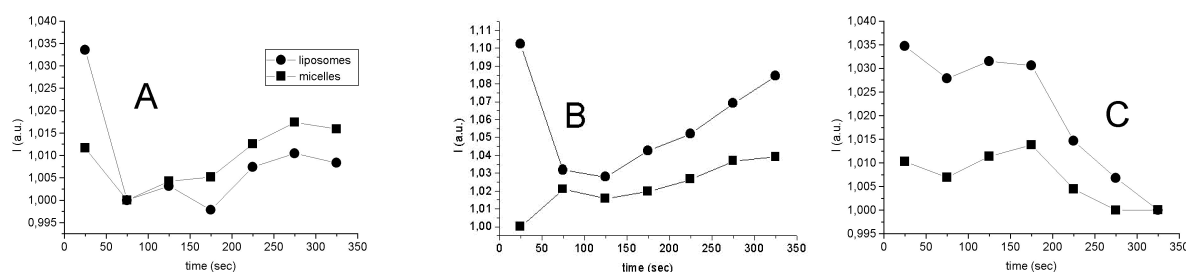


Figure 3. Intensity of the peaks associated with the liposome bilayer (●) and micelles (■) as a function of time. Liposomes used were cationic (A), anionic (B) and non-ionic (C) at high ionic strength.

These results seem to indicate that, in presence of the anionic surfactant SDS, liposomes containing 20% of ionic lipids show faster kinetics of both absorption of surfactant and desorption of mixed micelles than non-ionic liposomes. This could be related with the fact that the presence of electrostatic charge in cells may facilitate some adsorption and/or desorption processes.

Our experiments also indicate that the kinetics of the processes inducing liposome solubilization can be modulated by the ionic strength of the medium, although this modulator effect is dependent on the electrostatic charge of the membranes. Thus, in charged liposomes the ionic strength accelerates the interaction lipid-surfactant, whereas in neutral liposomes the ionic strength seems to slow down this interaction.

References:

- [1] O. López, M. Cócera, J. Pereira, H. Amenitsch, J. Caelles, L. Coderch, J.L. Parra, A. de la Maza and R. Pons; Processing stopped-flow saxs data to study the kinetic of liposome-surfactant systems; *Biophys. J.*, 86(1), 76a, (2004)
- [2] M. Cócera, O. López, R. Pons, H. Amenitsch, and A. de la Maza; Effect of the electrostatic charge on the mechanism inducing liposome solubilization: a kinetic study by synchrotron radiation SAXS; *Langmuir* 20(8), 3074 – 3079 (2004).
- [3] O. López, M. Cócera, L. Coderch, J.L. Parra, L. Barsukov and A. de la Maza; Octyl glucoside-mediated solubilization and reconstitution of liposomes: Structural and kinetic aspects; *J. Phys. Chem. B* 105, 9879-9886, (2001).
- [4] J.B. Hayter and J. Penfold; Determination of micelle structure and charge by neutron small-angle scattering; *Colloid Polym Sci* 261, 1022-1030 (1983).

PRESSURE INDUCED SUBUNIT DISSOCIATION OF DIMERIC BETA-LACTOGLOBULIN

P.Mariani¹, M.G.Ortore², F.Spinozzi¹, G.Onori² and H. Amenitsch³

1.) Dipartimento di Scienze Applicate ai Sistemi Complessi, Università Politecnica delle Marche, via Ranieri 65, 60131 Ancona, Italy

2.) Dipartimento di Fisica, Università degli Studi di Perugia, via A. Pascoli, 06123 Perugia, Italy

3.) Institute of Biophysics and X-Ray Structure Research, Austrian Academy of Sciences, Graz, Austria

The application of high pressure to a protein solution perturbs the structure of the protein and its interactions with solvent in a controlled way [1,2]. In vitro increasing pressure induces dissociation of oligomers and then protein denaturation.

Beta-lactoglobuline is a 18.400 Da protein, belonging to the lipocaline family and is abundantly contained in mammalian milk. At neutral pH the structure is dimeric, while at acidic pH (a condition more similar to the physiological one) the quaternary structure is lost, with a partial dissociation into two monomers still showing a fairly ordered structure.

In a paper we reported experimental data concerning structural properties of beta-lactoglobulin in acidic solutions (pH 2.3), at several values of ionic strength in the range 7-507 mM [3], evidencing the presence of a monomer-dimer equilibrium affected by the ionic strength. Moreover in a second paper [4] we improved the calculation of the theoretical average structure factor, using a new approximation to the protein-protein correlation functions $g_{ij}(r)$. This study has been able to reproduce the interference peak present at low Q as a function of a simple screened electrostatic potential among charged monomer and dimer. In continuation of our previous works, we performed an experiment at acidic pH (pH=2.3), at protein concentration 10mg/ml under mechanical pressure (up 1800bar) and changing the ionic strength of the solution from 0 to 200 mM NaCl. Also we used buffers with different percentages of ethylene-glycol (0%-50%) in order to evidence modifications of monomer-dimer equilibrium. Kratky plots of our data confirm that even the presence of 50% w/w E.G. induce no protein denaturation.

The radius of gyration of beta-lactoglobulin decreases when we apply high pressures [Fig.1], suggesting a transition from dimer to monomer. In each experiment at a fixed ionic strength the application of increasing pressure induces dissociation of oligomers [Fig.2]. The presence of ethylene-glycol seems to modify this behaviour translating the transition to higher pressures.

Ethylene-glycol modify solvent's permittivity in a controlled and continuous way, so that we can derive informations about protein-protein effective interactions.

We report a preliminary analysis that will be followed by a more detailed one. Since the form factors of both the species are known, we can obtain the average structure factor in order to determine protein-protein effective interactions. The experimental prospect shows that the monomer-dimer equilibrium can be modified by different conditions of ionic strength, pH, pressure and organic solvents. The characterisation of these different conditions is the first step to improve the study of protein-protein interactions.

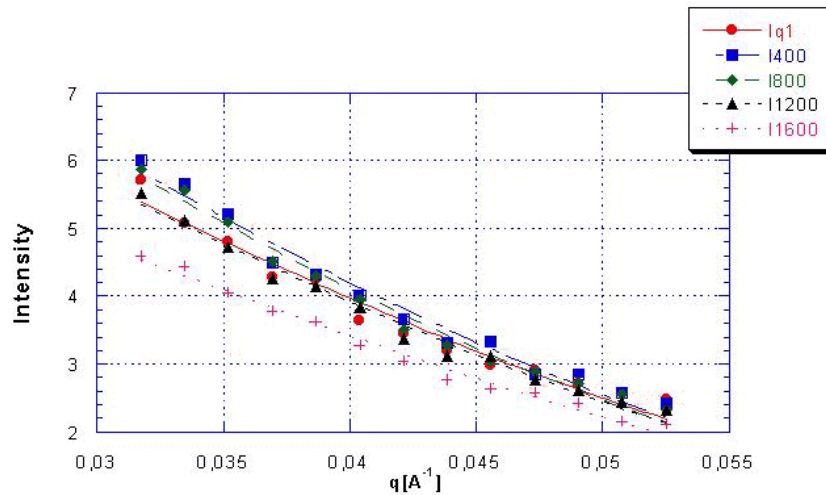


Figure 1. X-ray scattering pattern of beta-lactoglobulin in 10% w/w ethylene-glycol, pH=2.3, $C_{\text{protein}}=10\text{mg/ml}$, Ionic strength:12mM, $T=25^\circ\text{C}$.

● : 1 bar. ■ : 400bar. ◆ : 800bar. ▲ : 1200bar. + : 1600bar.

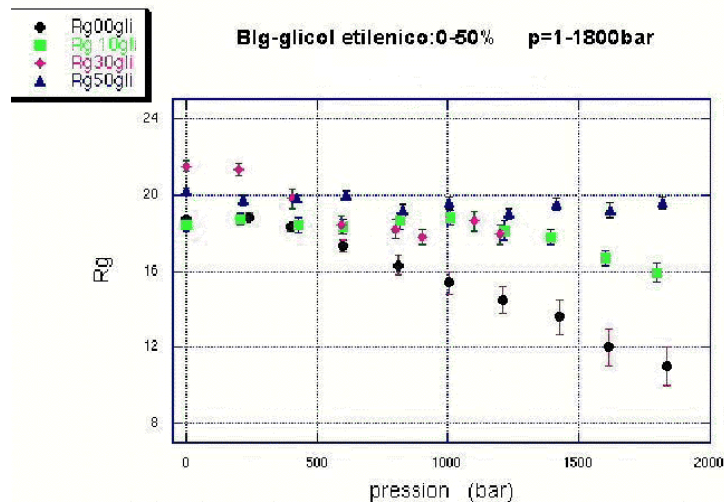


Figure 2. Radius of gyration at different EG fractions versus pressure. pH=2.3, $C_{\text{protein}}=10\text{mg/ml}$, Ionic strength:12mM, $T=25^\circ\text{C}$.

+ : 0% EG. ■ : 10% EG. ◆ : 30% EG. ▲ : 50% EG.

References:

- [1] Hawley, S.A. 1971. Reversible pressure-temperature denaturation of chymotrypsino- gen. *Biochemistry* 10: 2436-2442
- [2] Smeller, L. 2002. Pressure-temperature phase diagrams of biomolecules. *Biophys. Biochim. Acta* 1595:11-29
- [3] Baldini G, Beretta, S. G. Chirico, E. Maccioni, F. Spinozzi, P. Mariani, H. Franz. 1999. Salt-Induced Association Of Beta-Lactoglobulin By Light And X-Ray Scattering. *Macromolecules*, 32:6128-6138
- [4] Spinozzi, F., D. Gazzillo, A. Giacometti, P. Mariani and F. Carsughi. 2002. Interaction of proteins in solution from small angle scattering: a perturbative approach. *Biophys. J.*, 82:2165–2175

STRUCTURE AND FLUCTUATIONS IN THE ANOMALOUS SWELLING REGIME OF PHOSPHATIDYLCHOLINES

G. Pabst, H. Amenitsch, P. Lagner and M. Rappolt

Austrian Academy of Sciences, Institute of Biophysics and X-ray Structure Research, Schmiedlstraße 6, A-8042 Graz, Austria

We have determined the structural properties and bending fluctuations of fully hydrated phosphatidylcholine dispersions in the fluid phase near the main phase transition temperature (T_M). The number of carbons, n_{HC} , per acyl chain varied from 14 to 20 [1].

All lipids exhibit a nonlinear increase of the lamellar repeat distance d upon approaching T_M from above (Fig 1A), which is known as anomalous swelling from several previous studies [2]. The nonlinear increase reduces with chain length, but levels off above $n_{HC} = 18$. A detailed analysis of the diffraction patterns in terms of a global model [3] shows that anomalous swelling has two components: One is due to the water layer, d_w (Fig. 1B). This contribution reduces with chain length (Fig. 1B i–1B iii) and finally vanishes for $n_{HC} > 18$ (Fig. 1B iv). The second component is due to the bilayer thickness, d_B (Fig. 1C). In contrast to the behavior of the water layer, the increase of d_B upon decreasing temperature remains for all studied lipids unchanged, including a nonlinear component of about 0.5 Å in the vicinity of T_M .

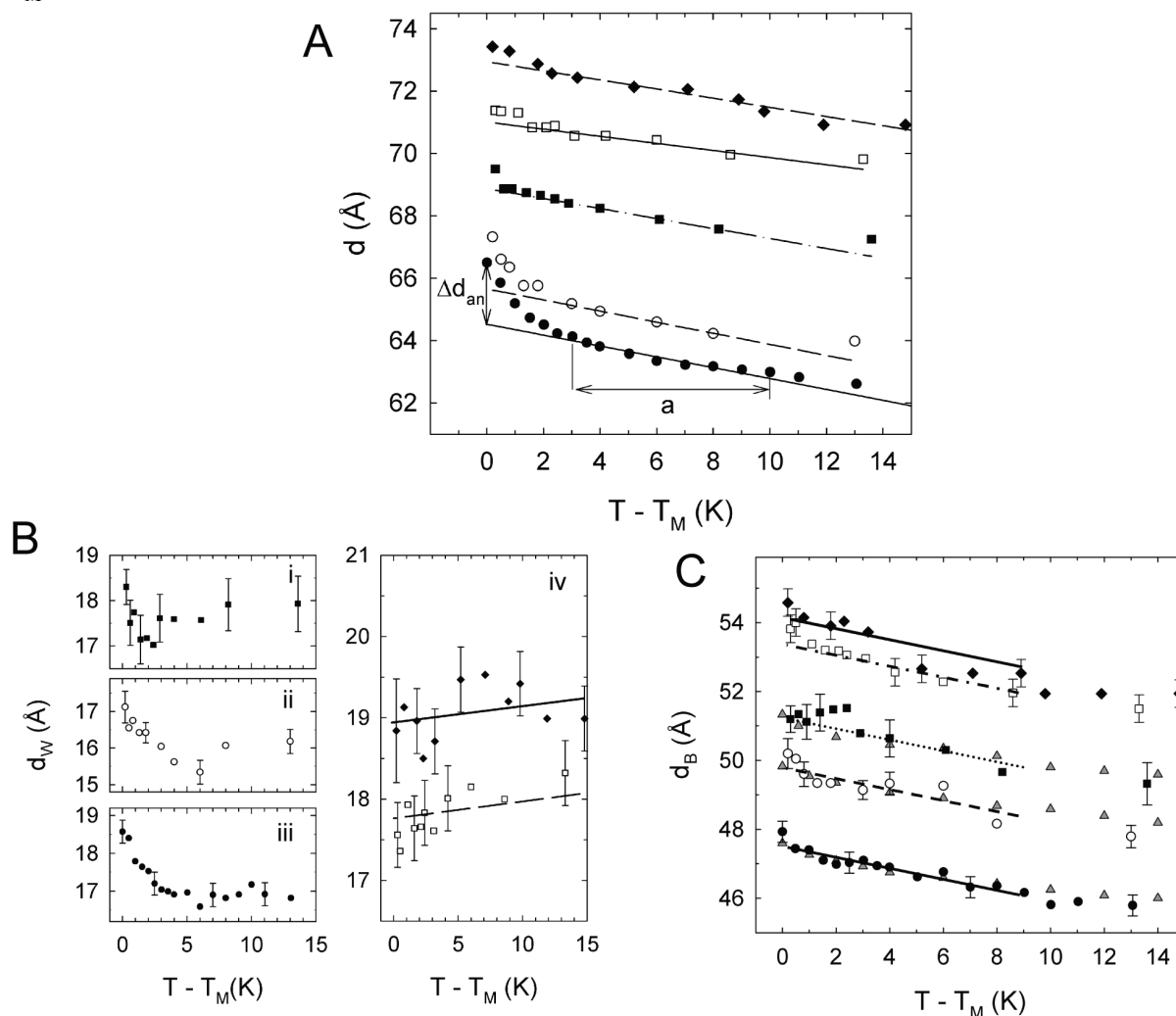


Figure 1 (see previous page). Chain length dependence of anomalous swelling. Panel (A) shows the temperature dependence of the d spacing for dimyristoyl phosphatidylcholine (\bullet , $n_{HC} = 14$), dipalmitoyl phosphatidylcholine (\circ , $n_{HC} = 16$), distearoyl phosphatidylcholine (\blacksquare , $n_{HC} = 18$), dinonadecanoyl phosphatidylcholine (\square , $n_{HC} = 19$) and diarachidoyl phosphatidylcholine (\blacklozenge , $n_{HC} = 20$). Panel (B) gives the results for the water layer and (C) for the membrane thickness. Panel (C) also contains NMR data [4] on the hydrocarbon chain length (gray Δ s) scaled to d_B .

Thus, anomalous swelling above 18 hydrocarbons per chain is due to the pretransitional effects on the membrane only. These results are additionally supported by a bending fluctuation analysis. Here, we find increased undulations close to T_M only for the short chain lipids (data not shown).

References:

- [1] Data submitted for publication.
- [2] See, for example, G. Pabst, J. Katsaras, V.A. Raghunathan, and M. Rappolt, Structure and Interactions in the Anomalous Swelling Regime of Phospholipid Bilayers, *Langmuir*, **19**, 1716-1722 (2003).
- [3] G. Pabst, M. Rappolt, H. Amenitsch, and P. Laggner, Structural Information from Multilamellar Liposomes at Full Hydration: Full q-range Fitting with High-Quality X-ray Data, *Physical Review E*, **62**, 4000-4009 (2000).
- [4] M.R. Morrow, J.P. Whitehead, and D. Lu, Chain-length Dependence of Lipid Bilayer Properties Near the Liquid Crystal to Gel Phase Transition, *Biophysical Journal*, *Biophys. J.*, **63**, 18-27 (1992).

HYDROSTATIC PRESSURE EFFECTS ON PHASE BEHAVIOUR OF LIPID MIXTURES: SAXS STRUCTURAL STUDIES

L. Paccamiccio¹, H. Amenitsch², S. Bernstorff³ and P. Mariani¹

1.) Dipartimento di Scienze Applicate ai Sistemi Complessi, Università Politecnica delle Marche, Ancona, Italy

2.) Institute of Biophysics and X-Ray Structure Research, Austrian Academy of Sciences, Graz, Austria

3.) Sincrotrone Trieste, Area Science Park, Trieste, Italy

DOPE (L- α -dioleoyl phosphatidylethanolamine) and DOPC (L- α -dioleoyl phosphatidylcholine) are phospholipids extensively studied as a membrane model system. In order to elucidate the structural properties, phase behavior and energetic of such lipid systems, high pressure X-ray diffraction analysis was continued on DOPE-DOPC lipid mixtures equilibrated in excess of water in the presence of tetradecane.

Samples were obtained by combining the appropriate amounts of the component lipids, dissolved in chloroform, with DOPC molar fraction (X_{DOPC}) ranging from 0 to 0.75. The solvent was evaporated and the mixtures were prepared in excess of water after the addition of tetradecane, which is known to stabilize hexagonal phases characterized by small curvatures at the water-lipid interface[1]. In order to obtain homogeneous mixtures, the samples were subjected to heat shock cycles.

Diffraction experiments were performed at the SAXS beamline at ELETTRA Synchrotron (Trieste, Italy) with $\lambda = 1.54 \text{ \AA}$ and $0.03 < Q < 0.6 \text{ \AA}^{-1}$. The wide-angle X-ray scattering detector was used to monitor diffraction patterns in the Q-range from 0.7 to 2.5 \AA^{-1} . Pressure cells with diamond windows, which allow to measure diffraction patterns at hydrostatic pressures up to 3 kbar, were used. Particular care has been taken to check for radiation damage and for equilibrium conditions. Measurements were repeated several times at the same constant pressure to account for stability in position and intensity of Bragg peaks. Accordingly, samples were gently compressed at a rate of 0.5-2 bar/s to ensure the onset of equilibrium conditions. The diffraction patterns were collected at 25°C. For each mixture, a series of diffraction patterns were measured as a function of pressure, from 1 bar to 2 Kbar, with step of 100 bar.

Figure 1 shows a series of X-ray diffraction profiles obtained at different pressures for three different mixtures. The pressure-concentration phase diagram referred to DOPE-DOPC-tetradecane-water mixtures is reported in Figure 2.

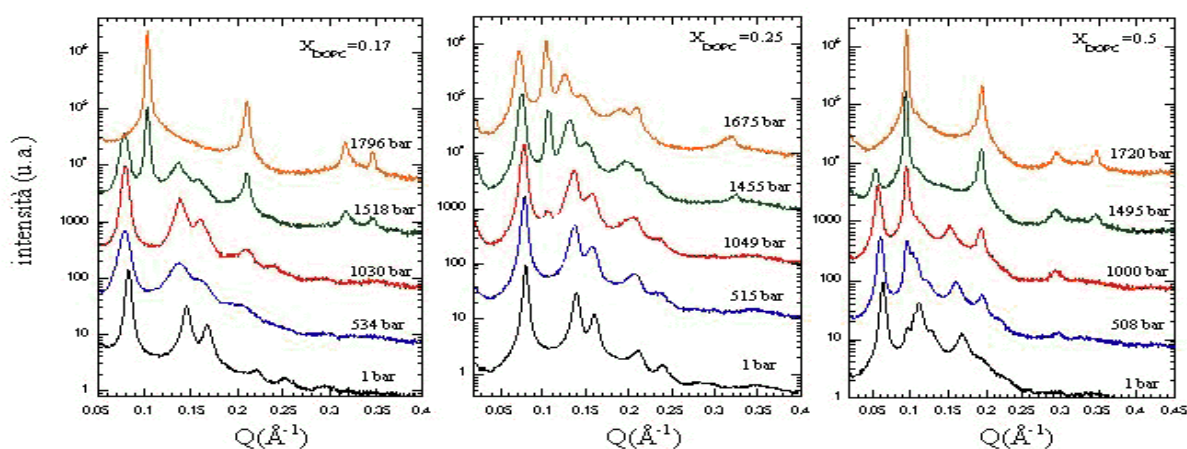


Figure 1. Low angle X ray diffraction profile form DOPE-DOPC mixtures at different pressure and at the following concentration: $X_{\text{DOPC}}=0,17$; $X_{\text{DOPC}}=0,25$; $X_{\text{DOPC}}=0,50$.

It can be observed the presence of the inverse hexagonal phase at room temperature and at ambient pressure at all the investigated concentrations. It can also be observed that pressure induces the H_{II} - L_{α} phase transition [2], and that for increasing DOPC concentration, the transition occurs at lower pressure. This behavior confirms the tendency of DOPC to form lamellar phase. This effect is combined with a larger coexistence region, in which inverted hexagonal and lamellar phases are both present.

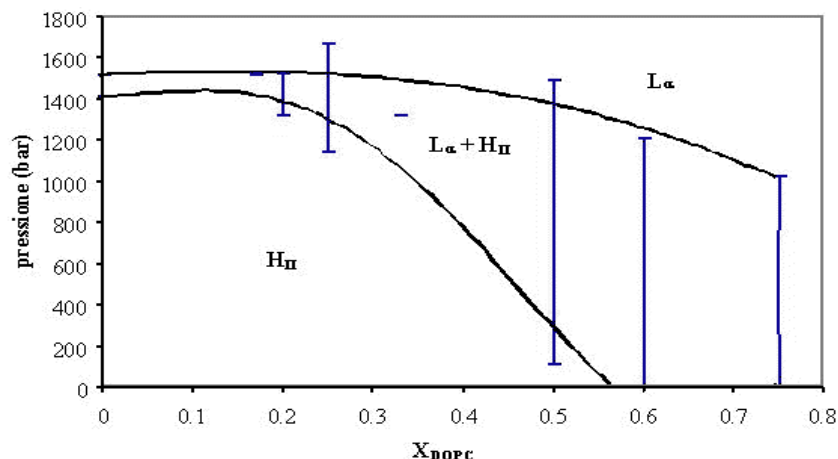


Figure 2. Phase diagram of the lipid mixture-water-tetradecane system at room temperature.

The unit cell dimension of H_{II} phase, measured at ambient pressure, increases as DOPC is added to the mixture (see Figure 3), likewise the L_{α} unit cell dimension, measured at the phase transition, shows a strong dependence on the lipid composition of the mixture.

These data confirm a general effect on the molecular characteristic of the hydrostatic pressure. At all the investigated concentration, high pressure increases the thickness of the hydrocarbon lipid layer, while the area at the lipid-water interface decreases: as a consequence, the curvature of the polar-apolar interface reduces so that the lamellar phase becomes more stable.

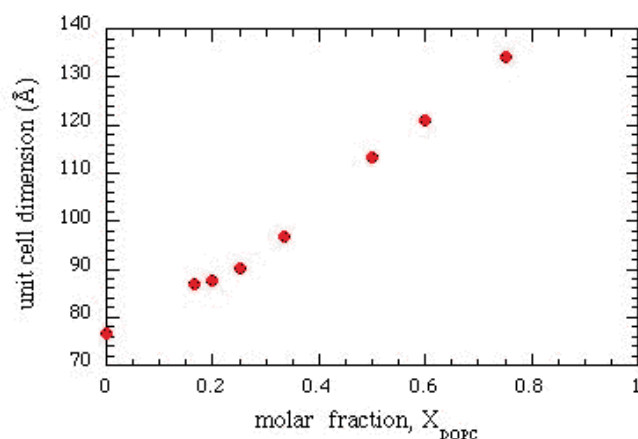


Figure 3. DOPC concentration dependence of the unit cell dimensions of the hexagonal phase in lipid mixture prepared in excess water and tetradecane at room temperature and ambient pressure

References:

- [1] R.P. Rand, N.L. Fuller, S.M. Gruner and V.A. Parsegian. Membrane curvature, lipid segregation, and structural transitions for phospholipids under dual-solvent stress. *Biochemistry*. **29** (1), 76-87 (1990)
- [2] M. Pisani, T. Narayanan, G.M. Di Gregorio, C. Ferrero and P. Mariani. Compressing inverse lyotropic systems: structural behavior and energetics of dioleoyl phosphatidyl ethanolamine. *Phys. Rev. E*, **68**, (2003)

X-RAY DIFFRACTION OF MIXED CHAIN PHOSPHATIDYLETHANOLAMINE AND PHOSPHATIDYLGLYCEROL

B. Pozo Navas, E. Sevcsik, G. Deutsch, H. Amenitsch and K. Lohner

Institute of Biophysics and X-ray structure Research. Schmiedlstraße 6. A-8042 Graz, Austria

Liposomes of PE and PG, combined at selected molar ratios, have been already described as simple models to mimic certain bacterial membranes, since both are the most abundant phospholipid species in bacterial membranes [1]. At certain ratios these mixtures constitute a model system for the cytoplasmic membrane of both Gram-negative and Gram-positive bacteria, which serve as basis for other investigations related to membranes. For example, phospholipid models consisting of mixtures of various lipid components mimicking bacterial and mammalian cell membranes are of interest to study the interaction of antimicrobial peptides, in order to gain insight into their specificity towards particular lipid components [2].

The aim of this investigation was to determine the structures of the mixtures of 1-palmitoyl-2-oleoyl-sn-glycero-3-phosphoethanolamine (POPE) and 1-palmitoyl-2-oleoyl-sn-glycero-3-[phospho-rac-(1-glycerol)] (Na salt) (POPG) as a function of the temperature, i.e. in the gel (L_{β}) and liquid-crystalline (L_{α}) phase. At the SAXS beamline samples were investigated using X-ray diffraction and differential scanning calorimetry simultaneously. This set up allows the measurement at temperatures below zero, which are necessary for the characterization of the mixtures rich in POPG, since they have a low chain melting temperature.

The information obtained from the on- and offset temperatures of the thermograms will be the input parameters for the regular solution theory to simulate the solidus and liquidus coexistence lines of the phase diagram of the POPE/POPG mixtures. Furthermore, X-ray diffraction revealed distinct phase regions composed of vesicles differing in lamellarity and correlation of the lipid lamellae.

References:

- [1] Lohner, K., Latal, A., Degovics, G., Garidel, P. (2001): Packing Characteristics of a Model System Mimicking Cytoplasmic Bacterial Membranes. *Chem. Phys. Lipids* **111**, 177-192.
- [2] Lohner, K. The Role of Membrane Lipid Composition in Cell Targeting of Antimicrobial Peptides. in: "Development of Novel Antimicrobial Agents: Emerging Strategies", (Ed. K. Lohner), Horizon Scientific Press, Wymondham, Norfolk, U.K. (2001) pp. 149-165.

THE NON-EQUILIBRIUM FORMATION OF THE CUBIC DIAMOND PHASE IN MONOOLEIN/WATER SYSTEMS

M. Rappolt¹, H. Amenitsch¹, G. Pabst¹, P. Laggner¹, M. Almgren², G.M. Di Gregorio³ and P. Mariani³

- 1.) Austrian Academy of Sciences, Institute of Biophysics and X-ray Structure Research, Schmiedlstraße 6, A-8042 Graz, Austria
- 2.) Department of Physical Chemistry, Uppsala University, O Box 532, 75121 Uppsala, Sweden
- 3.) Dipartimento di Fisica e Ingegneria dei Materiali e del Territorio, Università Politecnica delle Marche, Ancona, Italy

Lipid/water systems display a rich polymorphism, which in this extent is not shared with any other class of chemical compounds. However, concerning cell membranes only the fluid phases which are stable under excess of water conditions may be considered biological relevant, namely, the bicontinuous cubic diamond phase Q224, the micellar cubic phase Q227, one lamellar and the inverted hexagonal phase. The biological significance of the spongy structure of the Q224 phase has been discussed widely (for a review see [1]), e.g. in the action of lipolytic agents and membranes fusion. Further, the diamond type phase exists as cubic membranes in mammalian cells, but also gyroid type foldings of the membrane (Q230) have been reported. Finally, bicontinuous cubic phases have received increasing attention in recent years, because of their potential to serve for the crystallization of membrane-proteins. In time resolved X-ray studies we investigated the non-equilibrium formation of the cubic diamond phase in monoolein/water systems. The analysis of this data is in progress.

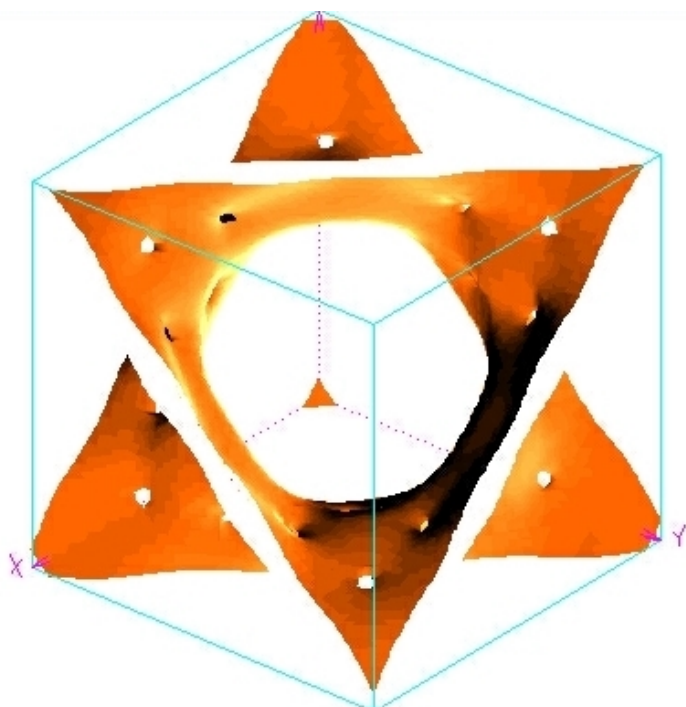


Figure 1. Electron density map of monoolein/water at room temperature. The surface plot highlights the minimal surface of the cubic phase Q224 within the unit cell, i.e. the surface in orange shows the mid-plane region of the bilayer.

References:

- [1] V. Luzzati. Biological significance of lipid polymorphism: the cubic phases. *Current Opinion in Structural Biology* 7: 661-668 (1997).

COMBINED MICROSAXS-MICROSCOPY STUDIES ON COLLOIDAL DISPERSIONS

M. Rappolt¹, H. Amenitsch¹, P. Laggner¹, D.-A. Cojoc², E. Ferrari², and E. Di Fabrizio²

1.) Austrian Academy of Sciences, Institute of Biophysics and X-ray Structure Research, Schmiedlstraße 6, A-8042 Graz, Austria

2.) TASC-INFN National Laboratory, Strada Statale 14, Km 163.5 in Area Science Park, 34012 Basovizza (Trieste), Italy

In general the superstructure of colloidal dispersion such as liposomal suspensions can be widely characterised by small angle X-ray scattering SAXS [1]. However, the recorded scattering pattern displays only an average structural picture of the investigated sample, i.e. in a typical experiment with a beam size of 0.5 mm^2 about one million individual vesicles give rise to the scattering signal. Thus, topological particularities within the dispersion can not be resolved. Plenty of interesting questions concerning details on the microscopic level can not be answered by the standard SAXS method. Only with the set-up of a micro-focus it is feasible to 'look' at individual parts of the sample [2], and distinguish different domains in the sample. In figure 1A for instance one can see hexagonal phase regions (1) coexisting with liposomes (2), and in figure 1B a cluster of liposomes is depicted.

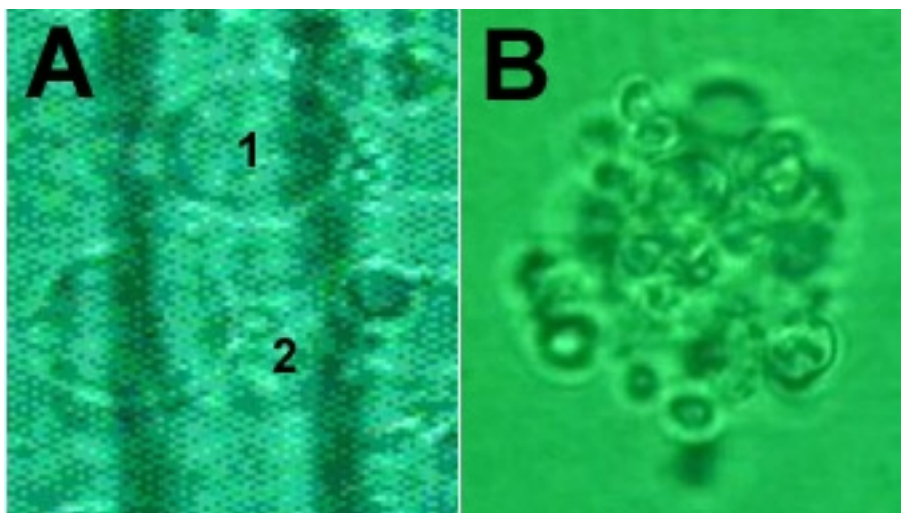


Figure 1.

A: Snapshot of a phospholipid dispersion during the lamellar-hexagonal phase transition.

B: A liposome cluster is seen. The magnification in both pictures is about 1000.

Out of the enormous variety of different colloidal systems, which may be interesting to be investigated with the combined microSAXS-microscopy method, we limited ourselves in a first pilot stage on the topological analysis of multilamellar vesicle suspensions only. Our main goal is to show that it is possible to individualise different microscopic domains and characterise each their nano-structural composition by SAXS.

References:

- [1] J. Seddon and G. Ceve. *In: Phospholipid handbook*. Ceve, G. (edt.). Marcel Dekker Inc., New York. pp. 403-454 (1993).
- [2] E. Di Fabrizio, F. Romanato, M. Gentili, S. Cabrini, B. Kaulich, J. Susini and R. Barrertt. High efficiency multilevel zone plates for keV X-rays”, *Nature* **40**: 895-898 (1999).

LAYER AND AGE SPECIFIC TENSILE TESTING OF HUMAN CARDIAC ARTERIES

F. Schmid^{1,2}, G. Sommer¹, H. Amenitsch², M. Rappolt², P. Laggner², G.A. Holzapfel¹, C.A.J. Schulze-Bauer¹

1.) Institute of Structural Analysis, Computational Biomechanics, Graz University of Technology, Austria

2.) Institute of Biophysics and X-ray Structure Research, Austrian Academy of Sciences, Graz, Austria

The understanding of the static and dynamic mechanical behaviour of the different layers of an artery is an essential prerequisite for the design of a constitutive computer model. It is generally agreed on that collagen fibres are the mechanically most important constituent of arteries. Hence the coupling between the nano-structural orientation of the collagen fibres and the direction of the applied macroscopic load yields important information for simulation. This study is using SAXS (Small Angle X-ray scattering) to determine the orientation and stretch of collagen fibres during tensile testing.

The samples are prepared right after autopsy of the patients of different ages. The arteries are excised, separated into their layers (intima (inner), media and adventitia) and cut into stripes of different orientation. A custom made tensile testing apparatus is used for uniaxial stretching (continuously in-/decreasing load, jump-relaxation) of the samples. Simultaneously 2D diffraction patterns are recorded.

First results of the evaluation of an adventitial sample are shown in Figures 1–3. For this sample 190 images have been taken during an in- and decrease cycle. The intensities for the 3rd order peak were integrated and fitted to a Gaussian.

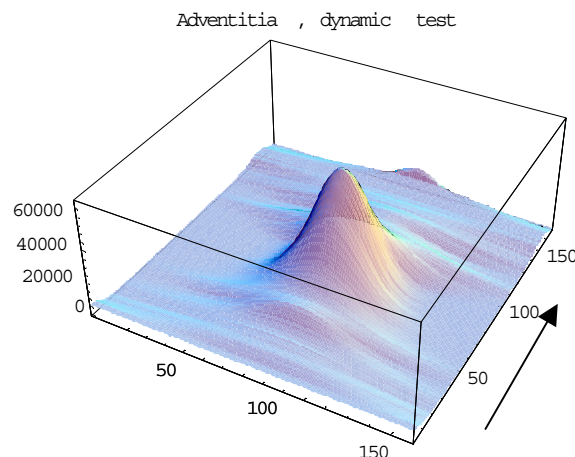


Figure 1: Fibre orientation over time (arrow), fitted to a Gaussian.

The result – representing the change of fibre orientation over time¹, indicated by the arrow – is shown in Figure 1. The higher and sharper the peak, the more fibres are aligned in the same direction at a certain time. This is even better demonstrated by Figure 2, which shows the azimuthal peak sigma over time. Again, it is clearly seen, that order increases towards higher elongation and decreases at release. Figure 3 is a cut through the centre of the Gaussian fits, indicating the intensity maxima.

¹ Actually the graphs do not show time but single frames. One frame equals roughly 10 seconds.

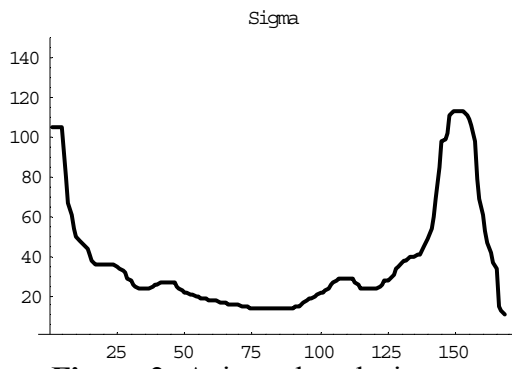


Figure 2: Azimutal peak sigma.

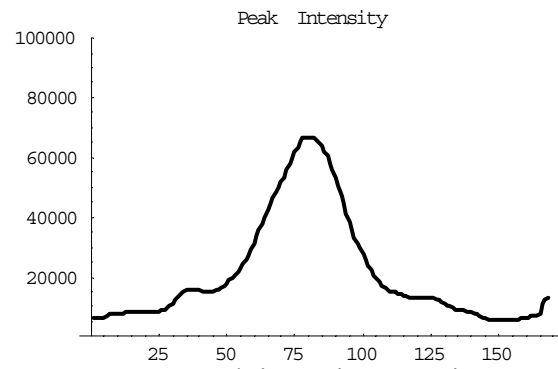


Figure 3: Peak intensity over time.

Further evaluation including the stretch of the collagen fibres during elongation are still in progress.

3. Chemistry

TIME RESOLVED “IN SITU” SAXS STUDY OF THE SYNTHESIS OF SBA-1, SBA-2 AND SBA-3 SILICA

N. Baccile¹, M. Lindén², A. Riley³, S. Tolbert³, H. Amenitsch⁴ and F. Babonneau¹

- 1.) Chimie de la Matière Condensée, Université Pierre et Marie Curie, 4 place Jussieu, 75252 Paris, France
- 2.) Department of Physical Chemistry, Åbo Akademi University, Porthaninkatu 3-5, FIN-20500 Turku, Finland
- 3.) Department of Chemistry and Biochemistry, University of California, Los Angeles, California 90095, USA
- 4.) Institute of Biophysics and X-Ray Structure Research, Austrian Academy of Sciences. Schmiedlstr. 6, A 8042 Graz, Austria

During the last ten years, many groups developed novel mesostructured inorganic-organic hybrid materials by combining sol-gel chemistry and the structuring effect of self assembling surfactants. The structure directing agents that have been used so far range from cationic to anionic and non-ionic surfactants having different forms and dimensions and whose interaction with the inorganic network varies according to their polar head group charge and pH [1,2]. The control of the final nanostructure can be achieved through a large number of experimental parameters (solution pH, surfactant type, operating temperature conditions and presence of organic solvents). The samples can be shaped as powders with controlled size, thin films or monoliths. The large versatility of this synthetic process to access materials with highly ordered porosity makes it highly attractive in a large range of application fields (catalysis, chromatography, drug delivery, sensing...).

In 1996 Huo and al. [3] demonstrated the large influence of synthetic parameters to tune the final mesophase structure. In particular, they pointed out the influence of the surfactant molecule geometry on the well-known micellar packing parameter “g”, introduced by Israelachvili et al. in 1976 [4]. A number of single chain, gemini and divalent cationic surfactants have been explored as structure-directing agents under various conditions and led to the synthesis of the SBA-type silicas: SBA-1 (Pm3n micellar cubic phase), SBA-2 (P6₃/mmc micellar hexagonal phase) and SBA-3 (P6m hexagonal).

Based on this study, we have followed by “in-situ” time resolved SAXS experiments, the synthesis from solution precipitation, of the SBA-1, SBA-2 and SBA-3 mesostructured silica powders using three cationic surfactants with different polar head groups (Table 1). Our objective was to see how the organization of the mesostructure develops, depending on nature of the surfactant polar head group.

Table 1. Description of the surfactant used in the SBA synthesis

Phase	Surfactant
SBA-1	CTEAB CH ₃ -(CH ₂) ₁₅ - N ⁺ (CH ₂ CH ₃) ₃ , Br ⁻
SBA-2	MMG CH ₃ -(CH ₂) ₁₅ - N ⁺ (CH ₃) ₂ - (CH ₂) ₃ - N ⁺ (CH ₃) ₃ , 2Br ⁻
SBA-3	CTAB CH ₃ -(CH ₂) ₁₅ - N ⁺ (CH ₃) ₃ , Br ⁻

The SBA-1, SBA-2 and SBA-3 materials have been synthesized either under acid or basic conditions according to literature data. Fig.1 presents a comparison between the X-ray diffraction patterns of the three final dried powders. The corresponding cell parameters are: a = 44,1 Å (bidimensional hexagonal cell) for SBA-3; a = 85,2 Å (Cubic cell) for SBA-1; a = 49,3 Å and c = 81 Å for the 3D-hexagonal SBA-2, with a c/a ratio at 1,64, in agreement with a hcp unit cell.

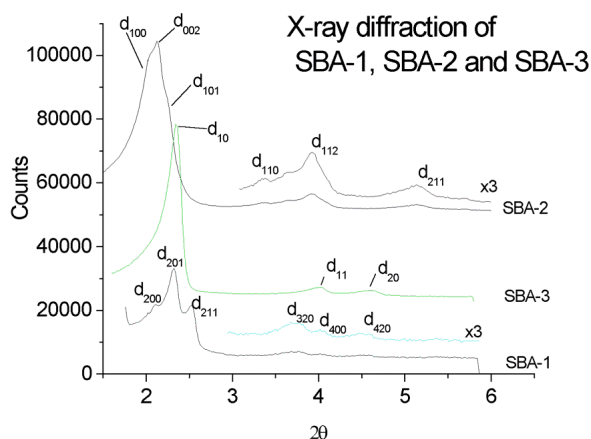


Figure 1. Comparison between the XRD patterns of SBA-1, SBA-2 and SBA-3 powders.

The time resolved experiments were performed using a batch reactor, previously described in the literature [5]. The initial solution is prepared by mixing the water, hydrochloric acid (or sodium hydroxide) and surfactant together and left under stirring during 10-15 minutes. The solution is then placed in the experimental setup. It will flow through a 1mm quartz capillary, and will be recycled by pumping it back to the batch reactor. The silica precursor (tetraethoxysilane) is added at $t=0$ when the pump and the beam are activated. The acquisition time is 1 frame per second with a maximum of 1024 frames collected for each experiments.

Fig.2-c shows the collection of the diffraction patterns for SBA-3. The lighter lines with respect to the background correspond to high intensity peaks. The presence of a high intensity peak at low values of $q = 1,5 \text{ nm}^{-1}$ and the presence of two smaller peaks at $q = 2,6 \text{ nm}^{-1}$ and $q = 3,0 \text{ nm}^{-1}$ are characteristic for a 2-D hexagonal mesophase. The mesophase formation takes place almost immediately when the white precipitate forms and the initial peak is the one corresponding to the (10) diffracting planes. The mesophase formation, in the case of SBA-3, takes place directly, without going through any other intermediate phase. This result has been already reported by Lindén et al [5]. The mechanism proposed is the cooperative self-assembly between the surfactant in solution and the silicon oxy-hydroxide oligomers in solution.

Fig.2-a shows the diffraction patterns for SBA-1, which has a final cubic Pm3n structure. The mesophase, just as before, forms directly; however, in contrast, the three low angle peaks appear simultaneously. One can however notice that a broad, diffuse signal is present prior to the appearance of the 3 peaks, in the same q -range. There is a slight cell contraction between the initial cubic cell ($a = 99,2 \text{ \AA}$) and the final one ($a = 86,0 \text{ \AA}$) certainly due to the higher degree of silica condensation around the micelles in the final material.

Fig.2-b shows the results for SBA-2, which is obtained, no longer with a monovalent, but with a divalent surfactant. Once again, the mesophase forms directly after 240 seconds circa. The appearance of all the diffraction peaks is quasi-simultaneous, even if the large overlap of the peaks at low q -values prevents to clearly distinguish them individually.

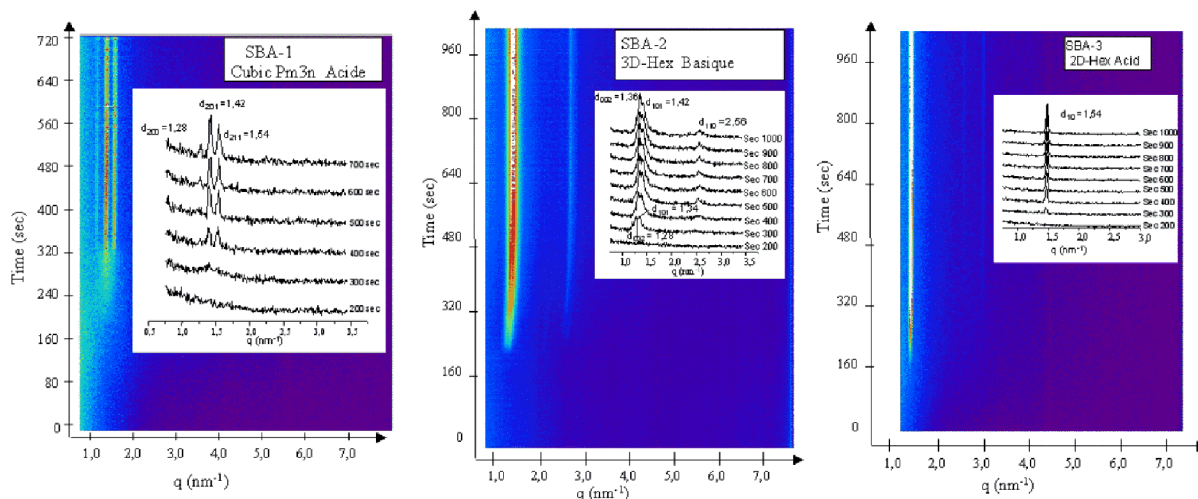


Figure 2. a) Time resolved SAXS diagrams of mesoporous silica SBA-1. b) Time resolved SAXS diagrams of mesoporous silica SBA-2. c) Time resolved SAXS diagrams (seen parallel to the “counts” axes) of mesoporous silica SBA-3. All pictures are represented parallel to the “counts” axes. In the upper right end corner of each figure, it is shown the sequence of diffraction diagrams at interval of 100 s each.

In conclusion, we have investigated the formation of SBA-1, SBA-2 and SBA-3 mesostructured silicas by means of time resolved in-situ SAXS experiments. In all the cases, the mesophase forms directly without any intermediate phase. Interestingly, one can notice that only for SBA-1, a diffuse halo in the same q -range appears prior to the diffraction peaks. This might suggest different self-assembly mechanisms that are currently under investigation.

References:

- [1] G. J. de A. A. Soler-Illia, C. Sanchez, B. Lebeau, and J. Patarin, *Chem. Rev.* **102**, 4093 (2002)
- [2] J. Patarin, B. Lebeau, R. Zana, *Curr. Opin. Colloid Interface Sci.* **7**, 107 (2002)
- [3] Q. Huo, D. Margolese, D. Stucky, *Chem. Mater.* **8**, 1147 (1996)
- [4] J. N. Israelachvili, D. J. Mitchell, B. W. Ninham, *J. Chem. Soc. Faraday Trans. I* **72**, 1528 (1976)
- [5] P. Agren, M. Linden, J.B. Rosenholm; R. Schwarzenbacher, M. Kriechbaum, H. Amenitsch, P. Laggner, J. Blanchard, F. Schueth, *Journal of Physical Chemistry B* **103** (1999) 5943-5948.

COCRYSTALLIZATION DYNAMICS IN LAMELLAR SYSTEMS OF POLYMER BLENDS IN VICINITY OF MELTING TEMPERATURE

J. Baldrian¹, M. Steinhart¹, A. Sikora¹, J. Kasparová², H. Amenitsch³, S. Bernstorff⁴

- 1.) Institute of Macromolecular Chemistry, Academy of Sciences of the Czech Republic, Heyrovsky Sq.2, 16206 Prague, Czech Republic
- 2.) Faculty of Chemical Technology, University of Pardubice, Studentská 95, Pardubice, Czech Republic
- 3.) Institute of Biophysics and X-ray Structure Research, Austrian Academy of Sciences, Schmiedlstr. 6, 8042 Graz, Austria
- 4.) Sincrotrone Trieste, Basovizza, 34012 Trieste, Italy

The aim of this project was to study new structural phenomena appearing in two different kinds of two-component crystalline/crystalline systems: polymer/polymer and symmetrical tri-block-copolymer/polymer during crystallization at temperatures near the melting-points of the components to obtain thorough insight in the development and transformation of blends morphology and process variables. Complicated structure development in both of these technologically important systems opened questions concerning the origin of cocrystalline lamellar systems development.

PEO/PEO blends

Binary mixtures of a low-molecular-weight fractions ($M_w \sim 2000, 3000, 4000$ and 6000 , Fluka AG – labelled as P2, P3, P4, P6) of poly(ethylene oxide) (PEO) and these polymers with a symmetrical tri-triblock copolymer PEO-*b*-PPO-*b*-PEO ($M_w \sim 3340-1760-3340$, Pluronic 6800 - P68, BASF) of 8/2, 6/4, 4/6 and 2/8 compositions were prepared. The copolymer was chosen because its PEO tails have M_w close to the M_w of neat PEO fractions used. The middle poly(propylene oxide) (PPO) block is amorphous. The blends were studied by the time-resolved SAXS/WAXS method on the synchrotron and by DSC. Measurements were performed in the course of cooling from the melt at $60\text{ }^\circ\text{C}$ to $35\text{ }^\circ\text{C}$ with the rate of $2\text{ }^\circ\text{C}/\text{min}$ and subsequent heating from $35\text{ }^\circ\text{C}$ to $65\text{ }^\circ\text{C}$ with the rate of $0.5\text{ }^\circ\text{C}/\text{min}$. Different rates were chosen for better mapping of structure changes near to melting points of the components.

Crystallization proceeds during cooling and heating in two steps:

- | | |
|--------------------|--|
| <i>First step</i> | very small changes of lamellar structure |
| <i>Second step</i> | steep thickening of lamellae near T_m |

Starting lamellar structures in the blends reflect molecular weights and crystallization behavior of components. Molecular-weight ratio 1:2 in blends P2/P4 and P3/P6 (Fig. 1) causes crystallization of lamellae, in which extended form (EC) of shorter and 1F of longer chains cocrystallize. Since the length of extended P2 (EC) molecules (P2 chains can not fold) is comparable with thickness of non-integrally folded chains (NIF) of P3 lamellae, P3 reveal strong tendency to form NIF lamellae at the beginning of crystallization. For this reason starting cocrystalline lamellae in P2/P3 blends consist of chains of the described conformations. Strong tendency of P3 to form NIF lamellae and P4 to form stable 1F lamellae cause that they cocrystallize at the beginning of crystallization as a mixture of these conformations. The lamellae are not very stable, since later they recrystallize to lamellae, where both components are in EC form. This behavior is dependent on composition.

In all studied polymer/polymer blends strong thickening of lamellar periodicity starts near T_m of components (Fig.1). In many cases the periodicity exceeds lengths of longest chains in

studied blends. Crystallinities in this temperature region strongly decrease (Fig.2) and DSC shows only one broad melting peak. These structure changes can not be completely explained by recrystallization. Thickening of lamellae near the melting points is at least partly caused by partial melting of lower-molecular-weight component and by diffusion of melted chains in the interlamellar amorphous regions.

F68/PEO blends

Blends copolymer/polymer have different behavior. Cocrystalline structures are not so well developed as in the case polymer/polymer. The structure of blends can be lamellar and hexagonal. Also the thickening of lamellae during heating does not proceed so quickly. This effect could be caused by the facts, that the copolymer chains are longer than the chains of the second components and the presence of amorphous middle block PPO of copolymer which reduces relatively strongly the crystallinity. The crystallinity of copolymer is around 45% in comparison with the values for more pure PEO, which are near 80 % (Fig.2). Thickening of lamellae near the melting points can be explained similarly to the case of polymer/polymer blends.

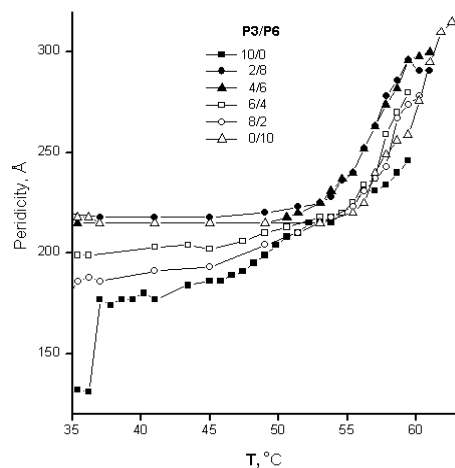


Figure 1. Temperature changes of lamellar periodicities in P3/P6 blends.

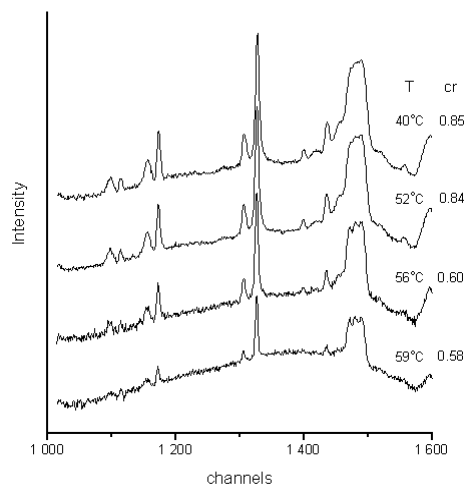


Figure 2. Changes of crystallinity in P3/P4 blend of 6/4 composition during heating.

HIGH PRESSURE PHASE TRANSITION OF ALCOHOL INTERCALATED ZIRCONIUM PHOSPHATE

L. Benes¹, V. Zima¹, K. Melánová¹, M. Steinhart², M. Kriechbaum³, H. Amenitsch³, S. Bernstorff⁴

- 1.) Joint Laboratory of Solid State Chemistry of Institute of Macromolecular Chemistry of Academy of Sciences and University Pardubice, Studentská 84, Pardubice, Czech Republic
- 2.) Department of Physics, University Pardubice, Studentská 84, Pardubice, Czech Republic
- 3.) Institute of Biophysics and X-ray Structure Research, Schmiedlstr. 6, 8042 Graz, Austria
- 4.) Sincrotrone Elettra, Trieste, Basovizza, 34012 Trieste, Italy

Intercalation represents a reversible insertion of mobile atomic or molecular guest species into solid layer host lattice. Intercalates of zirconium phosphate (α -Zr(HPO₄)₂·H₂O, hereafter ZrP) [1] belong among largely studied compounds. In our previous measurements on ZrP-liquid alcohol systems [2], we observed a phase transition induced by temperature changes. In this phase transition the bimolecular film of alkanols intercalated undergoes a change from an *all-trans* conformation to a conformation in which the O-C1-C2-C3 torsion angle changes from 180 to 136° during cooling the samples. This leads to the change of the alkyl chain inclination from 59.6° to 47.1°. These two phases differ in their basal spacing. Since the interlayer distance is connected with the thickness of the whole crystal a pressure dependence of the phase behavior can be expected.

Both static and time-resolved measurements were performed at the SAXS channel of the Elettra Synchrotron facility (Trieste, Italy). Further details of the high-pressure system and experimental aspects are given elsewhere [3].

The intercalates of 1-nonanol, 1-octanol and 1-decanol show different behavior. For the 1-nonanol intercalate (see Fig. 1), there is a gradual linear decrease of the basal spacing with increasing pressure at constant temperature up to a certain value of pressure, when a second phase appears. The basal spacing of this second phase also decreases with increasing pressure. Both phases are present in the area of the phase transition. For 1-octanol intercalated ZrP (Fig. 2), the basal spacing vs. pressure dependence is more complicated. At first, this dependence is linear. Just before the phase transition, a small increase of the basal spacing appears. It is followed by a steep decrease of the basal spacing of about 0.8 Å indicating a phase transition. In the intercalates containing a bimolecular film of the guest molecules with aliphatic chains which are not perpendicular to the host layers an even-odd effect can take place [4]. This effect is given by different orientations of the terminal methyl groups of the chains for even and odd numbers of the carbon atoms in the guest chains. Therefore, we can presume that the distinctly different dependence of the basal spacing on pressure in the case of the ZrP intercalate with 1-nonanol compared to the intercalates with 1-octanol and 1-decanol is probably connected with the even-odd effect.

The small increment of the basal spacing with pressure observed for the 1-octanol intercalate is very interesting. It can be caused by steric requirements of the methyl groups during the change of the angle, under which the chains are tilted to the layers, from 59.6 to 47.1°. This phenomenon was not observed for the 1-decanol intercalate, which has, like the 1-octanol intercalate, an even number of the carbon atoms in the chain.

A linear dependence of the phase transition was observed in the p-T diagrams of all three intercalates. The straight lines in the p-T diagrams have almost the same slope for all three alcohol intercalates, but differs distinctly in the temperature, at which the phase transitions occur at ambient pressure.

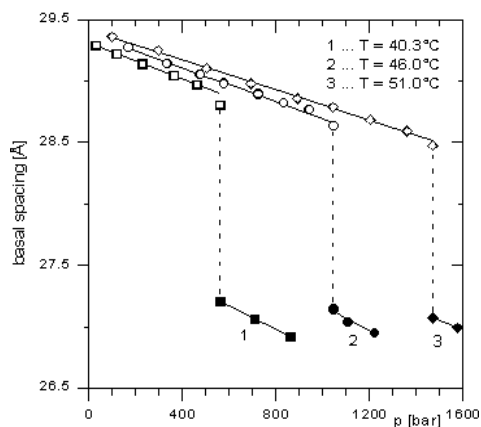


Figure 1. Dependence of basal spacing of $\text{Zr}(\text{HPO}_4)_2 \cdot 2\text{C}_9\text{H}_{19}\text{OH}$ intercalate on pressure measured at various temperatures.

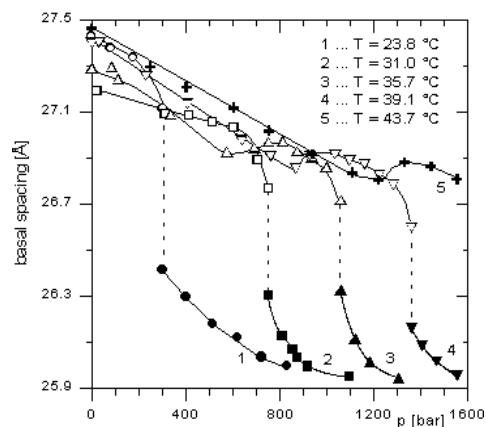


Figure 2. Dependence of basal spacing of $\text{Zr}(\text{HPO}_4)_2 \cdot 2\text{C}_8\text{H}_{17}\text{OH}$ intercalate on pressure measured at various temperatures.

Acknowledgement

This study was supported by the Grant Agency of the Czech Republic (GV 202/98/K002 and GA 202/01/0520). We would like to express our thanks to SAXS group for providing us with part of the in-house research time for our experiment.

References:

- [1] G. Alberti, U. Costantino in: J. M. Lehn (Ed), Comprehensive Supramolecular Chemistry, Vol. 7, Pergamon/Elsevier, Elmsford, 1996.
- [2] U. Costantino, R. Vivani, V. Zima, L. Benes, K. Melánova, Langmuir, 18, 1211-1217 (2002)
- [3] M. Steinhart, M. Kriechbaum, K. Pressl, H. Amenitsch, P. Laggner, S. Bernstorff, Rev. Sci. Instrum., 70, 1540-1545 (1999)
- [4] G. Lagaly, K. Beneke, Colloid. Polym. Sci., 269, 1198-1211 (1991)

TEMPERATURE DEPENDENT SAXS-MEASUREMENTS OF SUPRAMOLECULAR POLYMERS

W. H. Binder¹, C. Kluger¹, L. Petraru¹, M. Kunz¹ and D. Machl¹, V. Torma¹, H. Peterlik², S. Bernstorff³

- 1.) Institute of Applied Synthetic Chemistry, Division of Macromolecular Chemistry, Getreidemarkt 9 / 163 / MC, A-1060 Wien, Austria
- 2.) University of Vienna, Institute of Material Physics, Boltzmanngasse, A-1090 Wien, Austria
- 3.) Sincrotrone Trieste, 34012 Basovizza / Trieste, Italy

Introduction

Supramolecular polymers rely on the control of intermolecular interaction and the therefrom resulting molecular ordering of the polymeric chains into nanostructured domains. We are using an interplay between phase separation and molecular attraction to control the ordering of two different polymers (namely poly(etherketones) "PEK" and poly(isobutylenes) "PIB" bearing appropriate hydrogen bonding moieties at the chain ends. The binding constants are designed to cover the range from weak (i.e.: 25 M^{-1}) to medium (i.e.: $\sim 1000 \text{ M}^{-1}$) and strong interactions (i.e.: $> 35\,000 \text{ M}^{-1}$) (Figure 1). Details of the phase state and the experimental preparation of these pseudo-block copolymeric structures can be found in the references [1]. The main interest is the observation of the reversible nature of the hydrogen bonds, which should be broken during heating. This in turn was expected to lead to a change in nanostructure. Based on TEM-results from previous investigations [2] it was known, that there existed a nanostructure between $\sim 20 - 70 \text{ nm}$ depending on the length of the polymeric backbones. It was thus of interest to investigate the dynamic nature of the polymers upon heating, as well as the changes in their phase behavior.

Results and Discussion

Since SAXS-measurements represent the only possibility to study phase effects in the solid state by dynamic measurements in a reasonable time scale, measurements were performed at ELETTRA using a holder cell with a variable heating element, controllable with an external control element. Specimen were applied as powders in 2 mm glass capillaries, using approximately 10 mg of powdered material. The temperature was varied in steps of $20 - 60 \text{ }^\circ\text{C}$, depending on the effects observed. The measurement time for each sample was about 3 minutes, which - after equilibration of temperature - allowed a fast and steady measurement of all samples required. Figure 2 shows the temperature resolved scattering curve: At room temperature, the sample shows a clear periodicity of about 11.42 nm, which is in good correspondence to the size expected from extended polymer chains - the regularity is consistent with a lamellar-type structure, although with inhomogeneities within the phase structure. Upon heating there is little change up to a temperature of $130 \text{ }^\circ\text{C}$, indicative of a stable nanophase structures up to this temperature. At $140 \text{ }^\circ\text{C}$ the structures start to "melt", indicated by the change in periodicity, which is moving to higher values for the nanophased spacing. At $\sim 150 \text{ }^\circ\text{C}$ the periodicity is breaking down, which also corresponds to the glass transition temperature of the "hard" PEK-polymer. Upon further heating (up to $170 \text{ }^\circ\text{C}$) no changes are observed. Cooling of the sample does not lead to nanophase separation again, clearly demonstrated by the absence of the scattering peak.

The behavior can be clearly interpreted as follows (Figure 3) : At temperatures below $130 \text{ }^\circ\text{C}$ the material exists in a nanophase separated structure with little change. The hydrogen bonds (here with a binding strength of $\sim 1000 \text{ M}^{-1}$) are of sufficient strength to overcome the macrophase separation between the PEK- and PIB polymers. At temperatures higher than 130

°C the hydrogen bonds start to break, leading to an extension of the structure and – subsequently – to an increase of the repetitive nanostructured pattern within the material. At temperatures above 150 °C (the glass transition temperature of the PEK polymer) the nanostructure breaks down due to the "loosening" of the polymer chains above their glass transition temperature. The material is subjected to macrophase separation, which is irreversible due to the impossibility of the polymers to mix after cooling. The demonstrated material thus is a stimulus-responsive material, where small changes in temperature can lead to significant changes of the material structure (i.e.: the nanostructure) and the subsequent macroscopical nature of the polymer.

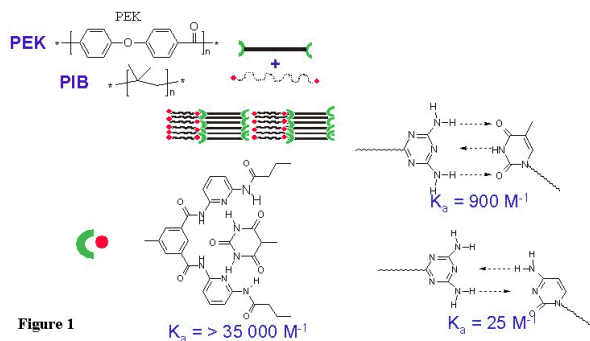


Figure 1. Schematic structure of the investigated polymers together with their hydrogen bonding elements inducing nanophase separation.

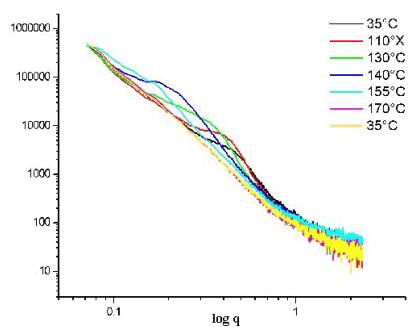


Figure 2. Temperature dependent SAXS-measurements on one polymer sample.

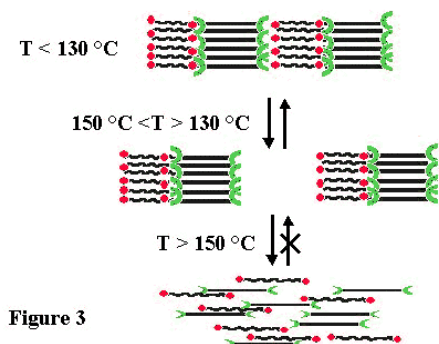


Figure 3. Schematic picture of the observed material behavior.

References:

- [1] (a) D. Farnik, C. Kluger, M. J. Kunz, D. Machl, L. Petraru, W. H. Binder, *Macromol. Symp.* in press (2004).
- (b) W. H. Binder, M. J. Kunz, C. Kluger, R. Saf, G. Hayn, *Macromolecules* 37, 1749 – 1759 (2004)
- (c) M. J. Kunz, G. Hayn, R. Saf, W. H. Binder, *J. Polym. Sci.* 42, 661 – 674 (2004)
- [2] W. H. Binder, M. J. Kunz, E. Ingolic, *J. Polym. Sci.* 42, 162 – 172 (2004)

SAXS ANALYSIS OF AEROSOL GENERATED MESOPOROUS PARTICLES

C. Boissiere¹, D. Grosso¹, H. Amenitsch², A. Coupé¹, N. Baccile¹, C. Sanchez.¹

1) LCMC, Université Pierre et Marie Curie, 4 place Jussieu 75252 Paris Cedex 5, France.

2) Institute of Biophysics and X-ray Structure Research, A.A.S., Schmiedlstr. 6, 8042 Graz, Austria

In order to understand and to have a better control on Evaporation Induced Self Assembly in spray drying, [1] it is of paramount importance to be able to follow *in situ* the structuration of the spherical particles in the carrying gas. However, the concentration of particles in the gas phase is very low (10^7 particles ($6 \mu\text{g}$ dry matter) per cm^3 , apparatus nominal value). Therefore, to reach a sufficiently high sensitivity, *in situ* SAXS characterization was performed using high flux (8 keV) third generation synchrotron (ELETTRA-Italy). The experimental setup shown in Figure 1 is composed of the aerosol generator (TSI 3076) from which drying droplets ($1 \mu\text{m}$ initial mean diameter) are carried by dry air ($3 \text{ l}\cdot\text{min}^{-1}$) into an evaporation chamber first, followed by an oven and a X-ray transparent cell. The amount of matter analysed was raised to $5\cdot 10^{-8}$ g by lengthening the sampling cell to 70 mm (optimised distance to conserve a good resolution). Residence time of aerosol into the evaporation chamber was modulated from 0 to 270 s at 25°C by varying its volume. Further evaporation and stabilisation took place in the heater at various temperatures ranging from 25°C to 500°C (2.5 s heating time). This thermal treatment is critical because it causes the hardening of the particle surface, preventing their coalescence. Depending on the system, a minimum heating temperature comprised between 125 and 250°C is required.[2,3] The initial solution contains CTAB:TEOS:H₂O:EtOH:HCl (molar ratio 0.14:1:5:20:0.13).

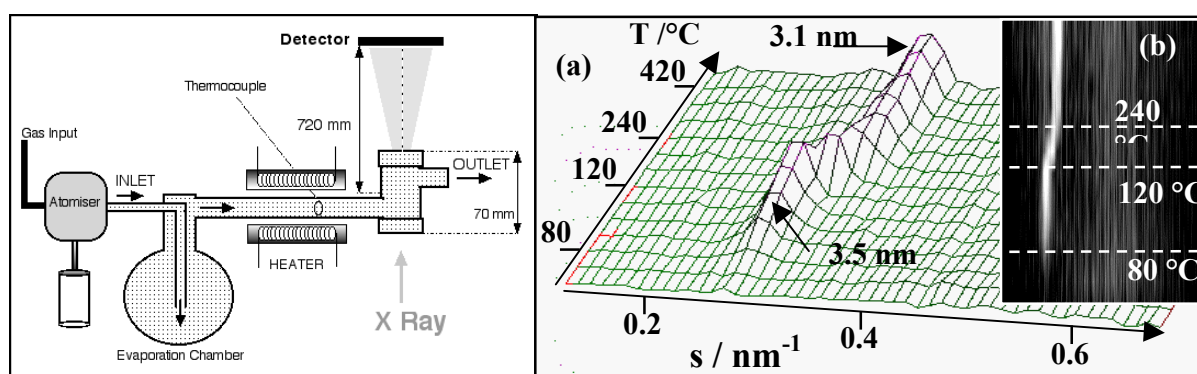


Figure 1. (a) Scheme of the experimental set-up and (b) scattering signal obtained versus the temperature within the oven.

In situ SAXS experiments were performed by progressively increasing heating temperature up to 500°C (100 s acquisition time). In the typical temperature resolved SAXS diagram shown in Figure 1(b), the low quantity of analysed matter did not allow to observe higher order correlation peaks. The order appeared above 80°C . At higher temperatures, the correlation peak shifted systematically to higher angles and remained at a fix angle above 250°C . This shift may have two origins: phase transition and/or shrinkage. Indeed, epitaxial cubic \leftrightarrow 2D hexagonal phase transition, observed when the same solution is deposited in thin films, [4] can explain this shift. In addition, it is likely that high temperature induces shrinkage by evaporation-condensation. It is important to emphasise that organisation occurs above 80°C , whatever the resting time in evaporation chamber, suggesting that temperature-assisted evaporation is one of the critical factor in this process. Exactly the same shift is observed for water rich systems, except that the final structure is less ordered and the

mesoorganisation is present from 25°C. As a result, the mesostructuration is influenced by the solvent nature and its evaporation rate which is enhanced at high temperature.

In the present aerosol process, the concentration of particles in the carrying gas is fixed, suggesting that evaporation stops when equilibrium in diffusion is reached. Since temperature greatly influences the evaporation rate through a variation of vapour pressure, chemical composition of the particle inside the heater is temperature dependant. Indeed, saturated vapour pressures of pure ethanol and water at 26°C are 0.09 and 0.033 atm. respectively, and increase to 1.00 and 0.47 atm. at 80°C. Because no organisation is observed before 80°C with ethanol rich systems, one expect the evaporation to be not completed before the heater and thus the mesostructuration to be promoted by the fast and almost total departure of ethanol at, and above, 80°C. This structuration is therefore allowed by elimination of the ethanol co-surfactant perturbing effect, concomitantly with the increase of medium polarity. [5] On the other hand, the lower saturated vapour pressure of water and its strong interactions with silica and CTAB polar head groups make it more difficult to evaporate than ethanol. The residual amount of water at 80°C promotes self-assembly.[6] This effect is confirmed for the water rich system, where the meso-ordering readily takes place at room temperature, as a result of the high water to ethanol ratio. Final particles prepared from alcohol rich solution exhibit better organisation than those prepared from water rich solution. Since a competition between condensation and self-assembly describes the EISA process, this lower order is due to a higher degree of silica condensation, favored in aqueous medium, which prevents complete self assembly into highly ordered structure.[7]

The self-assembly of aerosol generated templated particles is controlled by the diffusion of water and ethanol out of the particles during drying. After the first evaporation step, the proportion of water and ethanol that remains within the wet particles depends on the initial solution composition and on the corresponding saturated vapour pressures. During the following thermal treatment, the latter constants increase with the temperature, inducing further evaporation. The meso-ordering was observed from room temperature for water rich systems, and from 80°C for ethanol rich systems, suggesting that the self-assembly requires the total elimination of ethanol but the presence of a slight amount of water, which can be achieved by adjusting the temperature. After self-assembly, initial structures obtained with all studied systems, undergo phase transition and/or shrinkage at higher temperatures, suggesting that the structure is still flexible.

We demonstrate in this work that the critical parameters are both chemical and processing in nature and must be perfectly controlled. This *in situ* SAXS experiments shed a lot of light on the complex mechanisms occurring at the curved hybrid interfaces of spray-dried droplets during their mesostructuration, and open a land of possibilities for the reproducible design of inorganic or hybrid spheres having hierarchical structure.

References:

- [1] Y. Lu, H. Fan, A. Stump, T. L. Ward, T. Rieker, C. J. Brinker, *Nature*, 1999, **398**, 223.
- [2] D. Grosso, G. J. A. A. Soler-Illia, E.L. Crepaldi, C. Sanchez, *Adv. Funct. Mater.*, 2003, **13**, 37.
- [3] M. T. Bore, S. B. Rathod, T. L. Ward, A. K. Datye, *Langmuir*, 2003, **19**, 256.
- [4] D. Grosso, F. Babonneau, G. J. A. A. Soler-Illia, P.A. Albouy, H. Amenitsch, *Chem. Comm.*, 2002, 748.
- [5] K. Fontel, A. Khan, B. Lindstrom, D. Maciejwaska, S.P. Puang-Ngern, *Colloid and Polym. Sci.*, 1991, **269**, 7
- [6] F. Cagnol, D. Grosso, G. J. A. A. Soler-Illia, E. L. Crepaldi, F. Babonneau, H. Amenitsch, C. Sanchez, *J. Mater. Chem.*, 2003, **13**, 61.
- [7] D. Grosso, F. Babonneau, P.A. Albouy, H. Amenitsch, A.R. Balkenende, A. Brunet-Bruneau, J. Rivory, *Chem. Mater.*, 2002, **2**, 931.

PRENUCLEATION CLUSTER FORMATION AND NUCLEATION PROCESS IN SUPERSATURATED SOLUTIONS OF SMALL ORGANIC MOLECULES

S. Chattopadhyay¹, D. Erdemir², H. Amenitsch³, J.M.B Evans², C. U. Segre^{1,4},
A. S. Myerson²

- 1.) MR-CAT, Advanced Photon Source, Building 433B Sector 10, Argonne National Laboratory, 9700 South Cass Avenue, Argonne, Illinois 60439, USA
- 2.) Department of Chemical Engineering, Illinois Institute of Technology, Chicago, Illinois 60616, USA
- 3.) Institute of Biophysics and X-Ray Structure Research, Austrian Academy of Sciences, Strada Statale 14, 34012 Basovizza, Italy
- 4.) Biological, Chemical and Physical Sciences Department, Illinois Institute of Technology, Chicago, IL 60616, USA

Crystallization, especially that of small molecules from their supersaturated solutions, is not yet fully understood though the process is frequently used for synthesis and purification of industrially important chemicals such as pharmaceuticals, explosives, dyes and photographic materials. The early stages of the formation of the particles from solution can play a decisive role in determining the properties of the solid in its final state so it is important to gain a full understanding of the nucleation phenomena in order to have a control on the shape, size, morphology, structure and the quality of the crystals. Previous works focused on obtaining evidence on existence of molecular clusters in supersaturated solutions and structural data on the growth of these clusters, which ultimately would give rise to nucleation. Ginde et al. [1] showed that sodium chloride and potassium chloride exist mainly as a monomer in supersaturated solution and urea exists as an oligomer. Berkovitch-Yellin [2] hypothesized the existence of a glycine precursor in the form of cyclic dimer. Diffusion coefficient measurements by Myerson et al. [3,4], which yielded an average cluster size of 1.8 molecules in supersaturated solution, supported the hypothesis. They also observed a large decrease in the critical cluster size with increasing supersaturation. More recently, grazing incidence X-Ray measurements by Gidalevitz et al. [5] determined the centrosymmetric dimer as the essential building block for glycine grown out of water. In addition to these, recent molecular simulation studies [6-8] suggested that Classical Nucleation Theory (CNT) is not qualitatively correct and crystallization from solution is in fact a two step process, where the first step involves the formation of a liquid like cluster of solute molecules and the second step is the organization of such a cluster into an ordered crystalline structure. However, there is not much experimental evidence that supports this two-step nucleation theory. In this work, we utilized Small Angle X-ray Scattering in order to monitor the formation of clusters of small organic molecules in supersaturated solutions and to obtain an accurate description of the mechanism of nucleation.

Supersaturated solutions of urea, glycine, L-alanine and glycylglycine are chosen to be the model systems to be investigated because they have reasonable solubility values and crystallization is achieved relatively faster than the other small organic molecules. Also, the previous indirect measurements of glycine and urea cluster sizes in supersaturated solutions [1-4] provide us with reference points for the interpretation of our experimental data. Because of its small size and simple structure, glycine is used as a model compound for study of peptides and proteins. L-alanine is the smallest amino acid with a α -chiral carbon so it is useful in modeling of more complex systems.

Two different methods were used to prepare the solutions. In the first method, the chemical and deionized water were combined in test tubes with screw-on caps and the tubes were sonicated in an ultrasonic water bath at 55 °C until the chemical was completely dissolved. In the second method, the solutions were prepared by dissolving the chemical in water on a

magnetic hot plate. The samples were measured in thin walled 2 mm special glass capillaries, thermostated with KPR (Peltier heating/cooling) sample holder. The temperature control of the holder was achieved by a programmable temperature control system MTC-4.2 and temperature was monitored continuously during each experiment via a thermocouple connected to the sample holder. The samples were introduced to the beam with photon energy of 8 keV, either by transferring the solutions into the capillaries by using syringe needle and placing them in the preheated sample holder, or using an apparatus where the solution was withdrawn from a reservoir into the capillary, which had been already glued into a cuvette with vacuum tight connections and placed in the sample holder. As for the first method, the syringe and the syringe needle were placed in an oven beforehand to bring them above the solution temperature in order to prevent the solutions from crystallizing during the transferring process. The advantage of the second method was that we were able to cool the solutions rapidly and start the data acquisition immediately since the syringe motor was controlled from outside of the hutch. Supersaturation was achieved by cooling the solutions and SAXS patterns were recorded every 5 seconds with a one dimensional linear sensitive gas detector, monitoring the s-ranges between 0.014 nm^{-1} and 0.4 nm^{-1} , from the beginning of the cooling process till the samples were crystallized. An additional one dimensional PSD was used for recording diffraction in the wide angle regime, with the d-spacing range of 3.33 to 10 \AA , which allowed us to detect the time of crystallization and provided information on the polymorphic form of the crystal.

For the duration of our beamtime, we were able to perform eight successful urea runs. For the first four runs, the solutions were cooled from $50 \text{ }^\circ\text{C}$ to $2 \text{ }^\circ\text{C}$ with a cooling rate of $5 \text{ }^\circ\text{C}/\text{min}$, where the crystallization was achieved in a span of one to two hours and for the other four runs the solutions were withdrawn from a reservoir into the capillary at $2 \text{ }^\circ\text{C}$ by syringe pump, which provided relatively shorter induction times. Solutions with three different concentrations were examined in order to obtain information on the effect of supersaturation level on the cluster formation process. Among the five successful L-alanine runs, three of them were performed with a cooling rate of $10 \text{ }^\circ\text{C}/\text{min}$ and other two solutions with different concentrations were cooled from $60 \text{ }^\circ\text{C}$ to $2 \text{ }^\circ\text{C}$ with a cooling rate of $2 \text{ }^\circ\text{C}/\text{min}$. Two glycine solutions were successfully crystallized in the beam, where the cooling rate of $2 \text{ }^\circ\text{C}/\text{min}$ was used. In addition, we performed undersaturated solution measurements at different temperatures for each system in order to capture any changes in scattering intensity with decreasing temperature due to the interaction effects. This would be useful during the data interpretation; in distinguishing the changes due to the cluster formation from the interaction induced ones.

The raw data has been normalized and water background subtractions have been performed, and data analysis is currently under way to gain a better understanding of the nucleation phenomena.

References:

- [1] R. M. Ginde and A. S. Myerson ; Journal of Crystal Growth 116, 41-47 (1992)
- [2] Z. Berkovitch-Yellin; Journal of American Chemical Society 107, 8239-8253 (1985)
- [3] A. S. Myerson and Y. L. Pei; Journal of Crystal Growth 99, 1048-1052 (1990)
- [4] A. S. Myerson and Y. L. Pei; Journal of Crystal Growth 110, 26-33 (1991)
- [5] D. Gidalevitz, R. Feidenhans'l, S. Matlis and L. Leiserowitz; Angew Chem. Int. Ed. Engl. 36, 955-959 (1997)
- [6] P.R. Wolde and D. Frenkel; Science 277, 1975-1978 (1997)
- [7] J. Anwar and P. K. Boatang; Journal of the American Chemical Society 120, 9600-9604 (1998)
- [8] J. D. Shore, D. Perchak and Y.J. Shnidman; J. Chem. Phys 113, 6276-6284 (2000)

<IN-SITU> SAXS STUDY OF SIZE AND MORPHOLOGY VARIATIONS OF ZINC AEROSOL NANOPARTICLES UNDERGOING OXIDATION PROCESS

S. di Stasio¹, G. Verrengia¹, A. Onischuk², H. Amenitsch³

- 1.) Istituto Motori C.N.R., Aerosol and Nanostructures Lab, Via Marconi 8 – 80125 Napoli – Italy
E-mail: s.distasio@im.cnr.it
- 2.) Institute of Chemical Kinetics and Combustion, Siberian Branch of the Russian Academy of Sciences, 630090, Novosibirsk, Russia
- 3.) Institute of Biophysics and X-ray Structure Research, Austrian Academy of Science, Schmiedlstr. 6, 8042 Graz, Austria

Metal oxides nanoparticles powders are frequently produced by the so-called gas-phase processes, namely, by those routes that allow for the formation of solid particles within a carrier gas. The main advantages of aerosol synthesis are the good control of the process parameters, the low-cost with respect to other synthesis methods (for instance, vacuum techniques) and the possibility to control easily the physical (size, concentration, crystal growth, agglomeration, porosity) and chemical (stoichiometry, surface state) properties of the resulting products [1]. In our experiment # 200 2319 we attempted for the first time an <in-situ> SAXS investigation of gas-born nanoparticles smaller than 100 nm. The aim was to study the process of formation, aggregation and growth of the particles nucleating at high temperature from metallic vapours. The preliminary results [2,3] from TEM, XRD and Diffusion Batteries Aerosol Size Spectrometry had shown the existence of a mechanism of competition between chemical oxidation and physical evaporation of zinc nanoparticles during the exposure to the oxygen flux at high temperatures (400-1000°C). In particular, the size of oxidized particles has been found to be smaller with respect to that of the original zinc nanoparticles.

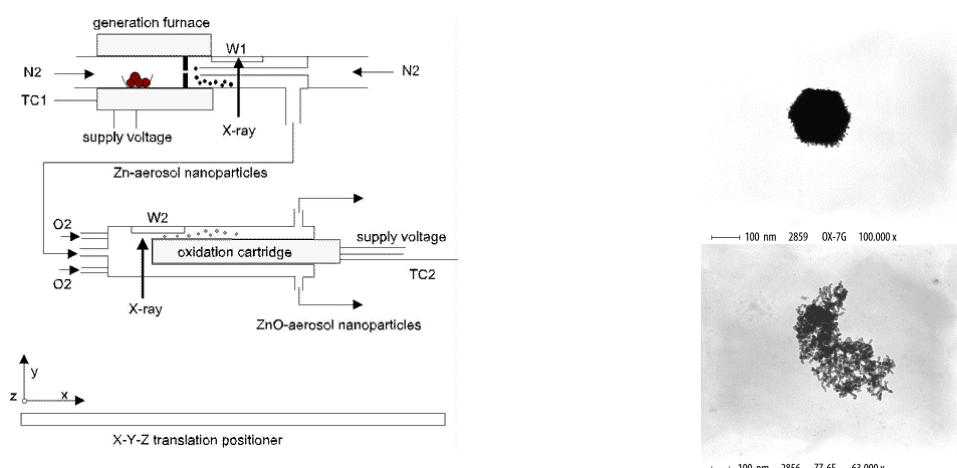


Figure 1. (left) Experimental set-up; (right-top), TEM image of a ZnO sample, $T_{\text{evap}}=490\text{ }^{\circ}\text{C}$, $T_{\text{oxid}}=1000\text{ }^{\circ}\text{C}$ (right-bottom), TEM micrograph of Zn aggregate, $T_{\text{evap}}=490\text{ }^{\circ}\text{C}$, average primary size $17\pm 4\text{ nm}$. At the surface of the main hexagonal crystal a necklace of very small particles has been formed as effect of partial re-evaporation occurring during the oxidation process. Average dimension of the primary particles is $7\pm 2\text{ nm}$

The set-up shown in Fig. 1 was composed of two quartz reactors, the first for generation, supplied with commercially available Zn grains, and the second for oxidation of zinc aerosol, which were designed on purpose by our group for the experiment at ELETTRA. Each of them

was cut carefully and equipped with 20 μm thickness Mica windows. The Zn and ZnO aerosols were probed through the pairs W1 and W2, respectively, by adjusting the XYZ-micro-positioners available at SAXS beamline. Evaporation of zinc grains was performed within a nitrogen carrier gas flux (1 Liter/min) at temperatures 440-600 $^{\circ}\text{C}$. The cooling of metallic vapours was produced by expansion through a diaphragm and contemporary dilution with fresh nitrogen. Thus, supersaturation of vapours was created and homogeneous nucleation of new born nanoparticles started up. The second reactor was supplied with oxygen (about 0.5 liter/min) and used to oxidizing Zn nanoparticles at controlled temperature (850 $^{\circ}\text{C}$). As well known, following evaporation-condensation routes the particle size, concentration and morphology do depend on the saturation vapour pressure inside the generation reactor, which is increasing with the evaporation temperature T_{evap} . In our case, at higher T_{evap} larger hexagonal prism or “butterfly” crystals were found to coexist with hierarchical aggregates of dimension several microns, which were composed by sub-units that, in turn, were cluster of smaller particles or crystals. At lower T_{evap} the condensation of Zn vapours was observed to generate Zn aggregates of primary particles, size about 10 to 50 nm, in the range 460 to 600 $^{\circ}\text{C}$, and, less frequently, larger crystals 100-300 nm. The size of the primary particles in such aggregates was found to increase with the T_{evap} from TEM. The process of oxidation was observed by TEM to induce the formation of large crystals and shrinkage of the smaller primary particles. Fig. 1(right) is an example of such a mechanism. SAXS patterns recorded at W1 for different evaporation temperatures confirmed the previous TEM result, in that smaller Zn particle were observed to form in correspondence of lower T_{evap} . Moreover, at the same evaporation temperature a slight increase of particle size was found to occur at different abscissas out of the furnace, thus demonstrating that the growth and eventually aggregation process of particles continues out of the furnace within the carrier gas flux for distance of about 1.5-2 mm, corresponding to residence times about 10 ms, depending on T_{evap} . Fig. 2(left) show the SAXS signals recorded at $T_{\text{evap}} = 577$ $^{\circ}\text{C}$ at the exit of generation oven in correspondence of different abscissas. In Fig.2(right) we report the size distribution of Zn particles obtained by the reduction of the experimental curves by GIFT software available at SAXS beamline. It is possible to observe that the radius modal peak is about 12 nm immediately at the exit of the furnace $x=0.0$ mm. Moreover, modal particle size it is augmenting at larger abscissas, which is explained as the effect of the agglomeration process which continues further up to $x=2.0$ mm. Fig. 3(left) represents the SAXS intensity recorded in correspondence of the oxidation section with $T_{\text{oxid}}=850$ $^{\circ}\text{C}$. The oxidation is obtained by a fire-rod cartridge with tip placed at $x=20$ mm. The abscissa $x_7=15.5$ mm represents the hottest section, being slightly lower the temperature at position more far from the cartridge tip. The elaboration of the signals, Fig.3(right) demonstrated that as far as particles were approach the hotter sections then the size distribution progressively exhibit modes with smaller radii. We note that the PSD observed at $x_5=5.0$ mm, relatively far from the heater tip, was identical to that observed, Fig.2(right), in the case of not-oxidized Zn particles. Thereafter, at $x_8=15.0$ mm the reduced PSD indicated the formation of smaller particles with the appearing of one mode at radius 9 nm, which further shifted towards lower values at $x_7=15.5$ mm, with radius 6 nm.

This is consistent with our previous observations at TEM and confirm the fact that the smaller particles, differently with respect to the larger ones, do undergo partial re-evaporation contemporarily to oxidation process. Intriguing is the fact that these very small particles (diameter about 5 nm, about 4000 atoms) originated from the re-evaporation process are often observed in TEM to be single crystals which preserve the hexagonal prism geometry just as the bulk (size larger than 100 nm) structural units revealed by the XRD and TEM/SEM.

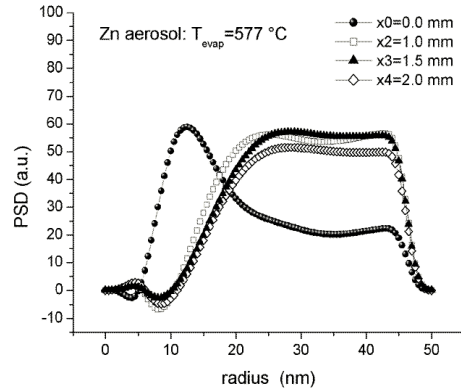
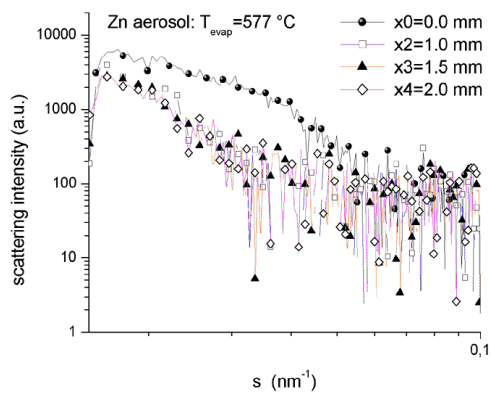


Figure 2. SAXS intensity pattern (left) and relative radius size distribution PSD (right) of Zn aerosol particles at $T_{\text{evap}}=577^\circ\text{C}$ and in correspondence of different abscissas out of the generation furnace.

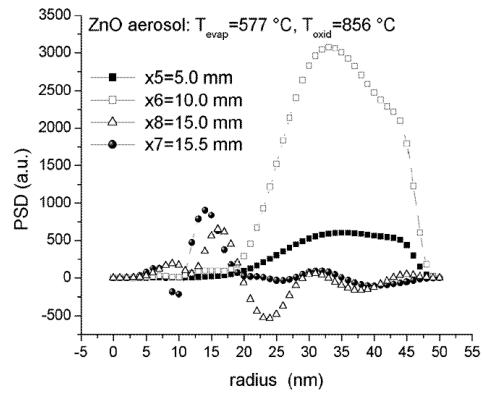
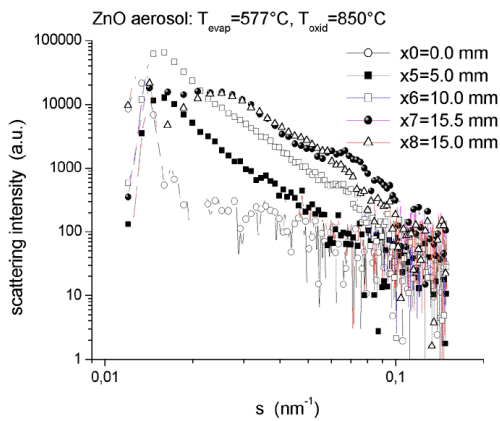


Figure 3. SAXS intensity pattern (left) and relative radius size distribution PSD (right) of ZnO aerosol particles previously generated at $T_{\text{evap}}=577^\circ\text{C}$ and oxidized at $T_{\text{oxid}}=850^\circ\text{C}$.

References:

- [1] F.E. Kruis, H. Fissan, A. Peled, *J. Aerosol Sci.* 29, 511-535 (1998)
- [2] S. di Stasio, A. Onischuk, A. Baklanov, *Proc. of the Int'l Aerosol Conf. IAC2002, Taiwan*, pp.343-344 (2002)
- [3] S. di Stasio, H. Amenitsch *J. Aerosol Sci.* In preparation (2004)
- [4] S. di Stasio, V. Dal Santo, B. Caruso, *Proc. of the PARTEC 2004, International Conf, Nurnberg*, 21.4 (2004)

ORTHORHOMBIC MESOSTRUCTURED SILICA FILM WITH HIGH THERMAL STABILITY

P. Falcaro¹, H. Amenitsch², P. Innocenzi³

- 1.) Dipartimento di Ingegneria Meccanica, settore materiali, Università di Padova, Via Marzolo 9, 35131 Padova, Italy.
- 2.) Institute of Biophysics and X-ray Structure Research, Austrian Academy of Sciences, Schmiedelstraße 6, A-8042, Graz, Austria.
- 3.) Laboratorio di Scienza dei Materiali e Nanotecnologie, Dipartimento di Architettura e Pianificazione, Università di Sassari, Palazzo Pou Salid, Piazza Duomo 6, 07041 Alghero (Sassari), Italy.

Silica mesoporous films have been synthesized via Evaporation Induced Self-Assembling (EISA) using Pluronic F-127 as templating agent. Our goal was to obtain a high thermal stability minimizing the amount of OH on the surface with a good degree of silica network densification. An optimised thermal process to stabilize the silica walls has been performed, the silica films exhibited an excellent thermal stability in a large range of temperatures and the 3D mesostructural order has been lost only for a temperature between 950°C and 1050°C [1]. The mesostructural evolution has been studied using the SAXS apparatus (in transmission for the sample as made and in grazing angle for all the other samples). An initial distorted $Im3m$ cubic mesostructure (sample as made, Figure 1) has been detected and a transition to orthorhombic symmetry has been observed.

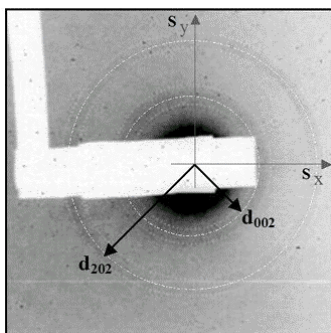


Figure 1. Transmission SAXS image of a sample as made.

In a phase transition from a body centred cubic cell ($Im3m$ in the space group) only few new symmetries are allowed and if we consider all the transitions, the possible phases that we should find are the $Fmmm$ and $Fddd$ (in the space group), which are both orthorhombic. From a computer simulation, done using the CMPR programme (B.Toby, NIST), only the $Fmmm$ diffraction patterns fit the spot positions recorded by the CCD detector (Figure 2).

The gradual change of the symmetry is strongly depending on the thermal process, it starts weakly from the sample as made and up to now it has been identified only as a distorted cubic phase without attribution with space group.

The precursor sol has been obtained adding tetraethoxysilane (silica alkoxyde), to ethanol, a reactant to hydrolyze the silicon precursor (water), an acid catalyst (HCl) and three-block copolymer surfactant (Pluronic F127) as templating agent [2].

The mesostructured silica films were deposited via dip coating in controlled conditions of humidity and temperature. All the depositions were performed at 30% RH, with a withdrawal speed of 20 cm min⁻¹ and 28°C. After the deposition the films were maintained in the deposition chamber for 10 minutes and then fired at 150°C for one hour in air. Thermal treatments at higher temperatures were performed introducing the samples directly in the oven. The firing process was done in sequence, i.e. all the samples were fired at 150°C, then at 250°C and so on, up to 1050°C.

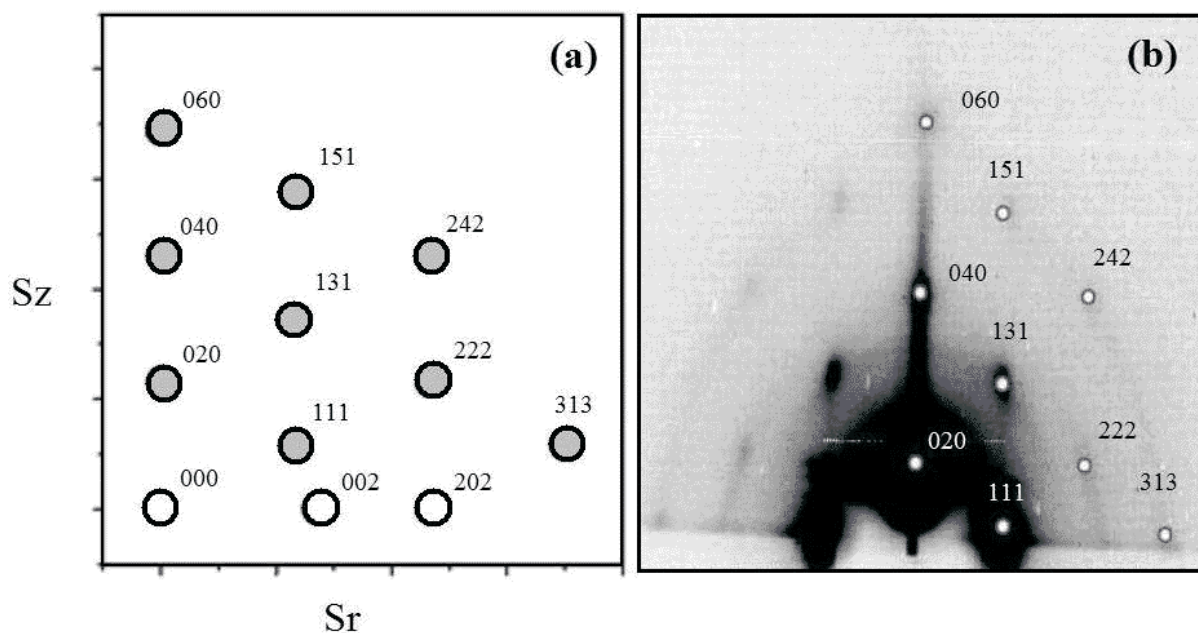


Figure 2. Comparison between CMPR simulation (a) and the recorded CCD image with high saturation to evidence the maximum spot number (b).

Using our thermal treatment, the change showed in the representation of Fig. 3 has been strongly observed at 250°C yet.

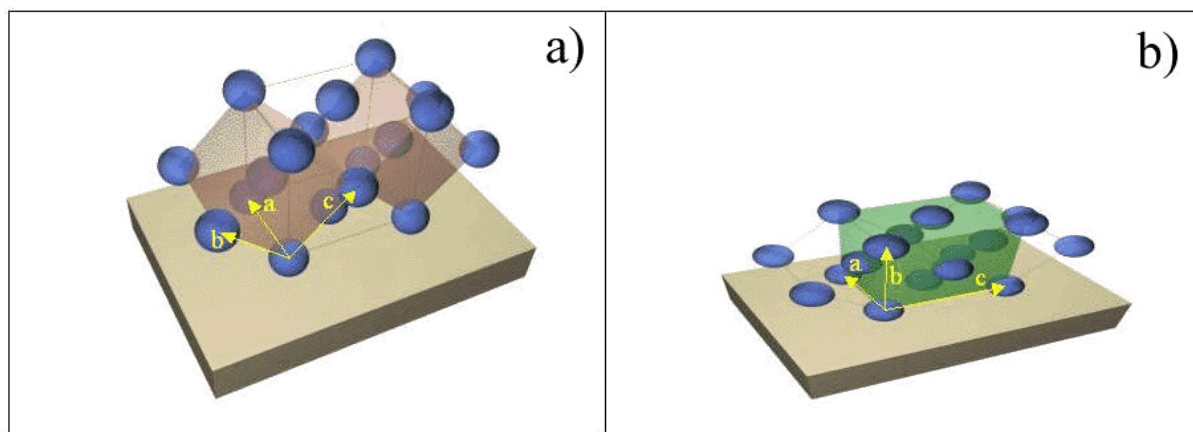


Figure 3. Symmetry change between the initial $Im\bar{3}m$ (a) and the final $Fmmm$ (b) mesophases.

Fourier transformed infrared spectroscopy has shown that the high thermal stability is correlated with a progressive strengthening of the silica structure during thermal induced polycondensation reactions and structural rearrangements of 4-fold rings present in the silica walls Figure 4.

It is interesting to note that whilst the thermal dehydroxylation of the silanol species present in hydrogen-bonded chains or silanol pairs is completed at 750°C, to eliminate the single silanols formed during dehydroxylation, larger temperatures are required. In the range of temperatures 750-950°C only isolated silanols are detected because residual isolated silanols are more difficult to remove due to the lower possibility to condense.

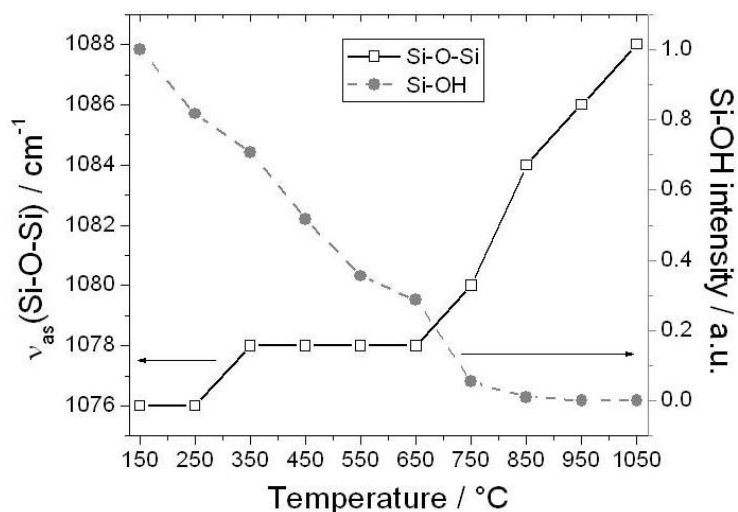


Figure 4. Change of the Si-OH and $\nu_{as}(\text{Si-O-Si})$ wavenumber as a function of the temperature of thermal treatment of the samples.

It means that 750°C with our thermal treatment is the right temperature to achieve a 3D ordered mesostructure (200, 111, 020 *Fmmm* spots are discernable), a good reticulation degree (ν_{as} Si-O-Si close to 1080 cm^{-1}), a low amount of OH group. These conditions are promising to use this kind of mesostructured materials as dielectric materials for electronic device.

References:

- [1] P. Falcaro, D. Grosso, H. Amenitsch, P. Innocenzi, J. Phys. Chem B, *in press*.
- [2] G. J. de. A. A. Soler-Illia, C. Sanchez, B. Lebeau, J. Patarin, Chem. Rev. 102, 4093-4138 (2002)

AN IN SITU SYNCHROTRON SMALL ANGLE X-RAY SCATTERING/X-RAY DIFFRACTION STUDY OF THE FORMATION OF SBA-15 MESOPOROUS SILICA

K. Flodström¹, C.V. Teixeira², H. Amenitsch³, V. Alfredsson¹, M. Lindén^{2,4}

1.) Physical Chemistry 1, Lund University, P.O. Box 124, SE- 221 00, Lund, Sweden

2.) Department of Physical Chemistry, Abo Akademi University, Porthansgatan 3-5, FI-20 500, Turku, Finland

3.) Institute of Biophysics and X-Ray Structure Research, Austrian Academy of Sciences, Schmiedlst. 6, A-8042 Graz, Austria

4.) Department of Heterogeneous Catalysis, Max-Planck-Institute for Coal Research, Kaiser-Wilhelm-Platz 1, D-45470, Mülheim/Ruhr, Germany

The initial stages of the formation of SBA-15 have been studied under acidic conditions by *in situ* SAXS/XRD using synchrotron radiation.[1] This is an extension of our previous work on the formation of MCM-41 under alkaline conditions. The interactions between the surfactant serving as the structure-directing agent and the polymerizing silica are different in the two cases, since while electrostatic interactions dominate in the case of MCM-41, hydrogen-bonding interactions are the main driving force for the formation of SBA-15.

A time-resolved SAXS/XRD pattern measured during the formation of SBA-15 is shown in Figure 1. Initially, only scattering from micelles is observed, the intensity of which increases with time. This is indicative of an increasing electron density contrast of the micelles due to adsorption of silica species to the palisade layer. A sudden appearance of a sharp reflection appears at $s = 0.080 \text{ nm}^{-1}$ ($d = 12.5 \text{ nm}$) together with two other less intense reflections at $s = 0.138 \text{ nm}^{-1}$ ($d = 7.25 \text{ nm}$) and $s = 0.160 \text{ nm}^{-1}$ ($d = 6.25 \text{ nm}$), respectively, which can be indexed as the (10), (11), and (21) reflections of a 2D hexagonal mesophase.

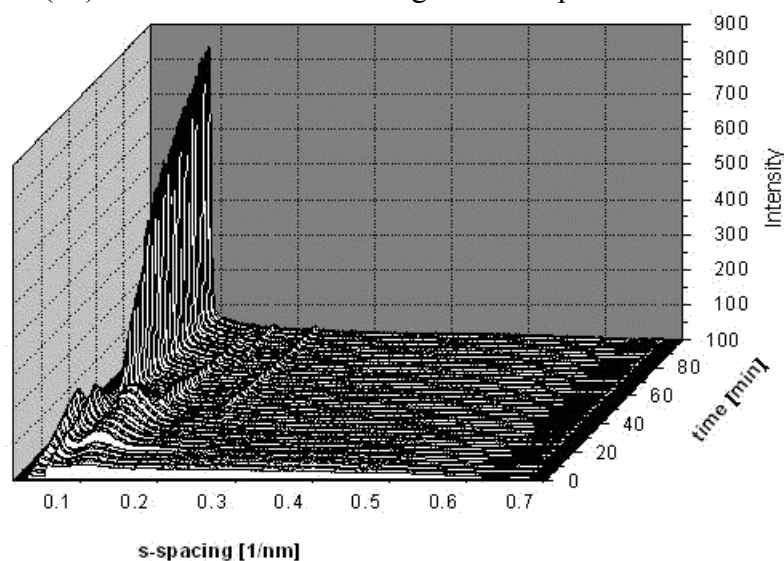


Figure 1. Time resolved SAXS pattern of the P123-TMOS system. A data accumulation time of 1 minute per frame was used.

Note that the (20) reflection does not appear at this stage. The micellar scattering reflection initially co-exists with the (10) reflection, but its intensity decreases rapidly and it is no longer present at a reaction time of 45 minutes. The full-width-at-half-maximum, FWHM, of the (10) reflection was $6.5 \cdot 10^{-3} \text{ 1/nm}$ at a reaction time of 45, but reaches a constant value of $6 \cdot 10^{-3} \text{ 1/nm}$ after about 55 minutes. The (20) reflection appears 65 minutes into the reaction, after which the intensity of this reflection increases continuously with time. The intensities of

the (11), and (21) reflections, on the other hand, actually decrease with time. Furthermore, the structure contracts continuously with time and has reached an s -value of 0.086 nm^{-1} (11.6 nm) 90 minutes into the reaction.

Analysis of the micellar scattering curve reveals that the micelles are spherical all the way up to the point where the 2D hexagonal phase starts to nucleate and grow. Fifteen minutes after the addition of TMOS, a total micellar radius R_T of 68 \AA is reached, with a micellar core radius close to 45 \AA . The analyses also reveal the increasing electron density with time of the palisade layer of the micelles, as discussed above.

Modeling of the the X-ray diffraction patterns obtained at different stages of the reaction results in a detailed description of the evolution of the 2D hexagonal phase. 2D electron density maps shown in Figure 2 are calculated based on the intensities of the Bragg reflections.

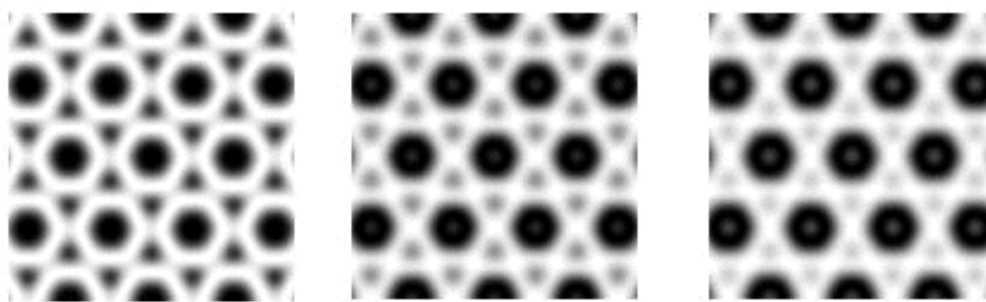


Figure 2. Two-dimensional electron density maps (4 times 4 unit cells) created using the intensities and positions of the (10), (11), (20), and (21) reflections at specific reaction times as input data; from left to right; 40 minutes, 71 minutes, and 92 minutes. White areas correspond to areas of high electron density and dark areas to areas of low electron density.

The initial absence of the (20) reflection is a consequence of a Fourier phase transition occurring during the early stages of the reaction.

It is evident that the degree of inter-micellar condensation is very low initially, and increases continuously with time. The observed contraction of the mesophase can be attributed to this increase in the degree of intermicellar condensation.

References:

[1] K. Flodström, C.V. Teixeira, H. Amenitsch, V. Alfredsson, M. Lindén, *Langmuir*, *in press*

IN-SITU SAXS INVESTIGATIONS ON THE FORMATION OF MESOSTRUCTURED SILICA MONOLITHS AND THEIR DRYING IN SUPERCRITICAL CARBON DIOXIDE

N. Hüsing¹, D. Brandhuber¹, C. Raab¹, V. Torma¹, H. Peterlik², M. Steinhart³, M. Kriechbaum⁴, and S. Bernstorff⁵

- 1.) Institute of Materials Chemistry, TU Vienna, Getreidemarkt 9/165, A-1060 Vienna, Austria
- 2.) Institute of Materials Physics, University of Vienna, Boltzmanngasse 5, A-1090 Vienna, Austria
- 3.) Institute of Macromolecular Chemistry, Academy of Science of Czech Republic, Heyrovsky Sq. 2, 16206 Prague, Czech Republic
- 4.) Institute of Biophysics and X-ray Structure Research, Austrian Academy of Sciences, Schmiedlstraße 6. A-8042 Graz, Austria
- 5.) Sincrotrone Trieste, Strada Statale 14, Km.163.5, in AREA Science Park 34012 Basovizza/ Trieste, Italy

A novel precursor molecule (tetrakis(2-hydroxyethyl)orthosilicate, EGMS) was used in the presence of an amphiphilic block copolymer as structure directing agent in purely aqueous solution for the synthesis of highly porous silica-based materials. This precursor has the distinct advantage of being water-soluble and it shows a good compatibility with lyotropic phases of surfactant molecules, thus allowing for true liquid-crystal templating of LC mesophases with inorganic species. We were able to prepare *hierarchically organized porous silica monoliths* with macropores in the range of 200 to 800 nm in diameter and periodically arranged mesopores with a repeating unit distance of about 11 nm from this precursor.[1]

The aim of this SAXS study was to follow the inorganic network formation and to answer the question, whether the surfactant phase is sensitive towards the different processing steps which include mixing, gelation, aging in alcoholic solution, solvent exchange to liquid carbon dioxide and finally even supercritical drying in carbon dioxide at a temperature of 45 °C and pressure of 120 bar.

The SAXS measurements were carried out during the gelation process, thus continuously following network formation. In addition, preformed gels were investigated at different times during aging (1 to 7 days) following their network changes during solvent exchange processes (of gels that have been aged for seven days) and finally supercritical drying. Liquid samples and also preformed gel samples were placed in a home-made flow-through cell with a sample volume of about 1 cm³ to follow gelation, aging and solvent exchange processes. For supercritical extraction with liquid carbon dioxide, the wet gels were placed in a high-pressure cell.[2] After solvent exchange from methanol to liquid carbon dioxide at 20 °C and 70 bar, the temperature and pressure were raised to 45 °C and 120 bar using remote computer control.

Figure 1 (top part) shows the SAXS pattern of the surfactant/ water mixture (A) and a representative SAXS curve obtained during the formation of the gel network after addition of tetrakis(2-hydroxyethyl)orthosilicate (B) and a pattern of a dried sample (C). Addition of the silane to the surfactant/ water mixture changes the SAXS pattern considerably from a number of distinct reflections to one broad maximum of low intensity. Gelation (formation of a solid three-dimensional network) occurred after 5 minutes, however, the SAXS pattern is not changed significantly by this event, still showing a broad reflection which corresponds to a low degree of order in the material. With time, the intensity of the maximum is getting more pronounced (B), indicating an increasing degree of order during gelation (also supported by the second order reflection). After gelation, the material is still progressively changing due to the presence of uncondensed silane monomers and the dynamic behavior of the surfactant liquid crystal phases. The *d*-spacing (repeating unit distance) is decreasing with time to a value of 12.8 nm (Fig. 1, bottom) corresponding to a higher degree of crosslinking of the network.

To complete the cooperative self-assembly process and network condensation the gels were subjected to an aging procedure in the mother liquid (water/ ethylene glycol) for seven days at 30 °C. In this study, preformed gels were measured at different days of the aging procedure. The further decrease in d -spacing to a value of 12.3 nm corresponds well to the observed syneresis, during which the gel network is shrinking and solvent is expelled from the gel. Prior to drying of the wet gels a solvent exchange process from the aqueous ethylene glycol solution to methanol was performed. During this process, the block copolymer surfactant is partly extracted from the gel and the silanol groups on the silica surface are converted to methoxy-groups. In the SAXS pattern no distinct influence of this procedure on the intensity/ half width of the maximum is observed, however the maximum is shifting to smaller d -spacings again indicating contraction of the gel network. Drying of large monoliths is the crucial step in the synthesis process, since surface tension, the evolution of capillary pressure and the removal of templates often result in large shrinkage or even destruction of the whole gel body. One typical procedure to prevent cracking is drying with supercritical fluids since the building-up of a gas/ liquid interface is avoided during drying, hence no capillary pressures evolve. An *in-situ* SAXS study of a supercritical drying process with carbon dioxide was performed in this study, comprising an extraction step with liquid carbon dioxide to exchange methanol, an increase in temperature to 45 °C while simultaneously increasing the pressure (120 bar), thus putting carbon dioxide into the supercritical state, and finally a venting step to ambient pressure. These experiments were performed by putting a pre-prepared and aged, wet gel sample into the high pressure cell. The measurements indicate, that none of the steps is detrimental to the mesostructure in the silica monoliths. During exchange of the solvent to liquid carbon dioxide no significant changes in the d -spacing are visible. Interestingly, the transition from liquid to supercritical CO₂ at 31 °C and ca. 80 bar leads to a small increase in the repeating unit distance, which cannot be explained at the moment. Venting the system to ambient pressure results in a contraction of the gel network and a final d -spacing of 11.6 nm.

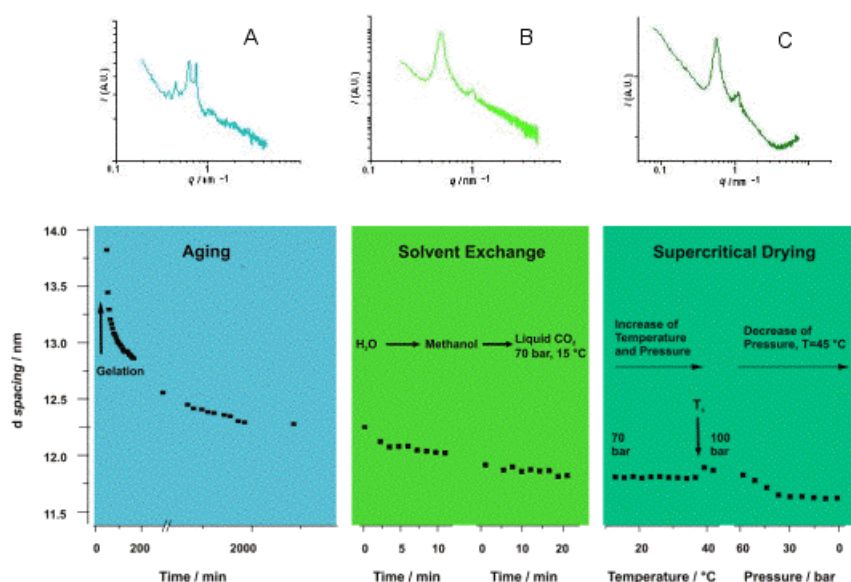


Figure 1. SAXS pattern of the water/surfactant mixture (A), shortly after gelation (B) and after supercritical drying (C), (top) and the evolution of the corresponding d -spacing during gel formation (30 sec/ measurement), solvent exchange from ethylene glycol/water mixture to methanol (in the liquid cell) to liquid carbon dioxide (in the high pressure cell) with preformed gels (30sec/ measurement) and supercritical drying with carbon dioxide (10sec/ measurement, bottom).

The liquid crystal (LC) templating process to highly porous silica monoliths with uniform periodic mesopores relies on the compatibility of the lyotropic liquid crystal-like phase of the surfactant with the inorganic network forming species. In addition, the stability of the network during surfactant removal and drying of the monoliths is of importance. We could not only follow the whole processing towards a monolithic silica-based sample, but also show that drying in supercritical carbon dioxide is not detrimental to the mesostructure formed through LC templating.

References:

- [1] N. Hüsing, C. Raab, V. Torma, H. Peterlik, A. Roig, *Chem. Mater.* 14, 2690 (2003).
- [2] M. Steinhart, M. Kriechbaum, K. Pressl, H. Amenitsch, P. Laggner, S. Bernstorff, *Rev. Sci. Instrum.* 72/2, 1540-1545 (1999), <http://www.ibr.oeaw.ac.at/beamline/publications.html>, *Annual Report of the Austrian SAXS-beamline* (2000), p. 27-29.

STRUCTURAL INVESTIGATION IN AQUEOUS SOLUTION OF COMPLEX POLYELECTROLYTES SYSTEMS

D. Lombardo¹, H. Amenitsch², S. Bernstorff³ and M. Rappolt²

1) CNR Istituto per i Processi Chimico Fisici (IPCF Sez. Messina), Via La Farina 237, I-98123 Messina, Italy

2) Institute of Biophysics and X-ray Structure Research, Austrian Academy of Sciences, Schmiedlstr. 6, A-8042 Graz, Austria

3.) Sincrotrone Trieste, Area Science Park, Basovizza/TS, I-34012, Italy

Recently there has been an increased interest in studying complexation between polyelectrolytes and oppositely charged macromolecular entities [1]. Apart the large variety of possible applications, those systems are particularly suited in advanced technology as molecular cages and controlled delivery agents (Guest-Host Systems) [2]. Although recent results clearly indicate the potential of these systems for advanced application in the field of biotechnology and material science, on the other hand a clear understanding of the process of formation of these complexes as well as their molecular behavior is still far to be attained [3]. The mechanism of polyelectrolyte-dendrimer complexation may be expected to play an important role in *transporting polyelectrolytes*, while the nature and criteria for its occurrence is certainly essential to our understanding and use of these materials as guest-host systems [4, 5]. Our research consists in the study of the equilibrium complexation behavior of Polyamidoamine dendrimers (PAMAM) with positively charged terminal groups (i.e. generations 2, 3, 4) to a negatively charged polystyrenesulfonate (PSSNa) polyelectrolyte in solutions.

Preliminary Laser Doppler Electrophoresis measurements revealed that the charge density plays an important role in determining the type of complex formed. Obtained results indicate, in fact, that complexes formed at lower salt concentrations may be disrupted by increasing the ionic strength above a critical threshold. In the experiment performed at Elettra, we tried to investigate the permeability of the dendrimer during complexation as a function of some relevant parameters of the system (such as polymer concentration and ionic strength). In this respect a series of SAXS measurements allowed to monitor the saturation of the long range electrostatic repulsion of the PSSNa polyelectrolytes due to the presence of dendrimers. The detection of the “effective dendritic charge” which influences dendrimer interaction with polyelectrolyte has been investigated for different ratios of the components.

The high charge detected even at the lowest polymer concentration employed has been evidenced by the presence of a pronounced peak in the SAXS spectra. In this respect the change in dimension of generated aggregates upon complexation requests measurements to be carried out in a larger polyelectrolyte concentration range. This is a necessary condition in order to clearly separate the information of the form factor $P(q)$ from the structure factor $S(q)$ in the corresponding SAXS spectra. Moreover also ionic strength revealed to be an important parameter which sensitively controls the main features of the electrostatic interaction. In this respect also for this parameter a detailed analysis requests a wider range of SAXS measurements to be performed.

SAXS experiments carried out with the first run are very promising but one more run will be needed to obtain a complete data set for our experiment.

References:

- [1] Li, Y.; Dubin, P. L.; Spindler, R.; Tomalia, D. A. *Macromolecules*, **28**, 8426-8431 (1995)
- [2] Ottaviani, M. F.; Sacchi, B.; Turro, N. J.; Chen, W.; Jockusch, S.; Tomalia, D. A. *Macromolecules*, **32**, 2275-2281 (1999)
- [3] Welch, P.; Muthukumar, M.; *Macromolecules*; **33**; 6159-6167 (2000)
- [4] N. Micali, L. Monsù-Scolaro, A. Romeo, D. Lombardo, P. Lesieur, F. Mallamace *Phys. Rev. E* **58**, 6229-6234 (1998)
- [5] F. Mallamace, D. Lombardo, A. Mazzaglia, A. Romeo, L. Monsù Scolaro, G. Maino. *Physica A*: **304**, 235-239 (2002)

MORPHOLOGY OF POLYOLEFIN-RESIN MIXTURES

A. Triolo¹, R. Triolo², M. Jeschke³

1.) Istituto per i Processi Chimico-Fisici, Consiglio Nazionale delle Ricerche, 98123 Messina, Italy

2.) Dipartimento di Chimica Fisica "F. Accascina", Università di Palermo, 90128 Palermo Italy

3.) Surface Specialties UCB, Wigton, Cumbria, UK

Polyolefins are presently attracting a great deal of attention as they are major components in a huge variety of manufactures. Their performances are routinely optimized by blending with other components such as inert fillers, other polymers and low molecular weight resins. The latter are of great interest as well as they are generally natural products with limited environmental impact and low cost. Moreover they have been found to play a major role in determining the morphological features when blended with polyolefins.

The experiment we report deals with characterization of morphological features of mixtures of isotactic polypropylene (iPP) and commercial resins. Moreover we also studied iPP-based copolymers (PP-b-polyethylene (PE)) (namely products RP220M and PMB6100, differing in the iPP:PE ratio) blended with the same resins. These mixtures are of industrial interest at UCB.

The two resins we explored have different properties: one of them (P125) is a hard (high-Tg) one ($T_g=85\text{ }^\circ\text{C}$), while the other resin (R1100) has a low temperature Tg ($T_g=30\text{ }^\circ\text{C}$). The mixtures were studied preliminarily by means of dynamic mechanical thermal analysis (DMTA). In Figure 1 we report a selection of these data, where $\tan \delta$ is plotted for 15% wt. mixtures of iPP with both P125 and R1100. The higher Tg of P125 leads to a more rigid sample when the resin is added to the polyolefin.

A detailed structural investigation has been carried out at the SAXS beamline at ELETTRA, where combined SAXS-WAXS data were collected at isothermal conditions between 30 and 180 °C for a series of polyolefin-resin mixtures.

In Figure 2, data reflecting the effect of R1100 addition to one of the iPP-PE copolymers (RP220M) are reported for $T=30\text{ }^\circ\text{C}$. It can be noticed that the lamellar spacing associated to the peak at about 0.5 nm^{-1} progressively shifts to shorter distances as the resin content increases. Moreover as soon as the resin content crosses from 11% to 15% a distinct feature appear at about 0.3 nm^{-1} .

On the other hand the same resin when blended with pure iPP does not present the layer feature: in Figure 3 data at 30 °C for iPP/R1100 are reported. The lamellar spacing, that in this case is associated to a peak at about 0.3 nm^{-1} , still shifts to longer sizes as the resin content increases. On the other hand no features at low Q occur as the concentration increases.

These observations are related to the different affinity of the polyolefins with the resins, which determine the phase diagram of the mixtures. Work is now in progress to interpret the data sets in combination with other thermal characterizations.

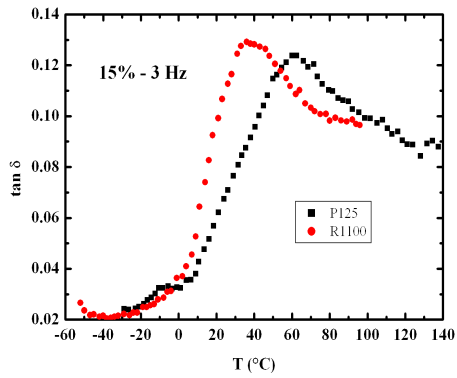


Figure 1. DMTA characterization of two iPP-resin mixtures. In particular iPP-R1100 and iPP-P125 (both 15 % wt.) are reported as a function of temperature.

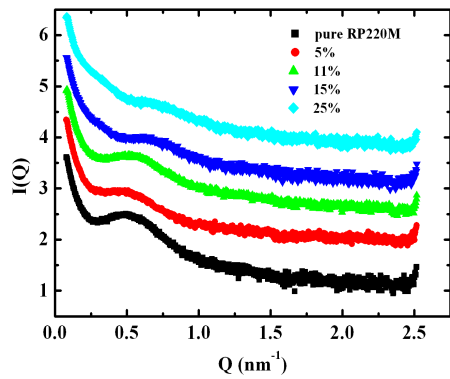


Figure 2. SAXS patterns from mixtures of RP220M with R1100 as a function of resin content, at T=30 °C.

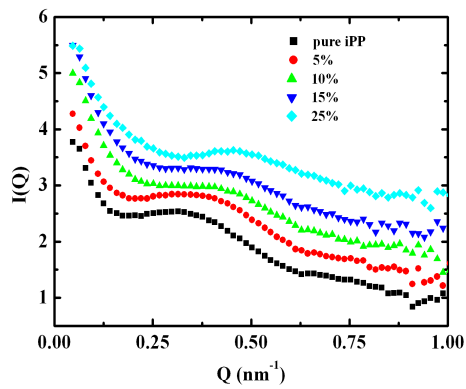


Figure 3. SAXS patterns from mixtures of iPP with R1100 as a function of resin content, at T=30 °C.

STUDY OF THE GROWTH OF SEMICONDUCTING ZnS NANOPARTICLES USING SAXS TECHNIQUE.

R. Viswanatha¹, S. Sapra¹, B. Sartori², H. Amenitsch² and D.D. Sarma¹

- 1.) Solid State and Structural Chemistry Unit, Indian Institute of Science, Bangalore-560012, India
- 2.) Institute of Biophysics and X-ray Structure Research, Austrian Academy of Sciences, Schmiedlstr. 6, 8042 Graz, Austria

It is now well-known that semiconducting nanoparticles provide us the unprecedented opportunity to tailor-make electronic and optical properties by varying the size of the nanoparticles via the quantum confinement effect [1]. The chemical approach to the synthesis of such nanoparticles, owing to its simplicity, flexibility and tunability [2-4], has been used extensively to prepare a wide range of systems so far; this method depends basically on stopping the reaction process leading to the formation of the semiconductor in a solution by adding a capping agent that binds to the surface of the growing nanoparticle and stops it from growing any further. The primary difficulty of this method is that the size along with the size distribution of the generated particles are determined primarily by the concentrations of the reactants and temperature in a way that is very little understood. Thus, the techniques of synthesis of high quality nanoparticles, indicated by the ability to grow a pre-defined size with a narrow size distribution, has remained largely in the realm of empiricism based on large number of hit-and-trial methods to fine-tune the synthesis parameters. The need to understand the growth process of these nanoparticles is obvious.

We have studied the thermal initiated growth of technologically important ZnS nanoparticles by investigating the time evolution of the formation as a function of the temperature using the 8 KeV Cu K α SWAXS camera at the small angle X-ray scattering (SAXS) beamline laboratory. The precursors were freshly prepared at room temperature and then sealed in 2 mm quartz capillary and the experiments were performed at various temperatures. The samples have been quickly heated to different temperatures. The evolution of the diffraction

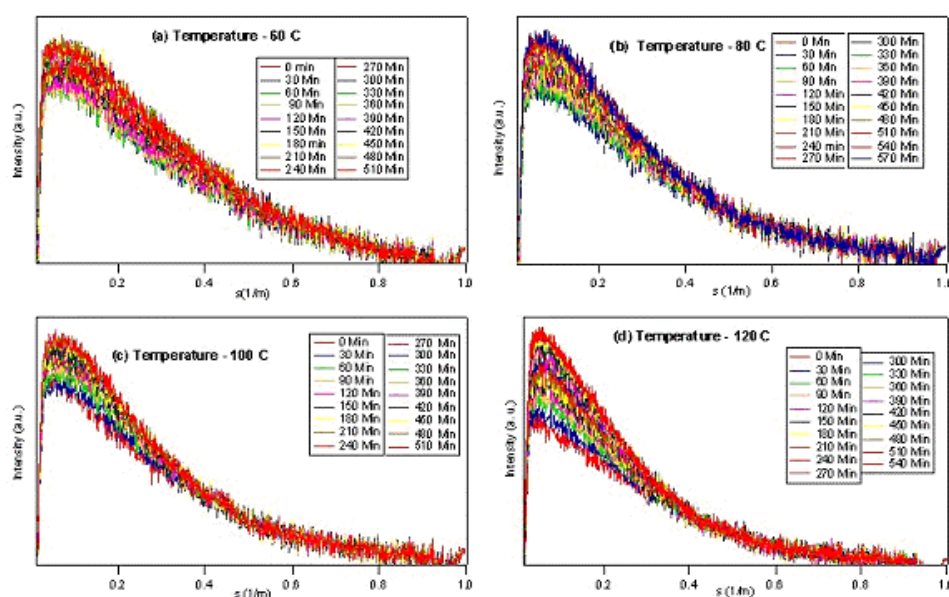


Figure 1. Experimental scattering curves measured during the thermal induced formation of ZnS particles with the laboratory SWAXS system at different temperatures indicated in the figure.

pattern of the system has been monitored with a time resolution of 30 min and the obtained time dependent diffraction patterns are shown in Fig. 1.

In order to obtain a more detailed understanding and to quantify the data we have obtained the forward intensity and the Guinier radius for the different reactions and are plotted in Fig.2. From the figure, it is clear that temperature has an effect on the formation of ZnS nanoparticles. It can be seen that the size of the particles increases with increase in temperature. We observe that a precipitation occurs at room temperature which dissolves into solution as we go to higher temperatures. However a temperature of 60°C is not sufficient to completely dissolve the precipitate. Due to the slow dissolution we see a decrease in the Guinier radius with increasing time in this case. At higher temperatures, the precipitate dissolves immediately and slowly grows as time progresses, though the growth is retarded due to effective interaction with the capping agent.

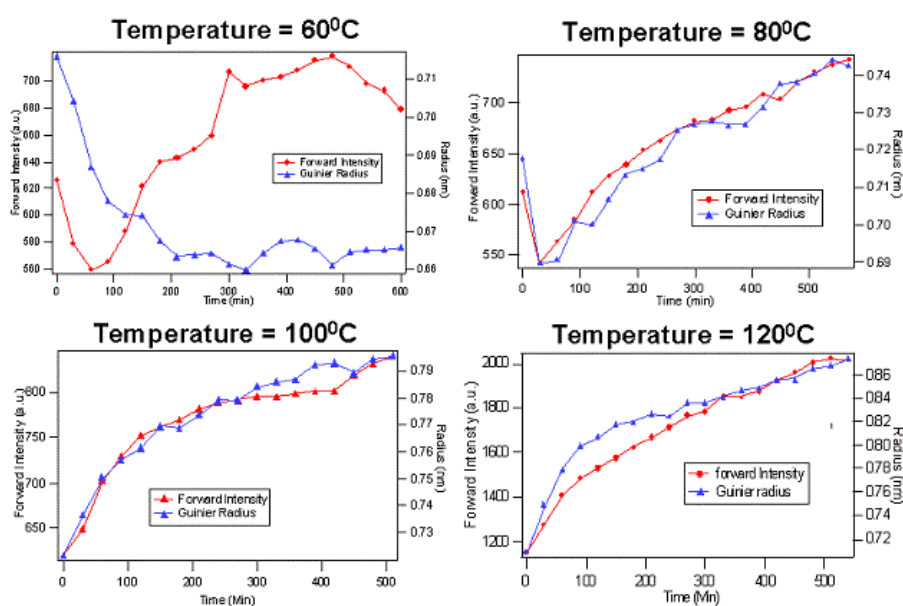


Figure 2. Evolution of the forward intensity and guinier radius determined from the scattering data at different temperatures, with resolved the fast formation in the beginning and the final particles with a nearly monodisperse radius at higher temperatures.

These results suggest that such SAXS measurements carried out on a faster time scale and different reaction conditions, like concentration of precursors and the capping agents would contribute to a deeper insight on the mechanism of growth in these nanocrystals. Following up on this idea, we are now in the process of carrying out such experiments at the SAXS beamline of Elettra and analyzing the results.

References:

- [1] Z. K. Tang, G. K. L. Wong, P. Yu, M. Kawasaki, A. Ohtomo, H. Koinuma, Y. Segawa, Appl. Phys. Lett. **72**, 3270 (1998).
- [2] T. Vossmeier, L. Katsikas, M. Giersig, I. G. Popovic, K. Diesner, A. Chemseddine, A. Eychmuller, H. J. Weller, J. Phys. Chem., **98**, 7665 (1994).
- [3] C. B. Murray, D. B. Norris, M. G. Bawendi, J. Am. Chem. Soc. **115**, 8706 (1993).
- [4] J. Nanda, S. Sapra, D. D. Sarma, N. Chandrasekharan and G. Hodes, Chem. Mater. **12**, 1018 (2000).

4. Instrumentation

DETECTOR DEVELOPMENT FOR TIME-RESOLVED SAXS IMAGING

A. Orthen¹, H. Wagner¹, S. Martoiu¹, H. Amenitsch², S. Bernstorff³, H.-J. Besch¹,
R.-H. Menk³, K. Nurdan¹, M. Rappolt², A.H. Walenta¹ and U. Werthenbach¹

1.) Universität Siegen, Fachbereich Physik, Walter-Flex-Str. 3, D-57072 Siegen, Germany

2.) IBR, Austrian Academy of Sciences, Schmiedlstr. 6, A-8042 Graz, Austria

3.) Sincrotrone Trieste, SS 14, Km 163.5, Basovizza, I-34012 Trieste, Italy

Urgent needs of fast imaging systems providing high time-resolutions in the microsecond time domain combined with a good spatial resolution in the range of 100-200 μm , a good efficiency for X-ray detection and large sensitive areas of several ten cm^2 led to the development of the 2D ViP (Virtual Pixel) imaging detector [1], presented in the following.

The single photon counter is based on a gaseous micro pattern detector, making use of gas amplification by three subsequent GEM [2] structures (triple-GEM). The triple-GEM setup offers high gas gains ($>5 \times 10^3$) even for xenon gas mixtures at a pressure of up to 3 bar (quantum efficiency $>80\%$ at 15 keV with 25mm conversion gap), a low fraction of back drifting ions (ion feedback) in the range of a few percent, decreasing distortions owing to space charge, and very short signals with lengths <50 ns (fwhm) [3]. Therefore, this concept is predestined for highly time-resolved applications which require in general the use of high photon rates.

By means of resistive charge division the event position is measured in two dimensions [4,5]. The interpolating concept of position determination offers large sensitive areas with an enormous reduction of electronic channels compared to pure pixel devices. The active area of the detector, presented here, amounts currently to $56 \times 56 \text{ mm}^2$ and is subdivided into 7×7 square interpolation cells. For a proper position reconstruction, a suited algorithm has been developed, providing nearly distortion free image reconstruction properties [6], as shown for a flatfield illumination and a diffraction image of silver behenate in Fig. 1 and 2, respectively. The spatial resolution has been measured to be in the range of 100-200 μm (fwhm) [7]. Since multiple events have to be rejected owing to a false position reconstruction, the rate capability of the presented system is limited to at least 10^6 photons s^{-1} (3×3 interpolation cells) $^{-1}$ with estimately 18% dead time loss due to paralyzable dead time. For a typical cellsize of $8 \times 8 \text{ mm}^2$, this value corresponds to an average detected flux $>2 \times 10^5$ photons $\text{s}^{-1} \text{ cm}^{-2}$. Therefore, the global counting rate acceptance of the readout structure is $>3 \times 10^6$ photons s^{-1} .

The electronic readout system, which used to be the bottleneck of the overall rate performance in previous systems [8,9], has been replaced by a new digitization and readout unit, which has the capability of proper event preprocessing [10]. Thereby, the event flux to the PC is increased by about 2 orders of magnitude compared to the old system, reaching nearly the rate limit determined by the readout structure.

We calculated that the time resolution of the overall detector system (triple-GEM+readout structure+readout electronics) for single photon detection is $<600\text{ns}$. For radiation stable samples, which withstand a large number of repetitive measurement cycles [11], this is the maximal time resolution. For sensitive samples, where the number of repetitions is limited, time slices in the ms- up to the 10 μs -range are feasible, as shown in a time-resolved temperature jump experiment of 1-Palmitoyl-2-Oleoyl-*sn*-Phosphatidylethanolaminin (POPE) in Fig. 3 [1]. It turns out the maximum change in d -spacing occurs in a time window between 3-30 ms after the laser trigger.

The prototype detector system, presented in this report, already shows the potential which can be exploited to its full extend in a future evolution of the detector. With optimised detector

parameters and an increased number of electronic channels, sensitive areas of $20 \times 20 \text{ cm}^2$ with a global rate capability $>3 \times 10^8 \text{ photons s}^{-1}$ seem feasible [1].

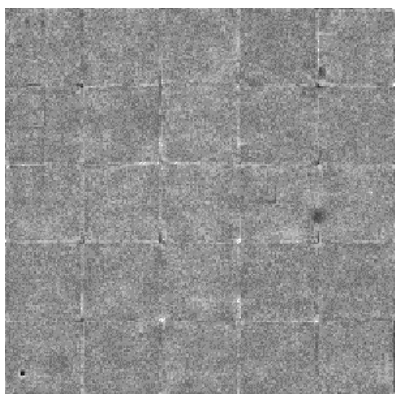


Figure 1. Reconstructed image of a flatfield illumination. The depicted area corresponds to $40 \times 40 \text{ mm}^2$. The image has been recorded with 6.4 keV fluorescence photons of a Fe scattering target in the 8 keV synchrotron beam of the SAXS beamline.

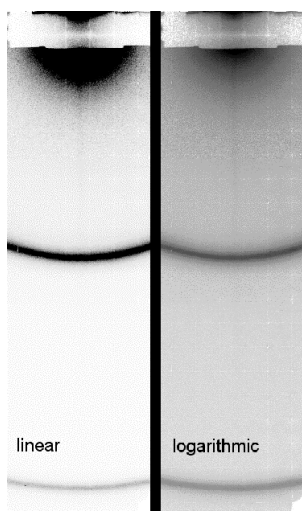


Figure 2. Diffraction image of silver behenate, recorded at the SAXS beamline. The depicted images in linear and logarithmic scale are composed of 1×4 single images, corresponding to an image size of $48 \times 168 \text{ mm}^2$.

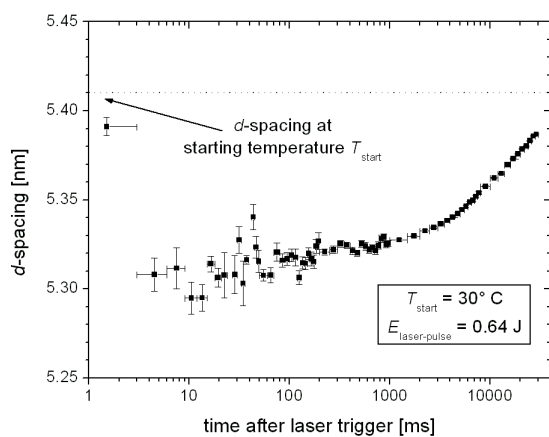


Figure 3. Measured d -spacing of the POPE lipid up to 30 s after the trigger of the laser pulse (at $t = 0$). The applied time-slices have variable width to give an overview over four orders of magnitude in time. The bars in the t -direction mark the slice-windows.

References:

- [1] A. Orthen, H. Wagner, S. Martoiu, H. Amenitsch, S. Bernstorff, H.-J. Besch, R.-H. Menk, K. Nurdan, M. Rappolt, A.H. Walenta and U. Werthenbach; Development of a two-dimensional virtual pixel X-ray imaging detector for time-resolved structure research; *J. Synchrotron Rad.* **11**, 177-186 (2004).
- [2] F. Sauli; GEM: A new concept for electron amplification in gas detectors; *Nucl. Instr. and Meth. A* **386**, 531-534 (1997).
- [3] A. Orthen, H. Wagner, H.J. Besch, S. Martoiu, R.H. Menk, A.H. Walenta, U. Werthenbach; Gas gain and signal length measurements with a triple-GEM at different pressures of Ar-, Kr- and Xe-based gas mixtures; *Nucl. Instr. and Meth. A* **512**, 476-487 (2003).
- [4] H.J. Besch, M. Junk, W. Meißner, A. Sarvestani, R. Stiehler, A.H. Walenta; An interpolating 2D pixel readout structure for synchrotron X-ray diffraction in protein crystallography; *Nucl. Instr. and Meth. A* **392**, 244-248 (1997).
- [5] H. Wagner, H.J. Besch, R.H. Menk, A. Orthen, A. Sarvestani, A.H. Walenta, H. Walliser; On the dynamic two-dimensional charge diffusion of the interpolating readout structure employed in the MicroCAT detector; *Nucl. Instr. and Meth. A* **482**, 334-346 (2002).
- [6] H. Wagner, A. Orthen, H.J. Besch, S. Martoiu, R.H. Menk, A.H. Walenta, U. Werthenbach; On image reconstruction with the two-dimensional interpolating resistive readout structure of the Virtual-Pixel detector; *Nucl. Instr. and Meth. A* **523**, 287-301 (2004).
- [7] H. Wagner, PhD-thesis, in preparation (2004).
- [8] R. Stiehler, M. Adamek, H. J. Besch, M. Junk, G. Menzel, E. Neuser, W. Meißner, A. Sarvestani, N. Sauer, S. Volkov, A. H. Walenta, R. H. Menk; A transient recorder system for applications in high rate detector systems; *Nucl. Instr. and Meth. A* **419**, 711-714 (1998).
- [9] A. Sarvestani, H. Amenitsch, S. Bernstorff, H.J. Besch, R.H. Menk, A. Orthen, N. Pavel, M. Rappolt, N. Sauer, A.H. Walenta; Biological X-ray Diffraction Measurements with a Novel 2D Gaseous Pixel Detector; *J. Synchrotron Rad.* **6**, 985-994 (1999).
- [10] S. Martoiu, A. Orthen, H. Wagner, H.-J. Besch, R.-H. Menk, K. Nurdan, A.H. Walenta and U. Werthenbach; to be published in *Nucl. Instr. and Meth. A* (2004).
- [11] A. Sarvestani, H.J. Besch, R.H. Menk, A. Orthen, N A. Pavel, N. Sauer, C. Strietzel, A.H. Walenta; Microsecond Time-resolved 2D X-ray Imaging of repetitive processes; *Nucl. Instr. and Meth. A* **465**, 354-364 (2001).

Publications

Publications in 2003

B. Alonso, A.R. Balkenende, P.A. Albouy, H. Amenitsch, M.N. Rager and F. Banonneau
Hybrid 3D ordered mesoporous thin films made from organosiloxane precursors
Journal of Sol-Gel Science and Technology 26, pp. 587-591 (2003)

Amenitsch, H., H. Edlund, A. Khan, E.F. Marques and C. La Mesa
Bile salts form lyotropic liquid crystals
Colloids and Surfaces A-Physicochemical and Engineering Aspects 213, pp. 79-92 (2003)

J. Baldrian, M. Horky, M. Steinhart, A. Sikora, M. Mihailova H. Amenitsch, S. Bernstorff,
and G. Todorova
SAXS and DSC study of co-crystallization of low-molecular weight PEO fractions in polymer blends
Fibers & Textiles in Eastern Europe, Vol 11, No. 5, pp. 46-49 (2003)

J. Baldrian, M. Steinhart, A. Sikora, G. Todorova, M. Kriechbaum, S. Bernstorff
Development of cocrystalline structures in polymer blends
In: Book of Abstracts. - Melbourne, Polymer Processing Society 2003. - S. 12.
[Annual Meeting of Polymer Processing Society /19./. Melbourne (Australia), 03.07.07-03.07.10 (WRD)]

Ludvík Benes, Vítězslav Zima, Klára Melánová, Milos Steinhart, Manfred Kriechbaum,
Heinz Amenitsch, Sigrid Bernstorff
High pressure phase transition of alcohol intercalated zirconium phosphate
Materials Structure 10, 80 – 81 (2003)

Johnny Mio Bertolo, Andrea Bearzotti, Paolo Falcaro, Enrico Traversa, Plinio Innocenzi
Sensoristic Applications of Self-assembled Mesostructured Silica Films
Sensor Letters, Vol. 1, 64-70, 2003

C. Boissiere, D. Grosso, H. Amenitsch, A. Gibaud, A. Coupe, N. Baccile, and C. Sanchez
First in-situ SAXS studies of the mesostructuration of spherical silica and titania particles during spray-drying process.
Chem Commun (Camb). 22, pp. 2798-2799 (2003)

M. Buljan, K. Salamon, P. Dubcek, S. Bernstorff, I.D. Desnica-Frankovic, O. Milat and U.V. Desnica
Analysis of 2D GISAXS patterns obtained on semiconductor nanocrystals
Vacuum 71, pp. 65-70 (2003)

F. Cagnol, D. Grosso, G.J.de.A.A. Soler-Illia, E.L. Crepaldi, F. Banonneau, H. Amenitsch and C. Sanchez
Humidity-controlled mesostructuration in CTAB-templated silica thin film processing. The existence of a modulable steady state.
Journal of Materials Chemistry 13, pp. 61-66 (2003)

G. Croce, A. Frache, M. Milanesio, D. Viterbo, G. Bavestrello, U. Benatti, M. Giovine and H. Amenitsch

Fiber diffraction study of spicules from marine sponges.

Microscopy Research and Technique 62(4), pp. 378-381 (2003)

J. De Roche, C.M. Gordon, C.T. Imrie, M.D. Ingram, A.R. Kennedy, F. Lo Celso, A. Triolo
Application of Complementary Experimental Techniques to Characterization of the Phase Behavior of [C16mim][PF6] and [C14mim][PF6]

Chem. Mater. 15-16, pp. 3089-9 (2003)

I.D. Desnica-Frankovic, U.V. Desnica, P. Dubcek, M. Buljan, S. Bernstorff, H. Karl, I. Großhans and B. Stritzker

Ion beam synthesis of buried Zn-VI quantum dots in SiO₂—a GISAXS studies

J. Applied Cryst. 36, 439-442 (2003)

U. V. Desnica, P. Dubcek, I.D. Desnica-Frankovic, M. Buljan, K. Salamon, O. Milat, S. Bernstorff and C.W. White

GISAXS studies of morphology and size distribution of CdS nanocrystals formed in SiO₂ by ion implantation

Nuclear Instruments and Methods B 200, 191-195 (2003)

U. V. Desnica, P. Dubcek, I.D. Desnica-Frankovic, M. Buljan, S. Bernstorff and S.W. White
GISAXS studies of the synthesis and growth of CdS quantum dots from constituent atoms in SiO₂ matrix

J. Applied Cryst. 36, 443-446 (2003)

P. Dubcek, U. V. Desnica, I.D. Desnica-Frankovic, S. Bernstorff and A. Meldrum
GISAXS study of shape and size of CdS nanocrystals formed in monocrystalline silicon by ion implantation

Nuclear Instruments and Methods B 200, 138-141 (2003)

P. Dubcek, B. Pivac, S. Bernstorff, F. Corni, R. Tonini, and G. Ottaviani
Grazing incidence small-angle X-ray scattering study of defects in deuterium implanted monocrystalline silicon

J. Applied Cryst. 36, 447-449 (2003)

P. Dubcek, B. Pivac, S. Bernstorff, R. Tonini, F. Corni and G. Ottaviani
GISAXS study of structural relaxation in amorphous silicon

Nuclear Instruments and Methods B 200, 110-113 (2003)

P. Dubcek, N. Radic and O. Milat
Characterization of grains in tungsten-carbon films

Nuclear Instruments and Methods B 200, 329-332 (2003)

O. Francescangeli, V. Stanic, L. Gobbi, P. Bruni, M. Iacussi, G. Tosi, and S. Bernstorff
Structure of self-assembled liposome-DNA-metal complexes

Phys. Rev. E 67, 011904 1 - 011904 11(2003)

D. Gracin, P. Dubcek, M. Jaksic and S. Bernstorff
Nanostructural properties of amorphous silicon carbide by GISAXS and optical spectroscopy
Thin Solid Films 433 (2003) 88-91

- D. Gracin, M. Jaksic, P. Dubcek, Z. Medunic
Investigation of the nano-structural properties of amorphous silicon carbon alloys by IBA technique, optical spectroscopy and GISAXS
 Vacuum 71, pp. 47-51 (2003)
- P.J. Griffiths, M.A. Bagni, B. Colombini, H. Amenitsch, S. Bernstorff, C.C. Ashley, and G. Cecchi
Myosin lever arm tilt during sinusoidal oscillations when the power stroke is suppressed
J. Physiol., 552P, C53 (2003)
- D. Grosso, F. Banonneau, C. Sanchez, G.J.de.A.A. Soler-Illia, E.L. Crepaldi, P.A. Albouy, H. Amenitsch, A.R. Balkenende and A. Brunet Bruneau
A first insight of the mechanisms involved in the self-assembly of 2D-hexagonal templated SiO₂ and TiO₂ mesostructured films during dip-coating
Journal of Sol-Gel Science & Technology 26, pp. 561-565 (2003)
- D. Grosso, G.J.D.A.Soler-Illia, E.L.Crepaldi, F.Cagnol, C.Sinturel, A.Bourgeois, A.Brunet-Bruneau, H.Amenitsch, P.A.Albouy and C.Sanchez
Highly porous TiO₂ anatase optical thin films with cubic mesostructure stabilized at 700 degrees C
Chemistry of Materials 24, pp. 4562-4570 (2003)
- D. Grosso, E.L.Crepaldi, G.J.D.Illia, F.Cagnol, N.Baccile, F.Babonneau, P.A.Albouy, H.Amenitsch and C.Sanchez
Phase transformations involved during silica modified silica, and non-silica mesoporous-organized thin films deposition. The role of evaporation
Studies in Surface Science and Catalysis 146 (Nanotechnology in Mesostructured Materials), pp. 281-284 (2003)
- H.S. Gupta, K. Misof, I. Zizak, P. Meßmer, P. Roschger, S. Bernstorff, K. Klaushofer, P. Fratzl,
Mineralized microstructure of calcified avian tendons: a scanning small-angle X-ray scattering study
Calcif. Tissue Int. 72, 567-576 (2003)
- F. Lo Celso, A. Triolo, F. Triolo, P. Thiyagarajan, H. Amenitsch, M. Steinhart, M. Kriechbaum, J.M.DeSimone and R. Triolo
A combined small-angle neutron and X-ray scattering study of block copolymers micellisation in supercritical carbon dioxide
J. Applied Cryst. 36, 660-663 (2003)
- M. Lucic-Lavcevic, D. Posedel and A. Turkovic
SAXS/WAXD on thermally annealed nanostructured CVD-obtained TiO₂ films
 in: "Chemical Vapor Deposition XVI and EUROCVD 14", Volume 2 / Allendorf, Mark D.; Maury, Francis ; Teyssandier, Francis (ed.), London, IBT Global, 2003

C. Michon, D. Kalnin, F. Mariette, G. Garnaud, P. Relkin, M. Ollivon, A. Davenel, P. Durosset and G. Cuvelier

Influence of fat Crystallinity on the texture of foams

Proceedings of ISFRS 2003 (3rd International Symposium on Food Rheology and Structure),
Editors: Fischer P. Marti I. Windhab E. ISBN: 3-905609-19-3, ZÜRICH, Switzerland, pp. 235-239 (2003)

E Occhipinti, P L Martelli, F Spinozzi, F Corsi, C Formantici, L Molteni, H Amenitsch, P Mariani, P Tortora, R Casadio

3D Structure of Sulfolobus solfataricus Carboxypeptidase developed by Molecular Modelling is confirmed by Site-directed Mutagenesis and Small-Angle X-Ray Scattering,

Biophys. J. 85, pp. 1165-1175 (2003)

A. Orthen, H. Wagner, H.J. Besch, R.H. Menk, A.H. Walenta, U. Werthenbach

Investigations of an optimised MicroCAT, a GEM and their combination by simulations and current measurements

Nucl. Instr. and Meth. A500 (2003) 163-177

A. Orthen, H. Wagner, H.J. Besch, S. Martoiu, R.H. Menk, A.H. Walenta, U. Werthenbach

Gas gain and signal length measurements with a triple-GEM at different pressures of Ar-, Kr- and Xe-based gas mixtures

Nucl. Instr. and Meth. A512, 476-487 (2003)

G. Pabst, J. Katsaras, V. A. Raghunathan, and M. Rappolt

Structure and Interactions in the Anomalous Swelling Regime of Phospholipid Bilayers.

Langmuir 19, 1716-1722 (2003)

G. Pabst, R. Koschuch, B. Pozo Navas, M. Rappolt, K. Lohner, and P. Lagner

Structural Analysis of Weakly Ordered Membrane Stacks

J. Appl. Cryst. 36 , 1378 - 1388 (2003)

Gerd Persson, Håkan Edlund and Göran Lindblom

Thermal behaviour of cubic phases rich in 1-monooleoyl-rac-glycerol in the ternary system 1-monooleoyl-rac-glycerol/n-octyl-beta-D-glucoside/water

European Journal of Biochemistry 270, pp. 56-65 (2003)

G. Persson, H. Edlund, H. Amenitsch, P. Lagner, and G. Lindblom

The 1-monooleoyl-rac-glycerol/n-octyl-beta-D-glucoside/water system: Phase diagram and phase structures determined by NMR and x-ray diffraction

Langmuir 19, 5813-5822 (2003)

B. Pivac, P. Dubcek, S. Bernstorff, A. Borghesi, A. Sassella, and M. Porrini

Small angle X-ray scattering study of oxygen precipitation in silicon

Nuclear Instruments and Methods B 200, 105-109 (2003)

B. Pivac, O. Milat, P. Dubcek, S. Bernstorff, F. Corni, C. Nobili and R. Tonini

Early stages of bubble formation in helium-implanted (100) silicon

Physica Status solidi (a) 198, No. 1, 29-37 (2003)

- B. Pozo-Navas, V. A. Raghunathan, J. Katsaras, M. Rappolt, K. Lohner, and G. Pabst
Discontinuous Unbinding of Lipid Multibilayers
 Phys. Rev. Lett. 91: 2, 028101-1-028101-3 (2003)
- M. Rappolt, A. Hickel, F. Bringezu and K. Lohner
Mechanism of the Lamellar/Inverse Hexagonal Phase Transition Examined by High Resolution X-Ray Diffraction
 Biophysical Journal 84, 3111-3122 (2003)
- M. Rappolt, M. Vidal, M. Kriechbaum, M. Steinhard, H. Amenitsch, S. Bernstorff, and P. Laggner
Structural, Dynamic and Mechanical Properties of POPC at Low Cholesterol Concentration Studied in Pressure/Temperature Space
 Europ. Biophys. J. 31, 575-585 (2003)
- John De Roche, Charles M. Gordon, Corrie T. Imrie, Malcolm D. Ingram, Alan R. Kennedy, Fabrizio Lo Celso, and Alessandro Triolo
Applications of complementary experimental techniques to the characterization of the phase diagram of [C16mim][PF6] and [C14mim][PF6]
 Chemistry of Materials 15, 3089 (2003)
- J.B. Rosenholm and M. Lindén
Controlled synthesis and processing of ceramic oxides – A molecular approach
 Handbook of Surface and Colloid Science, 2nd edition, CRC Press, p. 437 (2003)
- Matthias F. Schneider, Roman Zantl, Christian Gege, Richard R. Schmidt, Michael Rappolt and Motomu Tanaka
Hydrophilic/hydrophobic balance determines morphology of glycolipids with oligolactose headgroups
 Biophysical Journal 84, 306-313 (2003)
- F. Spinozzi, E. Maccioni, CV. Teixeira, H. Amenitsch, R. Favilla, M. Goldoni, P. Di Muro, B. Salvato, P. Mariani and M. Beltramini
Synchrotron SAXS studies on the structural stability of Carcinus aestuarii hemocyanin in solution.
 Biophys J. 85(4), pp. 2661-2672, (2003)
- M. Steinhart, M. Kriechbaum, M. Horky', J. Baldrian, H. Amenitsch, P. Laggner, S. Bernstorff
Time-resolved SWAXS measurements of effects induced by variation of pressure
 In: "Advances in Structure Analysis", Ed. R. Kuzsel and J. Hassek, J., Prague, Czech and Slovak Association 2003. - S. 463-472. ISBN: 80-901748-6-8
- L. Valkova, A. Menelle, N. Borovkov, V. Erokhin, M. Pisani, F. Ciuchi, F. Carsughi, F. Spinozzi, R. Padke, S. Bernstorff and F. Rustichelli
SAXS, SANS and neutron reflectivity studies of LB films of copper tetra-tert-butyl-azaporphyrines
 J. Applied Chryst. 36, 758-762 (2003)

K. Van Ouytsel, J. Boehmert and G. Mueller
A Small Angle X-ray Scattering Method to investigate the crack tip in metals
FZR-388 (2003)

H. Wagner, A. Orthen,, H.J. Besch, R.H. Menk, A.H. Walenta and U. Werthenbach
On the improvement of a flexible applicable gaseous 2D microCAT detector for highly time-resolved X-ray imaging
Nucl. Instr. and Methods A510 (2003) 145-149

I. Zizak, P. Roschger, O. Paris, Barbara M. Misof, A. Berzlanovich, S. Bernstorff, H. Amenitsch, K. Klaushofer, and P. Fratzl
Characteristics of Mineral Particles in the Human Bone-Cartilage Interface
J. Struct. Biol. 141, pp 208-217 (2003)

Publications in January to June 2004

P. Ausili, M. Pisani, S. Finet, H. Amenitsch, C. Ferrero and P. Mariani
Pressure effects on columnar lyotropics: anisotropic compressibilities in guanosine monophosphate four-stranded helices
J. Phys. Chem. B, 108: 1783-1789 (2004)

Josef Baldrian, Milos Steinhart, Antonin Sikora, Jana Kasparova, Heinz Amenitsch, Sigrid Bernstorff
SWAXS and DSC Study of PEO Cocrystalline Structures Development in Polymer Blends
Conference Proceedings, Long Abstract, pp. ??-??, (MACRO 2004 - 40th IUPAC World Polymer Congress, Paris, France, July 4-9, 2004)
(<http://www.upmc.fr/macro2004>)

L. Benes, V. Zima, K. Melanova, M. Steinhart, M. Kriechbaum, H. Amenitsch and S. Bernstorff
In situ high pressure phase transition of alcohol intercalated zirconium phosphate observed by synchrotron X-ray scattering
Journal of Physics and Chemistry of Solids 65, pp. 615-618 (2004)

M. Cócera, O. López, R. Pons, H. Amenitsch, and A. de la Maza
Effect of the electrostatic charge on the mechanism inducing liposome solubilization: a kinetic study by synchrotron radiation SAXS
Langmuir 20(8), 3074 - 3079 (2004)

G. Croce, A. Frache, M. Milanesio, L. Marchese, M. Causa, D. Viterbo, A. Barbaglia, V. Bolis, G. Bavestrello, C. Cerrano, U. Benatti, M. Pozzolini, M. Giovine and H. Amenitsch
Structural characterization of siliceous spicules from marine sponges
Biophysical Journal 86(1), pp. 526-34 (2004)

U.V. Desnica, M. Buljan, I.D. Desnica-Frankovic, P. Dubcek, S. Bernstorff, M. Ivanda and H. Zorc
Direct ion beam synthesis of II-VI nanocrystals
Nucl. Instrum. & Methods B 216, pp. 407-413 (2004)

- P. Dubcek, B. Pivac, O. Milat, S. Bernstorff and I. Zulim
Study of structural changes in krypton implanted silicon
 Nucl. Instrum. & Methods B 215, Issue 1-2, pp. 122-128 (2004)
- P. Dubcek, A. Turkovic, Z. Crnjak Orel, B. Etlinger and S. Bernstorff
Synchrotron Light Scattering on Nanostructured V/Ce Oxide Films Intercalated with Li⁺ Ions
 J. Chem. Inf. Comput. Sci. 44, 290-295 (2004)
- D. Gracin, P. Dubcek, H. Zorc and K. Juraic
Medium Range Ordering of Amorphous Silicon-Carbon Alloys Studied by GISAXS, Spectroscopy and IBA
 Thin Solid Films 459, 1-2; 216-219 (2004)
- P.J. Griffiths, M.A. Bagni, B. Colombini, H. Amenitsch, S. Bernstorff, C.C. Ashley, and G. Cecchi
SI structure under conditions of hypo- and hypertonicity
 J. Physiol., 555P, C169 (2004)
- D. Grosso, F. Cagnol, Galo J. de A. A. Soler-Illia, Eduardo L. Crepaldi, P. A. Albouy, H. Amenitsch, A. Brunet-Bruneau, and Clément Sanchez
Fundamental of mesostructuration through evaporation-induced self-assembly
 Advanced Functional Materials 14, 309-322 (2004)
- O. López, M. Cócera, J. Pereira, H. Amenitsch, J. Caelles, L. Coderch, J.L. Parra, A. de la Maza and R. Pons
Processing stopped-flow saxs data to study the kinetic of liposome-surfactant systems
 Biophys. J, 86(1), 76a, (2004)
- A. Orthen, H. Wagner, S. Martoiu, H. Amenitsch, S. Bernstorff, H.J. Besch, R.H. Menk, K. Nurdan, M. Rappolt, A.H. Walenta and U. Werthenbach
Development of a two-dimensional virtual-pixel X-ray imaging detector for time-resolved structure research
 J. Synchrotron Rad. 11, 177-186 (2004)
- G. Pabst, H. Amenitsch, P. Laggner, and M. Rappolt
Pretransitional swelling is not linked to ripple phase formation in phosphatidylcholines
 Biophysical Journal 86, 350A (2004)
- N. Radic, A. Tonejc, J. Ivkov, P. Dubcek, S. Bernstorff, Z. Medunic
Sputter-deposited amorphous-like tungsten
 Surface and Coatings Technology Vol 180-181C, pp 66-70 (2004)
- A. Raudino, F. Lo Celso, A. Triolo, and R. Triolo
Pressure-induced formation of diblock copolymer "micelles" in supercritical fluids. A combined study by small angle scattering experiments and mean-field theory. I. The critical micellization density concept
 J. Chem. Phys. 120, 3489 (2004)

A. Raudino, F. Lo Celso, A. Triolo, and R. Triolo
Pressure-induced formation of diblock copolymer "micelles" in supercritical fluids. A combined study by small angle scattering experiments and mean-field theory. II. Kinetics of the unimer-aggregate transition
J. Chem. Phys. 120, 3499 (2004)

Th. Schmidt, T. Clausen, J. Falta, S. Bernstorff, G. Alexe, T. Passow and D. Hommel
Investigation of CdSe/ZnS quantum dot ordering by grazing incidence small angle X-ray scattering
Phys. Stat. Sol. B241, No. 3, 523-526(2004)

Th. Schmidt, T. Clausen, J. Falta, G. Alexe, T. Passow, and D. Hommel and S. Bernstorff
Correlated stacks of CdSe/ZnS quantum dots
Appl. Phys. Lett. 84(22) 4367-4369 (2004).
and
Virtual Journal of Nanoscale Science & Technology, May 24, 2004 issue at
<http://www.vjnano.org>.

H. Wagner, A. Orthen, H.J. Besch, S. Martoiu, R.H. Menk, A.H. Walenta, U. Werthenbach
On image reconstruction with the two-dimensional interpolating resistive readout structure of the Virtual-Pixel detector
Nucl. Instr. and Meth. A523 287-301 (2004)

A. Turkovic'
Grazing-incidence small-angle X-ray scattering and reflectivity on nanostructured oxide films
Materials Science & Engineering B. 110, 1; 68-78 (2004)

Publications in print (June 2004)

S. Areva, C. Boissière, D. Grosso, T. Asakawa, C. Sanchez, M. Lindén
One-pot aerosol synthesis of ordered hierarchical mesoporous core-shell silica nanoparticles
Chem. Commun.

W. H. Binder, S. Bernstorff, C. Kluger, L. Petraru, M. J. Kunz, V. Torma
Poly(etherketone)-Poly(isobutylene) Pseudo-Block Copolymers: Phase Separation Behavior via SAXS
Polymer

G. Cecchi, M.A. Bagni, B. Colombini,, C.C. Ashley, H. Amenitsch, S. Bernstorff and P.J. Griffiths
Use of sinusoidal length oscillations to detect myosin conformation by time-resolved x-ray diffraction
Adv. Exp. Med. Biol.

P. Dubcek, B. Pivac, S. Bernstorff, F. Corni, C. Nobili and R. Tonini
Grazing incidence small angle X-ray scattering study of He irradiation induced defects in monocrystalline silicon
NIM B

Paolo Falcaro, David Grosso, Heinz Amenitsch, Plinio Innocenzi
Silica Orthorhombic Mesostructured Films with Low Refractive Index and High Thermal Stability
Journal Physical Chemistry B

K. Flodström, C.V. Teixeira, H. Amenitsch, V. Alfredsson and M. Lindén
An in situ Synchrotron Small Angle X-ray Scattering/X-ray Diffraction Study of the Formation of SBA-15 Mesoporous Silica
Langmuir

David Grosso, Cédric Boissière, Bernd Smarsly, Torsten Brezesinski, Nicola Pinna, Pierre A. Albouy, Heinz Amenitsch, Markus Antonietti and Clément Sanchez
Periodically Ordered Mesoporous Films with Nanocrystalline Multimetallic Oxide Walls
Nature Materials

Plinio Innocenzi, Paolo Falcaro, Stefano Schergna, Michele Maggini, Enzo Menna, Heinz Amenitsch, David Grosso, Galo Soler A.A. Illia, Clément Sanchez
One-Pot Self-Assembling of Mesostructured Silica Films and Membranes Functionalised with Fullerene Derivatives
Journal Material Chemistry

M. Pisani, T. Narayanan, G.M. Di Gregorio, C. Ferrero, H. Amenitsch and P. Mariani
Compressing inverse lyotropic phases: effects on dioleoyl phosphatidyl ethanolamine at low hydration
Phys. Rev. E

B. Pivac, P. Dubcek, S. Bernstorff, F. Corni and R. Tonini
GISAXS study of hydrogen implanted silicon
J. Alloys and Compounds

H. Wilhelm, A. Paris, E. Schafner, S. Bernstorff, J. Bonarski, T. Ungar, M. J. Zehetbauer,
Evidence of dislocations in melt-crystallised and plastically deformed polypropylene
Mater.Sci.Eng.A

International Conferences and Workshops in 2003

H. Amenitsch, P. Agren, M. Linden, F. Schueth, D. Grosso and F. Babonneau
Synthesis of mesoporous materials studied with small angle X-ray scattering: from bulk to surfaces
AIC-SILS Joint Congress, Trieste, 21-25 July 2003 (talk)

H. Amenitsch, C. V. Teixeira, M. Rappolt, M. Majerovic and P. Laggner
X-ray surface diffraction to study highly aligned phospholipids under influence of amphiphilic molecules and salt
AIC-SILS Joint Congress, Trieste, 21-25 July 2003 (talk)

H. Amenitsch, P. Agren, M. Linden, F. Schueth, D. Grosso and F. Babonneau
Synthesis of Mesoporous Materials Studied with Small Angle X-ray Scattering: From Bulk to Surfaces

International Conference on Materials for Advanced Technologies ICMAT 2003,
Singapore, December 7-12, 2003 (talk)

H. Amenitsch, C.A.J. Schulze-Bauer, G. Sommer, M. Rappolt, P. Laggner, G.A. Holzapfel
Layers of Age Specific Human Aortas During Tensile Testing: A Small Angle X-ray Scattering Study

International Conference on Materials for Advanced Technologies ICMAT 2003,
Singapore, December 7-12, 2003 (talk)

N. Baccile, M. Lindén, A. Riley, S. Tolbert, H. Amenitsch and F. Babonneau

Hybrid materials: from properties to applications

Ecole thématique CNRS "Galerie", Carcans – Maubuisson (France), September 14–19, 2003
(poster)

J. Baldrian, M. Steinhart, A. Sikora, L. Kasparova, H. Amenitsch and S. Bernstorff

SWAXS and DSC study of PEO crystallization in polymer blends

11th International Users' Meeting of ELETTRA, Trieste, Italy, 2.12.2003 (poster)

J. Baldrian, M. Steinhart, A. Sikora, G. Todorova, M. Kriechbaum, H. Amenitsch and S. Bernstorff

Real-Time Study of Cocrystalline Structure Development in Polymer Blends

International Conference on Materials for Advanced Technologies ICMAT 2003,
Singapore, December 7-12, 2003 (poster ICMATJ364 J-5-8-P)

Ludvík Benes, Vítězslav Zima, Klára Melánová, Milos Steinhart, Manfred Kriechbaum,
Heinz Amenitsch, Sigrid Bernstorff

High pressure phase transition of alcohol intercalated zirconium phosphate

STRUKTURA' 03 conference: "Computational methods in X-ray and neutron structure
analysis", 16. 6. - 21. 6. 2003, Nové Hradky, Czech Republik (Poster)

Proc. Materials Structure 10, 80 – 81 (2003)

S. Bernstorff, H Amenitsch, M. Kriechbaum, M. Rappolt and P. Laggner

*The SAXS-beamline at ELETTRA as a tool for fast time resolved structural studies on the
nanometer-scale*

13 th International Symposium on "Spectroscopy in Theory and Practice", Nova Gorica,
Slovenia, August 27-30, 2003 (invited talk)

W. Binder, M. Kunz, D. Machl and C. Kluger

Self assembly of hydrogen bonded supramolecular polymers

6th Austrian Polymermeeting, Vienna, Austria 2003

M. Buljan, K. Salamon, P. Dubcek, I.D. Desnica-Frankovic, U. V. Desnica, O. Milat

STRUKTURNA ANAKLIZA CdSc NANOKRISTALA u SiO2 SUPSTRATU

4th Meeting of Croatian Physical Society, Zagreb, Croatia, 13-15. 11. 2003 (Poster)

P. Bussian, P. Agren, M. Linden, W. Schmidt, H. Amenitsch, F. Schueth

ms time resolution small angle scattering study of Zinc sulfide precipitation in a liquid jet

AIC-SILS Joint Congress, Trieste, 21-25 July 2003 (poster)

M. Cocera, J. Pereira, O. Lopez, R. Pons, J. Caelles, I. Carrera, A. de la Maza and H. Amenitsch

Effect of Electrostatic Charges on the First Steps of Liposome Solubilization: a Time Resolved SAXS Study

AIC-SILS Joint Congress, Trieste, Italia, 21-25 July 2003 (poster)

G. Croce, M. Milanesio, D. Viterbo, M. Cadoni, A. Frache and L. Marchese

Synchrotron radiation structural study of MCM-22

AIC-SILS Joint Congress, Trieste, 21-25 July 2003 (poster)

G. Croce, M. Milanesio, D. Viterbo, H. Amenitsch, G. Bavestrello, M. Giovine

Structural organization in siliceous spicules from marine sponges and the biosilicification process

INDABA IV: patterns in nature Skuzuzu, South Africa 17-22 August 2003 (oral)

I.D. Desnica-Frankovic, P. Dubcek, U.V. Desnica, S. Bernstorff, H. Karl and I. Großhans, B. Stritzker

GISAXS studies on CdSe nanocrystals synthesized in thermally grown SiO₂

E-MRS 2003 Spring Meeting, Strasbourg, France, June 10 - 13, 2003 (poster A/PII 47)

I.D. Desnica-Frankovic, P. Dubcek, U.V. Desnica, S. Bernstorff, H. Karl, I. Gosshans and B. Stritzker

GISAXS Studies on CdS nanocrystals synthesized in thermally grown SiO₂

AIC-SILS Joint Congress, Trieste, 21-25 July 2003 (talk)

I.D. Desnica-Frankovic, P. Dubcek, U.V. Desnica, S. Bernstorff, H. Karl and I. Großhans

Combinational Approach to the Ion Beam Synthesis of CdSe monocrystals

Euro Nano Forum 2003, Trieste, December 9-12, 2003 (poster)

U.V. Desnica, I.D. Desnica-Frankovic, M. Buljan, P. Dubcek, and S. Bernstorff

Direct Ion Beam Synthesis of II-VI Nanocrystals

EuroNanoForum 2003, Trieste, Italy, 9.-12.12.2003 (poster)

U. V. Desnica, I.D. Desnica-Frankovic, M. Buljan, P. Dubcek, S. Bernstorff

Direct Ion Beam Synthesis of II-VI nanocrystals at room temperature

E-MRS 2003 Spring Meeting, Strasbourg, France, June 10 - 13, 2003 (talk)

U. V. Desnica, I.D. Desnica-Frankovic, M. Buljan, P. Dubcek, M. Ivanda, H. Zorc

Direktna sinteza nano _estica binarnth poluvodi _a ionskom implantacijom

4th Meeting of Croatian Physical Society, Zagreb, Croatia, 13-15. 11. 2003(Poster)

P. Dubcek, S. Bernstorff, K. Salamon, O. Milat,, and N. Radic

Grain structure of sputter-deposited tungsten carbide thin films

Symposia: 'A - Current trends in nanoscience - from materials to application'

E-MRS 2003 Spring Meeting, Strasbourg, France, June 10 - 13, 2003 (poster A/PII 64)

Paolo Falcaro

Advance on mesoporous films

Institute of Industrial Science, University of Tokyo, Japan, November 2003 (seminar talk)

Paolo Falcaro, Johnny Mio Bertolo, Andrea Bearzotti, Plinio Innocenzi
Ordered mesostructured silica films: effect of pore surface on its sensing properties
XII International Sol-gel Workshop, Sydney, Australia, August 2003 (poster)

D. Gracin, M. Jaksic, P. Dubcek, H. Zorc and K. Juraic
Medium range ordering of amorphous silicon-carbon alloys studied by GISAXS, optical spectroscopy and IBA
Abstracts of 8th European Vacuum Congress, Berlin, Deutsche Vakuumgesellschaft, p. 86 (2003)

P.J. Griffiths, M.A. Bagni, B. Colombini, H. Amenitsch, S. Bernstorff, C.C. Ashley and G. Cecchi
Myosin lever arm tilt during sinusoidal oscillations when the power stroke is suppressed
Joint Meeting of the "British Pharmacological Society" and "The Physiological Society", University of Manchester, UK, September 9-12, 2003 (talk)

David Grosso, Florence Cagnol, Aurélie Coupé, Niki Baccile, Cédric Boissière, Galo J. de A. A. Soler-Illia, Eduardo Crepaldi, and, Clément Sanchez
Amorphous and crystalline mesoporous materials prepared via evaporation
MRS Spring meeting 2003, San Francisco, USA (invited talk)

David Grosso, Florence Cagnol, Aurélie Coupé, Niki Baccile, Cédric Boissière, Galo J. de A. A. Soler-Illia, Eduardo Crepaldi, and, Clément Sanchez
Overview of Evaporation induced self-assembly
Euromat 2003, Lausanne, Suisse (invited talk)

N. Huesing, U. Lavrencic Stangar, G. Kickelbick, V. Torma, C. Raab, B. Launay
Spectroscopic tools in the synthesis and characterisation of liquid-crystal templated materials
13 th International Symposium on "Spectroscopy in Theory and Practice", Nova Gorica, Slovenia, August 27-30, 2003 (invited talk)

D. Kalnin, M. Ouattara, O. Schafer, H. Amenitsch and M. Ollivon
TAG Crystallization in Emulsions: DSC/XRDT study of Triacylglycerol Polymorphism influenced by emulsifier under process conditions
Joint Symposium of Lipid and Cereal Science in Europe, Vichy, France, 15-17 Nov 2003 (oral)

D. Kalnin, O. Schafer, H. Amenitsch and M. Ollivon
TAG Crystallization in Emulsions: DSC/XRDT study of Triacylglycerol Polymorphism influenced by emulsifier concentration
STK Meeting 2003, Swiss Society for Thermal Analysis & Calorimetry, Lausanne, Switzerland, 5 Nov, 2003 (oral)

D. Kalnin, O. Schafer, H. Amenitsch and M. Ollivon
TAG Crystallization in Emulsions: DSC/XRDT study of Triacylglycerol Polymorphism influenced by emulsifier concentration
GEFTA-Tagung 2003, Gesellschaft für Thermische Analyse e.V.; Augsburg, Germany 15-16. Sep 2003 (oral)

D. Kalnin, O. Schafer, H. Amenitsch and M. Ollivon
TAG Crystallization in Emulsions: Triacylglycerol Polymorphism influenced by emulsifier concentration
25th World Congress and Exhibition of the ISF, Bordeaux, France, 12-15 Oct 2003 (Poster)

T. Koch, S. Seidler, S. Bernstorff, and E. Halwax
Microhardness of quenched polypropylene
6th Austrian Polymer Meeting, Vienna, 15.-17.9.2003, Proceedings p82 (talk)

P. Laggner, M. Rappolt, G. Pabst, C.V. Teixeira, J. Strancar and H. Amenitsch
In-Situ Diffraction and Spin-Label ESR Studies on Membranes at Solid Surfaces
International Conference on Materials for Advanced Technologies ICMAT 2003,
Singapore, December 7-12, 2003 (talk)

M. Lucic-Lavcevic, D. Posedel and A. Turkovic
SAXS/WAXD on thermally annealed nanostructured CVD-obtained TiO₂ films
The Electrochemical Society INTERFACE / Rajeshwar, Krishnan (ed.)
Hookset, U.S.A., Cummings Printing Co., 2003. PS-64

M. Lucic-Lavcevic, D. Posedel, A. Turkovic
SAXS/WAXD on thermally annealed nanostructured CVD-obtained TiO₂ films
203rd ECS Meeting, Paris, France (2003)
Meeting Abstracts, CD / Allendorf, Mark D ; Maury, Francis ; Teyssandier, Francis (ed.)
London, IBT Global, p. 2188 (2003)

K. Melánová, L. Benes, V. Zima, M. Trchová, P. Čapková
In situ high pressure phase transition of alcohol intercalated zirconium phosphate followed by synchrotron X-ray radiation
12th. International Symposium on Intercalation Compounds, Poznan, Poland, 1 – 5 June
2003, Proc. page 152

R. Menk, H. Amenitsch, F. Arfelli, S. Bernstorff and H. Besch
Imaging with high dynamic using an ionization chamber
SPIE conference “Medical Imaging”, Session “Physics of Medical Imaging”, San Diego,
California, USA, 15 – 20 February 2003, Poster [5030-85]S12
(Besch+Menk haben auch: [5030-28]S6)

C. Michon, D. Kalnin, F. Mariette, G. Garnaud, P. Relkin, M. Ollivon, A. Davenel, P.
Durosset and G. Cuvelier
Influence of fat Crystallinity on the texture of foams
3rd International Symposium on Food Rheology and Structure (ISFRS 2003), Zürich ,
Switzerland, Feb 9-13, 2003

C. Michon, D. Kalnin, F. Mariette, G. Garnaud, P. Relkin, M. Ollivon, A. Davenel, P.
Durosset and G. Cuvelier
Effet de l'état de la matière grasse sur la texture de mousses aux différents étapes du procédé de fabrication
Colloque du GFR “Rhéologie & Physico-chimie des Produits Formulés”, BREST, France, 15-
17 Oct 2003 (poster)

M. Pisani, V. Stanic, P. Bruni, M. Iacussi, G. Tosi and O. Francescangeli
Supramolecular Structure of Self-Assembled Liposome-DNA-Metal Complexes
INFM Meeting, Genova, Italy, June 23rd-25th, 2003 (poster)

B. Pivac, P. Dubcek, S. Bernstorff, F. Corni, R. Tonini and G. Ottaviani
Grazing incidence small angle X-ray scattering study of He irradiation induced defects in monocrystalline silicon
E-MRS 2003 Spring Meeting, Strasbourg, France, June 10 - 13, 2003 (poster E/PI.19))

B. Pivac, P. Dubcek, O. Milat, S. Bernstorff, R. Tonini, F. Corni and G. Ottaviani
GISAXS comparative study of H and D implanted Si
E-MRS 2003 Spring Meeting, Strasbourg, France, June 10 - 13, 2003 (poster E/PI.16))

B. Pivac, P. Dubcek, I. Kovacevic, S. Bernstorff, I. Zulim, Ivan
Structural changes in amorphous silicon at low temperatures
2nd aSiNet Workshop on Thin Silicon and 9th Euroregional Workshop on Thin Silicon Devices, Book of Abstracts / Shubert, Markus B. ; Conde, Joao P. (ur.). Lisboa: Instituto Superior Tecnico, 2003 (talk)

R. Pons, J. Caelles, I. Carrera, H. Amenitsch.
Emulsification by temperature change followed by time resolved SAXS
XVII ECIS Conference, Florence (Italy), 21-26 September 2003 (poster)

D. Posedel, P. Dubcek, A. Turković and Z. Crnjak Orel
Grazing-incidence small-angle X-ray scattering of synchrotron light source on nanostructured V/Ce oxide films intercalated with Li⁺ ions
12th Croatian Slovenian Crystallographic Meeting, National Park Plitvice Lakes, Croatia, June 19 – 22, 2003 (talk)

G. Principi, A. Maddalena, Marcos Meyer, Simone Dal Toe', Ajay Gupta, Pooja Sharma, B.A. Dasannacharya, Neelima Paul, S. Bernstorff, H. Amenitsch
Structural Evolution of the Amorphous Grain Boundary Phase during Nanocrystallization of Fe₇₂Cu₁Nb_{4.5}Si_{13.5}B₉
International Conference on Magnetism (ICM2003), Rome, Italy, July 27 - August 1, 2003

N. Radic, A. Tonejc, J. Ivkov, P. Dubcek and S. Bernstorff
Sputter-deposited amorphous-like tungsten
E-MRS 2003 Spring Meeting, Strasbourg, France, June 10 - 13, 2003 (poster G/PII 30)

N. Radic,, S. Bernstorff, P. Dubcek, K. Salamon and O. Milat
Grain structure of sputter-deposited tungsten carbide thin films
AIC-SILS Joint Congress, Trieste, 21-25 July 2003 (poster)

Michael Rappolt
Modeling of diffraction data from fluid like multibilayer systems by means of an inverse Fourier method
Workshop on "Advances in experimental and teoretical methods for biological applications of Synchrotron radiation, Frascati, Rome, Italy, 27.- 29.2.2003 (invited talk)

Th. Schmidt, T. Clausen, J. Falta, S. Bernstorff, G. Alexe, T. Passow and D. Hommel
Correlation of stacked CdSe/Zn(S)Se quantum dots observed by small angle x-ray scattering
11th International Conference on II-VI Compounds (2003 II-VI), September 22-26, 2003,
Niagara Falls, New York, USA (talk)

Francesco Spinozzi

Structure of Sulfolobus solfataricus Carboxypeptidase Determined by Molecular Modelling and SAXS

Workshop on “Advances in experimental and teoretical methods for biological applications of Synchrotron radiation, Frascati, Rome, Italy, 27.- 29.2.2003 (invited talk)

A. Turkoviç, P. Dubcek, Z. Crnjak-Orel and S. Bernstorff

Nanoparticles in vanadium oxide and V/Ce oxide films

12th Croatian Slovenian Crystallographic Meeting, National Park Plitvice Lakes, Croatia, June 19 – 22, 2003 (talk)

A. Turkoviç, P. Dubcek, Z. Crnjak-Orel and S. Bernstorff

Synchrotron Light Scattering on Nanostructured V/Ce Oxide Films intercalated with Li+ Ions

Euro Nano Forum 2003, Trieste, December 9-12, 2003 (poster)

A. Turkovic and M. Gaberscek

Impedance spectroscopy and GISAXS on nanostructured TiO₂ films

Euro Nano Forum 2003, Trieste, December 9-12, 2003 (poster)

L.A. Valkova

Nanomaterials based on azaporphyrine LB films.

Report at round table: “Organic Materials for the Molecular Electronic: Nanostructures, Properties, Nanotechnologies” Conference: Scientific Activities in Classical University. Ivanovo, ISU, Russia, 20 Feb. 2003 (talk)

L. Valkova

Organic nanomaterials for sensor application: Crowned azaporphyrines

International School on Advanced Material Science and Technology, 26-29 August 2003, Jesi - Ancona, Italy (lecture)

L. Valkova

Organic nanomaterials for sensor application: Fullerene composites

International School on Advanced Material Science and Technology, 26-29 August 2003, Jesi - Ancona, Italy (lecture)

L.A. Valkova

Features of formation and structure of the azaporphyrine LB films.

Report at Seminar “Langmuir films and amphiphilic molecules assembly”, Institute of Crystallography, Moscow, Russia, 30 Sept. 2003 (talk)

D. Viterbo, G. Croce, M. Milanesio, H. Amenitsch, G. Bavestrello and M. Giovine

Structural organization in siliceous spicales from marine sponges and the biosilicification process

Joint congress AIC-SILS, Tieste, 21-25 July 2003 (poster)

H. Wilhelm, A. Paris, E. Schafler, S. Bernstorff, J. Bonarski, T. Ungar, M. J. Zehetbauer
Proof of dislocations in melt-crystallised and plastically deformed polypropylene
13th Int.Conf on “Strength of Materials, Fundamental Aspects of the Deformation and Fracture of Materials” (ICSMA-13), 25-30 August 2003, Budapest, Hungary (lecture)

H. Wilhelm, A. Paris, E. Schafler, S. Bernstorff, J. Bonarski, T. Ungar, M. J. Zehetbauer
Proof of dislocations in melt-crystallised and plastically deformed polypropylene
6th Austrian Polymer Days, University of Technology, Vienna, Austria (Sept. 2003) (poster)

M. J. Zehetbauer
Work hardening and ultrafine-grained microstructures at large plastic deformations
13th Int. Workshop on Computational Mechanics of Materials Otto von Guericke-University Magdeburg, Germany, September 22-23 (2003) (Invited lecture)

M. J. Zehetbauer
Principles and Modelling of severe plastic deformation providing ultra fine grained materials
Symposium "Microstructure and Property Design by Deformation Processing of Materials" at the occasion of the retirement of Prof.Etienne Aernoudt, Katholieke Universiteit Leuven, Belgium, October 6-7 (2003) (Invited lecture)

ELETTRA Highlights 2002-2003

N. Hüsing, D. Brandhuber; C. Raab; V. Torma, H. Peterlik, M. Steinhart, M. Kriechbaum and S. Bernstorff
In-situ SAXS Investigations on the Formation of Mesostructured Spider-Web Like Silica Monoliths
pp. 32-35 (2003)

PhD Thesis 2003

Pamela Ausili
Studio delle proprietà strutturali di quadrirelliche di guanosina mediante diffrazione dei raggi X: effetti della temperatura, concentrazione, forza ionica, pH e pressione meccanica
Università di Ancona, Italy

Mercèdes Cócera
Estudio de los efectos derivados de la incorporacion de alquilsulfatos sobre bicapas lipidicas
(Study of the effects due to the incorporation of alkyl-sulphate to lipid bilayers)
Universitat de Barcelona, Spain

Giordano M. Di Gregorio
Analisi strutturale di sistemi lipidici di interesse biologico tramite tecniche di diffrazione dei raggi X
Università di Ancona, Italy

Anna Lind

Characterization, and Further Processing of Surfactant Templated Mesoporous Silica Synthesized under Alkaline Conditions

Dept. Phys. Chem., Åbo Akademi University, Finland

Thomas Koch

Morphologie und Mikrohärte von Polypropylen-Werkstoffen (Morphology and microhardness of polypropylene materials)

Thesis Advisor: S. Seidler

Vienna University of Technology, Austria, August 2003

Michela Pisani

Effetti della pressione sulle proprietà strutturali di sistemi liotropici di interesse biologico

Università di Ancona, Italy

Master Theses (Tesi di Laurea) 2003

Niki Baccile

Study of mesoporous silica powders prepared by solution precipitation and aerosol processing

Thesis of DEA (Diplôme d'études approfondies) in inorganic chemistry, University Pierre et Marie Curie, Paris (France), June 2003

Julie Blin

Fabrication et caractérisation de nanocapsules lipidiques

DEA Pharmacotechnie Biopharmacie, Chatenay Malabry 2003

Aljoša KANCLER

Studij faznega prehoda med nematično in smektično A fazo v ograjeni geometriji poroznega stekla CPG

(Study of the nematic - smectic A phase transition in confined geometry of the CPG porous glass)

Faculty of Education, University of Maribor, Maribor, Slovenia, 2003

[COBISS.SI-ID 12435720]

Author Index

ALEXE, G.	39
ALFREDSSON, V.	102
ALMGREN, M.	78
AMENITSCH, H.	54, 56, 57, 59, 61, 65, 68, 69, 71, 73, 75, 77, 79, 80, 83, 86, 88, 92, 94, 96, 99, 102, 107, 110, 113
ASHLEY, C.C.	54
BABONNEAU, F.	83
BACCILE, N.	83, 92
BAGNI, M.A.	54
BALDRIAN, J.	86
BENES, L.	88
BERNSTORFF, S.	39, 41, 43, 45, 47, 49, 54, 61, 63, 65, 68, 75, 86, 88, 90, 104, 107, 113
BESCH, H.J.	113
BINDER, W.H.	90
BOISSIERE, C.	92
BRANDHUBER, D.	104
BULJAN, M.	41
CAELLES, J.	69
CARRERA, I.	69
CASTAGNA, R.	63
CECCHI, G.	54
CHATTOPADHYAY, S.	94
CLAUSEN, T.	39
CLEMENTONI, D.	63
CÓCERA, M.	69
COJOC, D.A.	79
COLOMBINI, B.	54
CONTI, C.	63
COUPÉ, A.	92
CROCE, G.	59
DE LA MAZA, A.	69
DESNICA, U.V.	41, 43
DESNICA-FRANKOVIC, I.D.	41, 43
DEUTSCH, G.	77
DI FABRIZIO, E.	79
DI GREGORIO, G.M.	78
DI STASIO, S.	96
DUBČEK, P.	41, 43, 45, 47
ERDEMIR, D.	94
EVANS, J.M.B	94
FALCARO, P.	99
FALTA, J.	39
FEDERICONI, F.	61
FERRARI, E.	79

FLODSTRÖM, K.	102
FRANCESCANGELI, O.	63
GRIFFITHS, P.J.	54
GROBHANS, I.	43
GROSSO, D.	57, 92
HOLZAPFEL, G.A.	80
HOMMEL, D.	39
HÜSING, N.	104
INNOCENZI, P.	99
IVKOV, J.	47
JESCHKE, M.	108
KALNIN, D.	65
KARL, H.	43
KASPAROVÁ, J.	86
KELLER, G.	65
KLUGER, C.	90
KOVACEVIC, I.	45
KRIECHBAUM, M.	68, 88, 104
KRUSE, C.	39
KUNZ, M.	90
LAGNER, P.	56, 57, 68, 73, 78, 79, 80
LINDÉN, M.	83, 102
LOHNER, K.	77
LOMBARDO, D.	107
LÓPEZ, O.	69
MACHL, D.	90
MARIANI, P.	61, 71, 75, 78
MARTOIU, S.	113
MATTIONI, M.	61
MEDUNIĆ, Z.	47
MELÁNOVÁ, K.	88
MENK, R.H.	113
MILANESIO, M.	59
MÜLLER, G.	51
MYERSON, A.S.	94
NURDAN, K.	113
NYILAS, K.	49
OLLIVON, M.	65
ONISCHUK, A.	96
ONORI, G.	71
ORTHEN, A.	113
ORTORE, M.G.	71
PABST, G.	57, 73, 78
PACCAMICCIO, L.	75
PEREIRA, J.	69
PETERLIK, H.	90, 104
PETRARU, L.	90
PISANI, M.	63
PIVAC, B.	45

PONS, R.	69
POZO NAVAS, B.	77
RAAB, C.	104
RADIĆ, N.	47
RAPPOLT, M.	56, 57, 59, 68, 73, 78, 79, 80, 107, 113
RILEY, A.	83
SANCHEZ, C.	92
SAPRA, S.	110
SARMA D.D.,	110
SARTORI, B.	56, 57, 110
SCHAFFER, O.	65
SCHAFLER, E.	49
SCHMID, F.	80
SCHMIDT, TH.	39
SCHULZE-BAUER, C.A.J.	80
SEGRE, C.U.	94
SEVCSIK, E.	77
SIKORA, A.	86
SOMMER, G.	80
SPINOZZI, F.	71
STANIC, V.	63
STEINHART, M.	68, 86, 88, 104
STRITZKER, B.	43
TEIXEIRA, C.V.	102
TOLBERT, S.	83
TONEJC, A.	47
TORMA, V.	90, 114
TRIOLO, A.	108
TRIOLO, R.	108
UETA, A.	39
UNGÀR, T.	49
VAN OUYTSEL, K.	51
VERRENGIA, G.	96
VIDAL, M.F.	68
VISWANATHA, R.	110
VITERBO, D.	59
WAGNER, H.	113
WALENTA, A.H.	113
WERTHENBACH, U.	113
ZEHETBAUER, M.	49
ZEIPPER, L.	49
ZIMA, V.	88